RV-17

NASA TECHNICAL MEMORANDUM

NASA TM X-1171

NASA TM X-1171

TRANSONIC CHARACTERISTICS OF BOTH LAUNCH AND FLYBACK CONFIGURATIONS OF A VTO REUSABLE LAUNCH VEHICLE

by Robert J. McGhee

Langley Research Center
Langley Station, Hampton, Va.

NATIONAL AERONAUTICS AND SPACE ADMINISTRATION • WASHINGTON, D. C. • NOVEMBER 1965

NASA TM X-1171

TRANSONIC CHARACTERISTICS OF BOTH LAUNCH AND FLYBACK CONFIGURATIONS OF A VTO REUSABLE LAUNCH VEHICLE

By Robert J. McGhee

Langley Research Center
Langley Station, Hampton, Va.

NATIONAL AERONAUTICS AND SPACE ADMINISTRATION

TRANSONIC CHARACTERISTICS OF BOTH LAUNCH AND FLYBACK CONFIGURATIONS OF A VTO REUSABLE LAUNCH VEHICLE*

By Robert J. McGhee
Langley Research Center

SUMMARY

An investigation has been conducted in the Langley 8-foot transonic pressure tunnel to determine the longitudinal and lateral-directional stability characteristics of a complete vertical-take-off launch vehicle and its first-stage reusable flyback vehicle. In addition, control effectiveness was obtained for the reusable first stage at both transonic and landing conditions. Some effects of forebody shape, shroud shape, body base boattailing, vertical-tail arrangements, and flyback engine nacelles are indicated. The complete launch vehicle was tested at angles of attack from -4° to 10°, over a Mach number range of 0.40 to 1.20, and angles of sideslip of 0° and 5°. The flyback vehicle was tested at angles of attack from -4° to 16°, over a Mach number range of 0.20 to 1.20, and over an angle-of-sideslip range of 0° to 6°. Test Reynolds numbers per foot (per 0.305 meter) varied from approximately 1.5×10^6 to 4.4×10^6.

The subsonic level of the zero-lift drag coefficient of the complete reusable launch vehicle was reduced to about the same as that of a similar but expendable launch vehicle. Based on an average estimated in-flight center-of-gravity location of 3.0 diameters forward of the model base, the complete launch vehicle was both longitudinally and directionally stable throughout the Mach number range.

The flyback vehicle was longitudinally stable throughout the Mach number range. Large wing-tip-mounted vertical tails employing 5° of toe-in provided directional stability. A maximum lift-drag ratio of about 6.3 at a Mach number of 0.60 was measured; however, this decreased to about 5.5 with both vertical tails toed in 5°. Longitudinal control effectiveness generally increased with Mach number up to a Mach number of 0.90 and thereafter did not decrease below the subsonic level effectiveness. Lateral control effectiveness remained approximately constant with both angle of attack and Mach number up to about a Mach number of 0.70; it then decreased about 25 percent. Directional control effectiveness decreased as much as 50 percent at transonic speeds.

No appreciable change in longitudinal stability or control effectiveness occurred at simulated landing conditions; however, there was a positive shift in the pitching-moment curve and a delay in pitch-up was observed, attributed to the presence of the ground plane.

---

*Title, Unclassified.

INTRODUCTION

The National Aeronautics and Space Administration is presently engaged in studies to determine the aerodynamic characteristics of reusable launch-vehicle systems. As the frequency of placing large payloads in orbit increases, reusable launch-vehicle systems may provide significant reductions in overall cost per launch, provided recoverability and refurbishment costs can be minimized. For future manned-space-flight missions, winged reusable launch-vehicle systems may offer significant improvements in safety and reliability.

Results of exploratory tests for a reusable first stage of a winged launch vehicle having a large body diameter compared with the wing span have been reported in reference 1. These exploratory tests showed severe longitudinal and lateral-directional stability deficiencies, as well as low subsonic lift-drag ratios. Results of the investigation of reference 1 were employed to design a new configuration of the first stage of a large-payload vertical-take-off reusable launch-vehicle system. The revised first-stage vehicle incorporated a change in wing planform and location as a result of a reassessment of the probable vehicle center-of-gravity and stability requirements, relocation and changes in the planform of the vertical tails, and relocation of the flyback turbine engines.

The present investigation was initiated to determine the stability of the complete launch vehicle at transonic speeds and the stability and control characteristics of the first-stage flyback vehicle at both returning cruise and landing conditions. Results at supersonic and hypersonic speeds are presented in references 2 and 3. Because of the severity of the lift-drag ratio problem encountered in reference 1, it was considered necessary to determine additional information on the effects of forebody shape, shroud shape, body base boat-tailing, vertical-tail arrangements, and flyback engine nacelles.

The tests were conducted in the Langley 8-foot transonic pressure tunnel over a Mach number range of 0.20 to 1.20 at angles of attack from -4° to 16° and sideslip angles of 0° and 5°; some additional data were obtained over an angle-of-sideslip range of -8° to 6°. The test Reynolds number per foot (per 0.305 meter) varied from approximately 1.5×10^{6} to 4.4×10^{6}.

SYMBOLS

Measurements for this investigation were taken in the U.S. Customary System of Units. Equivalent values are indicated herein parenthetically in the International System (SI) in the interest of promoting use of this system in future NASA reports. Details concerning the use of SI, together with physical constants and conversion factors, are given in reference 4.

The aerodynamic data are reduced to standard coefficient form. All data for the complete launch vehicle are referred to the body axes. All lateral-directional and control data for the first-stage winged reusable configuration

are referred to the body axes, whereas the longitudinal data are referred to the stability axes. The moment reference for all data was selected to be 0.90 body diameter forward of the model base. All coefficients are referred to the maximum body base area and maximum body diameter.

C_N normal-force coefficient, $\frac{\text{Normal force}}{q_\infty S_{ref}}$

C_A axial-force coefficient, $\frac{\text{Total axial force}}{q_\infty S_{ref}}$

C_L lift coefficient, $\frac{\text{Lift}}{q_\infty S_{ref}}$

C_D drag coefficient, $\frac{\text{Total drag}}{q_\infty S_{ref}}$

$\left(C_{D,b} + C_{D,i}\right)_{nacelle}$ internal and base drag coefficient for nacelle, $\frac{(\text{Internal drag} + \text{Base drag})_{nacelle}}{q_\infty S_{ref}}$

C_m pitching-moment coefficient, $\frac{\text{Pitching moment}}{q_\infty S_{ref} D}$

C_l rolling-moment coefficient, $\frac{\text{Rolling moment}}{q_\infty S_{ref} D}$

C_n yawing-moment coefficient, $\frac{\text{Yawing moment}}{q_\infty S_{ref} D}$

C_Y side-force coefficient, $\frac{\text{Side force}}{q_\infty S_{ref}}$

C_{N_α} normal-force-curve slope, $\frac{\partial C_N}{\partial \alpha}$, per degree at $C_N \approx 0$

C_{L_α} lift-curve slope, $\frac{\partial C_L}{\partial \alpha}$, per degree at $C_L \approx 0$

$C_{m_{C_N}}$ longitudinal stability parameter (referred to body axes), $\frac{\partial C_m}{\partial C_N}$ at $C_N \approx 0$

$C_{m_{C_L}}$ longitudinal stability parameter (referred to stability axes), $\frac{\partial C_m}{\partial C_L}$ at $C_L \approx 0$

C_{l_β} effective-dihedral parameter, $\frac{\Delta C_l}{\Delta \beta}$, per degree

C_{n_β} directional-stability parameter, $\frac{\Delta C_n}{\Delta \beta}$, per degree

C_{Y_β} side-force parameter, $\frac{\Delta C_Y}{\Delta \beta}$, per degree

C_{m_δ} longitudinal-control-effectiveness parameter, $\frac{\Delta C_m}{\Delta \delta_e}$, per degree where $\delta_e = \delta_{e,R} = \delta_{e,L}$

C_{l_δ} lateral-control-effectiveness parameter, $\frac{\Delta C_l}{\Delta \delta_e}$, per degree where $\delta_e = \delta_{e,R} = -\delta_{e,L}$

C_{n_δ} directional-control-effectiveness parameter, $\frac{\Delta C_n}{\Delta \delta_r}$, per degree

L/D lift-drag ratio

C_p pressure coefficient, $\frac{p - p_\infty}{q_\infty}$

c local chord, feet (meters)

$\bar{c}$ mean aerodynamic chord of exposed basic wing planform, feet (meters)

D maximum body diameter, feet (meters)

M free-stream Mach number

p static pressure, lb/sq ft (N/m^2)

p_∞ free-stream static pressure, lb/sq ft (N/m^2)

q_∞ free-stream dynamic pressure, lb/sq ft (N/m^2)

R Reynolds number per foot (per 0.305 meter)

S_{ref} model reference area, $\frac{\pi D^2}{4}$, square feet ($meters^2$)

t local airfoil thickness, feet (meters)

α angle of attack, degrees

β angle of sideslip, degrees

x,y,a,r coordinate system (see fig. 2(b))

$\frac{x_{cg}}{D}$ center-of-gravity location forward of model base

$\frac{x_{cp}}{D}$ center-of-pressure location forward of model base

$\delta_{e,R}$ right elevon deflection angle (positive when trailing edge is down), degrees

$\delta_{e,L}$ left elevon deflection angle (positive when trailing edge is down), degrees

δ_r rudder deflection angle (positive when trailing edge is to left), degrees

θ_c vertical-tail cant angle (positive tip outward), degrees

θ_t vertical-tail toe-in angle (positive when leading edge is inward), degrees

γ rocket-engine toe-in angle (positive inward), degrees

Subscripts:

o conditions at zero angle of attack or zero lift

max maximum

b body base

c balance chamber

i internal

r rocket engine base

s shroud base

MODEL DESCRIPTION

A two-vehicle configuration was employed in this investigation: the complete launch vehicle and the first-stage winged flyback vehicle. The basic body of the flyback vehicle was an axisymmetric cylinder to which various forebody and body base components, a trapezoidal wing, and vertical tails were

added, with further addition of air-breathing engine nacelles and a crew nacelle. General model arrangements for the configuration are shown in figure 1 with details of model components in figure 2. Table I presents the pertinent model dimensions. Photographs of the launch and flyback vehicles are shown in figure 3.

Complete Launch Vehicle

The complete launch vehicle model consisted of two stages arranged in tandem as shown in figure 1(a). The first stage was a flyback vehicle described later. The second stage consisted of an expendable booster with a length-diameter ratio of 2.92 (including interstage structure) and an ogival spacecraft having a length-diameter ratio of 2.21 (including interstage structure). Four rocket engines, displaced 45° from the vertical axis of symmetry, were mounted parallel to the body axes to simulate the launch arrangement. Two 15° half-conical shrouds were employed to provide protection of the two upper rocket engines, and the wing—body-juncture fairing was shaped to provide protection for the two lower engines from aerodynamic loads during launch. Details of the arrangement of the shrouds, rocket engines, and spacecraft are given in figures 2(a) and 2(b).

Reusable Flyback Vehicle

Arrangements of the first-stage winged reusable flyback vehicle are shown in figure 1(b). Generally, it consisted of two primary assemblies: the ballistic rocket booster and the winged reusable system attached thereto.

The ballistic first-stage rocket booster shown in figure 2(b) was cylindrical and had a length-diameter ratio of 3.65, excluding the forebody. Two interchangeable forebodies consisting of a 1:1 ellipse (spherical forebody) and a 1:2 blunt ellipse were constructed. Provision was made to change the shape of the rearward section (0.5D) of the basic body. Three interchangeable afterbodies were constructed: a plain cylinder (base 1), a base with a parabolic boattail fairing (base 2), and a base with a circular-arc boattail fairing (base 3). A set of parabolic shrouds were designed to provide the minimum cross-sectional area needed to enclose the engine gimbal struts and pylons. These shrouds were identical to those used in reference 1. As an alternate arrangement, the shrouds were removed, and a set of simulated engine actuator struts were installed. (See fig. 1(b).) The four simulated rocket engines were canted toward the center line 12° to reduce their resultant drag during flyback. They were oriented 45° from the vertical plane of symmetry; thus, only the two upper shrouds would be needed since the wing base and wing-body juncture would take the place of the two lower shrouds.

A trapezoidal wing (fig. 2(a)) with a 65° leading-edge sweep angle was mounted on the basic booster so that the center of gravity coincided with 22 percent of the exposed mean aerodynamic chord. The exposed planform area (trailing-edge extensions being neglected) was $7.5D^2$, the taper ratio was 0.35 and 5° of geometric dihedral was employed. The wing was mounted so that the

uppermost wing element at the plane of symmetry was tangent to the body diameter; that is, the chord plane was parallel to and located $t_{max}/2$ below the lowest body element. The basic airfoil section was identical to that used in reference 1 and consisted of a symmetrical 10-percent-thick circular arc with a leading-edge radius of $t_{max}/6$ and a trailing-edge thickness of $t_{max}/3$ with no twist or camber incorporated. A trailing-edge extension, which amounted to 15 percent of the local chord and consisted of a simple wedge section, was added to the wing, as shown in figure 2(a). At the center section, inboard of the 10-percent semispan station, a center flap with a straight trailing edge amounting to 15 percent of the local chord at the 10-percent station was provided. Arbitrary fairings between the body and wing surface made up the wing-body juncture. The original fairing was essentially a minimum-weight fairing, and therefore an alternate and more generous fairing (fig. 2(a)) was tested to improve aerodynamic stability characteristics.

The vertical tails (fig. 2(a)) were located outward at the wing tips and employed an outboard cant of 15°. Toe-in angles of 0° and 5° were provided by rotating the vertical tail about its midchord. The airfoil section was similar to that for the wing without the trailing-edge extensions. The taper ratio was 0.60.

The flyback engines were arranged in a six-abreast nacelle having a rectangular planform and were located at the center of the wing just rearward of the 41-percent chord station and mounted beneath it. (See figs. 1(b) and 2(b).) In this position the outboard nacelle leading edge was just rearward of the assumed wing front-spar location at about 18 percent of the local chord and it could be retracted without wing structure interference. This nacelle was considered to be retracted entirely within the wing during launch; hence, the lower surface shape coincided with the wing lower surface shape. Simple semicircular inlet lips were provided, and the duct was sized to provide an inlet mass-flow rate of approximately 0.60 at the assumed cruise-back Mach number of 0.60. A simple elliptic cylindrical pod, constructed to simulate a crew nacelle, was located on the wing leading edge at 20 percent of the left wing semispan. It was mounted with its axis on the wing-chord plane. Details of the flyback engine nacelle and the crew nacelle are shown in figures 2(a) and 2(b), respectively.

Control Surfaces

Nearly full-span elevons amounting to 20 percent of the basic wing chord were provided. They extended from 10 percent to 90 percent of the exposed semispan (not including tip fairing). Deflection angles of 0° and ±5° were provided with hinge plates. These elevons were considered to provide both pitch and roll control.

Directional control was provided by 0.30c control surfaces located on the trailing edge of the vertical tails and extending from approximately the 10-percent station to the tip. By means of hinge plates, provisions were made for deflection angles of 0° and ±5°.

APPARATUS AND TESTS

Range of Investigation

The tests were conducted in the Langley 8-foot transonic pressure tunnel. For the complete launch vehicle the tests were conducted over a range of Mach numbers from 0.40 to 1.20, at angles of attack from -4° to 10°, and angles of sideslip of 0° and 5°. Additional data were taken over an angle-of-sideslip range of -8° to 2° at an angle of attack of 0°. Test Reynolds number per foot (per 0.305 meter) varied from approximately 1.5×10^6 to 4.2×10^6. Tests for the flyback vehicle were conducted over a range of Mach numbers from 0.40 to 1.20, at angles of attack from -4° to 16°, and over an angle-of-sideslip range of 0° to 6°. Most of data was obtained at sideslip angles of 0° and 5°. Test Reynolds number per foot (0.305 meter) varied from approximately 1.5×10^6 to 3.8×10^6. Low-speed tests in the presence of a ground plane were conducted at Mach numbers from 0.20 to 0.40, and angles of attack from 0° to 16° with corresponding Reynolds number per foot (per 0.305 meter) from approximately 1.8×10^6 to 4.4×10^6. (See fig. 4.) Results of longitudinal-, lateral-, and directional-control deflections were obtained at cruise flight and landing conditions.

Ground Board

A ground board was employed to determine the effects of the proximity of the ground on the aerodynamic characteristics at landing of the first-stage winged flyback vehicle. The ground board spanned the tunnel, had a chord of 6 feet (1.83 meters), and had the trailing edge cut out to accommodate the support sting at high angles of attack. The center of rotation of the model was approximately 2 inches (0.051 meter) downstream from the model base and 2.90 inches (0.074 meter) above the ground board. Thus, for the 0.008 scale of this model, the vertical height simulated was about 30 feet (9.14 meters) or approximately 0.90 body diameter.

Transition Strips

All experiments were conducted with artificial transition, consisting of 0.10-inch-wide strips of No. 80 carborundum grains, located on each forebody and at the 0.10c station of both surfaces of the wings and vertical tails.

Measurements

Aerodynamic force and moment measurements were obtained by use of a six-component internally mounted strain-gage balance. Angles of attack and sideslip were corrected for balance and sting deflection under load. All drag data represent gross drag unless otherwise noted. The internal drag of the ducts was measured by use of a survey rake, and pressure measurements were also

made on the base of the flyback-engine nacelle. The nacelle drag was taken to be the sum of the internal air-flow drag together with the nacelle-base drag. Additional pressure measurements were made in the balance chamber, on the body base, and on various body-base components. (See fig. 1(b).)

PRESENTATION OF RESULTS

The results of this investigation have been divided into two major parts. The first consists of the data for the complete launch vehicle; the second, the data for the first-stage winged reusable flyback vehicle. The latter were further divided into the data applicable to cruise flight and landing conditions.

Figures 5 to 10 present the basic and summary aerodynamic characteristics of the complete launch configuration. Figures 11 to 21 include basic and summary data for the first-stage winged reusable flyback vehicle at cruise flight conditions. Figure 22 presents basic data at landing conditions of the first-stage winged reusable flyback vehicle. Finally, figure 23 summarizes the control effectiveness of the first-stage reusable flyback vehicle at landing and cruise flight conditions.

All force and moment data have been referred to the maximum area of the body base and its maximum diameter. All moments have been referred to the assumed center of gravity, which was 0.90 diameter forward of the model base - the estimated center of gravity for the first stage during flyback to the recovery site.

DISCUSSION OF RESULTS

The results of this investigation provide basic aerodynamic characteristics of a representative launch configuration of a large-cargo payload rocket-powered two-stage-to-orbit vertical-take-off launch vehicle for which the first stage is a winged reusable flyback vehicle and the second stage is an expendable booster. The results will further provide basic aerodynamic characteristics for the winged reusable flyback vehicle during the transonic and subsonic flight regions. Improvement in performance of the redesigned configuration over that of reference 1 will be indicated, and some initial information relative to longitudinal and lateral-directional control effectiveness is presented. Finally, some initial results concerning the landing aerodynamic characteristics and control effectiveness near the ground for the flyback vehicle are given.

Complete Launch Vehicle

Axial-force coefficient.- Figure 8 shows that the basic axial-force coefficient at an angle of attack of 0° remained relatively constant over the subsonic Mach number range to about $M = 0.8$ and was then followed by the usual abrupt transonic drag rise. At $M = 0.8$, $C_{A,o} = 0.70$ for the basic

configuration, whereas toeing the vertical fins in 5° added nearly 10 percent to the axial-force coefficient. The subsonic level of total axial-force coefficient was compared with that for an expendable launch vehicle (ref. 5) having somewhat similar geometry to the booster stages alone. (See fig. 8.) The small difference in $C_{A,o}$ for the expendable vehicle compared with the present reusable vehicle is initially surprising inasmuch as both wings and vertical tails have been added to the first stage. Reference 1, however, showed that by proper design, the zero-lift drag coefficient of the flyback vehicle could be reduced to a value below that for the basic expendable first-stage booster. The source of the high drag of the expendable booster was shown (ref. 1) to have been caused by excessively negative base pressures associated with base pumping action in the presence of the large 15° conical shrouds. Figure 8 shows the calculated average subsonic level of the base pressure coefficient from reference 5 (configuration 6), which at $M = 0.80$ is about -0.34 as compared with the much lower value of -0.23 for the present winged configuration.

Stability and control.- Normal-force-curve slopes C_{N_α} are shown in figure 8 to vary from about 0.64 to 0.84 and are about four times the side-force parameter C_{Y_β} shown in figure 9. Figure 5 also shows that approximately 1° of incidence will be required for a zero-normal-force trajectory. At launch ($M = 0$) the vehicle center of gravity has been estimated and is shown in figure 10 to be about 2.8D above the base; at $M = 1.2$ it is about 3.1D from the base. The indicated forward shift is caused by first-stage propellant consumption during this portion of the flight trajectory. Based on an average value of approximately 3.0D for the center-of-gravity location together with an aerodynamic center located only about 0.5D from the base, it is obvious that an extreme longitudinal stability normal to the wing plane exists. Furthermore, figure 9 shows that the launch configuration does not possess positive effective dihedral. Figure 10 shows that the lateral center of pressure of the launch vehicle is about 1.0D forward of the body base; therefore, based on an average center-of-gravity location of 3.0D forward of the body base, positive directional stability is indicated. The lack of 1:1 correspondence in the angle-of-attack induced forces coupled with lack of coincidence of the longitudinal and lateral centers of pressures may be expected to introduce severe aerodynamic-control problems since the control system must be designed to compensate for transverse winds of arbitrary orientation. The control-system problem will be degraded if a prescribed launch trajectory must be followed as compared with the possibility that a drifting flight trajectory might be allowed for some cases.

Cruise Aerodynamic Characteristics of Flyback Vehicle

Drag and lift-drag ratio.- The difficulty in obtaining high subsonic lift-drag ratios for the flyback cruise conditions was indicated in reference 1 to be associated primarily with the large body base and base pumping caused by the engine shrouds. For the present configuration the base drag problem was increased by lowering the wing by one-half the maximum root-chord thickness as compared with the configuration of reference 1. This change was made to effect a substantial improvement in the wing center section from a structural standpoint, and to allow employment of a fully retractable flyback engine nacelle

on the lower wing surface during launch. This design would also permit a center-section trailing edge which could provide protection of the lower rocket-engine nozzles from reentry heating and loads. (See fig. 1.) Lowering of the wing also required an enlarged wing-fuselage fairing (fig. 1) at the body base to insure aerodynamic protection of the engines from excessive loads during the launch phase of flight. The resulting increase in base area was about 20 percent. The zero-lift drag coefficient with no shrouds or rocket engines and with the basic booster cylindrical body is shown in figure 12 to be 0.45 at $M = 0.60$, which was estimated to approximate the optimum flyback Mach number. This value represents an increase of 0.04 in $C_{D,o}$ over that shown in reference 1 and is associated primarily with the physical changes just discussed. The best zero-lift drag coefficient for the earlier studies was 0.35 and was obtained only after considerable tailoring. From the earlier studies it had been concluded that a parabolic rocket-engine shroud shape provided a marked $C_{D,o}$ improvement. From considerations of the launch-vehicle requirements, the equivalent of the basic 15° shrouds would be needed to prevent excessive aerodynamic loads on the rocket engines. Since the parabolic shrouds would not be expected to provide this needed protection during launch, some additional hardware would be required. For flyback, this additional hardware would have to be ejected prior to subsonic cruise flight. An alternate arrangement would be to eject the 15° shrouds and thereby leave the rocket-engine actuators exposed during the subsonic portion of the flight. Figure 12 shows less than 0.010 penalty in $C_{D,o}$ for the actuator struts exposed, compared with that for the parabolic shrouds at $M = 0.60$. For this test no attempt was made to streamline the struts or the attachments; hence, some small improvement could be anticipated if this region were properly modified. Additional $C_{D,o}$ improvement, with the struts exposed, was achieved by a small amount of body boattailing rearward of the thrust-frame location on the body. The lowest $C_{D,o}$ value achieved for the present flyback vehicle is shown in the figure to be 0.475. Because of the importance of forebody length on interstage-structural weight, an additional shape, a 1:2 elliptical forebody (fig. 2(b)), was tested to determine the drag penalty. Figure 12 shows that $C_{D,o}$ has increased about 20 percent over that of the spherical forebody. The conclusion of reference 1 that the spherical forebody is nearly the optimum compromise between interstage weight and aerodynamic shape is validated.

For the configuration of reference 1, the maximum L/D was about 6.0 at $M = 0.60$, as compared with 6.3 for the present configuration. Figure 13 shows the large improvement in maximum L/D resulting from the special tailoring of the wing-body juncture fairing, which was incorporated because of a longitudinal pitch-up at subsonic speeds (to be discussed later). However, it is shown in figure 13 that when 5° of toe-in of the vertical tails was employed (which from references 2 and 3 was shown to be needed for supersonic and hypersonic directional stability), the maximum L/D can be expected to decrease by about 0.80 (from 6.3 to about 5.5).

Longitudinal stability.- Figure 13 shows a subsonic static margin of about 20 percent of the body diameter for the flyback configuration with both vertical tails toed in 5°, and it increases to about 43 percent at $M = 1.20$. Installation of the flyback engine nacelle with air flow resulted in an abrupt

decrease in stability at transonic speeds. Special tailoring of the wing-body juncture fairing (see fig. 2(a)) removed most of the irregularity of the stability parameter throughout the Mach number range.

Figure 11 shows favorable shifts in positive $C_{m,o}$ resulting from the tailoring of the wing-body juncture fairing. This shift in the pitching-moment curve would result in less control being required to trim the vehicle. A severe pitch-up is shown (fig. 11) to occur at lift coefficients of about 7 in the low-speed range and about 8 in the high-speed range. Results of several oil-flow tests revealed a strong vortex originating near the leading edge of the wing at the body juncture, which resulted in flow separation over a large part of the wing. Several means were employed to alleviate this problem; the greatest improvement was obtained by refairing to provide a more generous radius about the wing-body juncture. (See fig. 2(a).) This modification delayed the pitch-up about $\Delta C_L = 1$ throughout the Mach number range. Toeing in the vertical tails 5° resulted in a decrease in the level of the pitching-moment curves throughout the Mach number range; this decrease was caused by the expected increase in wing-tip loading. Installation of the flyback engine nacelle decreased the pitching-moment level and resulted in nonlinearity in the curves in the subsonic speed range; however, in this location the engine thrust would provide substantial increments in ΔC_m.

Lateral-directional stability.- The negative effective dihedral indicated by reference 1 has been eliminated at subsonic speeds (fig. 16); however, lateral instability still exists at transonic speeds at an angle of attack of 0°. Positive directional stability is shown in figure 14 when both vertical tails were toed in 5° over an angle-of-attack range between about 0° to 12°. The level of stability at $\alpha = 0°$ and $\alpha = 12°$ is shown in figure 16, the latter angle corresponding closely with the angle of attack for maximum L/D. The flyback engine nacelle reduced C_{n_β} at subsonic speeds (fig. 16) by about as much as the toed-in tails improved it. This result would be expected since the nacelle was located appreciably forward of the vehicle center of gravity.

Control effectiveness.- Longitudinal-control effectiveness increased to about $M = 0.90$ throughout the angle-of-attack range (fig. 23) and thereafter did not decrease below the subsonic level. Comparison of figures 16 and 20 shows negligible effects of C_{m_δ} on directional stability; however, a positive contribution to C_{l_β} at subsonic speeds is noted at $\alpha = 0°$ for an elevon deflection of 5°.

Figure 23 shows that roll-control effectiveness remained relatively constant at subsonic speeds up to an angle of attack of about 12°. A decrease in C_{l_δ} of about 25 percent occurred with increasing angle of attack for Mach numbers greater than about 0.80 in the low-angle range and 0.70 in the high-angle range. An adverse yawing moment resulted from differential elevon deflection, as shown by comparison of figures 14 and 18(b).

Directional-control effectiveness (fig. 23) decreased with an increase in angle of attack, but it increased with increasing Mach number up to about $M = 0.90$ and then deteriorated as much as 50 percent at transonic speeds. Comparison of figures 16 and 21 shows that when both rudders were deflected to the left ($\delta_r = 5^\circ$), a positive contribution to both C_{l_β} and C_{n_β} resulted at $\alpha = 0^\circ$.

Landing Aerodynamic Characteristics of Flyback Vehicle

Longitudinal stability.- Figure 22 shows the longitudinal aerodynamic characteristics in the presence of a ground plane. A positive shift in $C_{m,o}$ of about 0.30 at $M = 0.40$ is shown by comparison of figures 11(a) and 22(a). This favorable increase would result in less control being required for landing. No appreciable change in longitudinal stability is shown in the presence of the ground plane. A static margin of about 16 percent of the body diameter is indicated for all Mach numbers. At $M = 0.40$, the ground plane exerts a substantial influence on pitch-up as a delay from about $C_L = 8$ to $C_L = 9$. (See figs. 11(a) and 22(a).) As indicated by figure 11(a), tailoring of the wing-body juncture fairing would probably provide an additional increase in C_L to about 10 at $M = 0.40$. Based on an assumed wing loading of 45 lb/ft^2 (215.46 N/m^2) (calculated by basing both C_L and wing loading on total wing-planform area), the estimated landing speed required to stay within the stability region is about 210 knots.

Control effectiveness.- Figure 22(a) indicates that an up-elevon deflection of 5° removed most of the nonlinearity of the pitching-moment curve at $M = 0.20$. The data of figure 22 indicate that for an available landing C_L of about 10, an up-elevon deflection of about 10° would be required to trim at landing.

Figure 23 shows that no reduction in roll-control effectiveness occurred in the presence of the ground plane. An increase in positive $C_{m,o}$ at all Mach numbers resulted from differential elevon deflections of $\pm 5^\circ$ (fig. 22(a)) with about the same degree of adverse yawing moment in ground effect at $M = 0.40$ as was indicated for out-of-ground-plane effects. (Compare figs. 22(b) and 18(b).)

Deflection of both rudders 5° to the right is shown in figure 22 to have no influence on longitudinal characteristics. There was no appreciable effect on C_{n_δ} in the presence of the ground plane, as indicated by figure 23.

CONCLUSIONS

An investigation has been conducted to determine the longitudinal and lateral-directional stability characteristics of a complete vertical-take-off

launch vehicle and its first-stage reusable flyback vehicle. In addition, control effectiveness was obtained for the flyback vehicle at both transonic and landing conditions. Test data were obtained over a Mach number range from 0.20 to 1.20, angles of attack from -4° to 16°, and sideslip angles of 0° and 5°. Test Reynolds number per foot (per 0.305 meter) varied from approximately 1.5×10^6 to 4.4×10^6. The results indicate that the following conclusions are appropriate:

1. By proper attention to the base drag problem, the subsonic level of the zero-lift drag coefficient of the complete reusable launch vehicle was reduced to about the same as that of a similar but expendable launch vehicle. Based on an average in-flight center-of-gravity location of 3.0 diameters forward of the body base, the complete launch vehicle was longitudinally and directionally stable throughout the Mach number range.

2. The reusable flyback vehicle was longitudinally stable throughout the Mach number range, and wing-tip-mounted vertical tails employing 5° of toe-in provided directional stability. A maximum lift-drag ratio of about 6.3 at a Mach number of 0.60 was measured; however, this ratio decreased to about 5.5 with both vertical tails toed in 5°.

3. Longitudinal control effectiveness generally increased with Mach number up to a Mach number of 0.90 and thereafter did not decrease below that of the subsonic level. Lateral control effectiveness remained approximately constant with both angle of attack and Mach number up to about a Mach number of 0.70; it then decreased about 25 percent. Directional control effectiveness deteriorated as much as 50 percent transonically.

4. No appreciable change in longitudinal stability or control effectiveness occurred at simulated landing conditions; however, there was a positive shift in the pitching-moment curve and a delay in pitch-up was observed and was attributed to the presence of the ground plane.

Langley Research Center,
National Aeronautics and Space Administration,
Langley Station, Hampton, Va., July 29, 1965.

REFERENCES

1. Pierpont, P. Kenneth: Aerodynamic Investigation of a Large Winged Vertical-Take-Off Reusable Orbital Launch Vehicle at Mach 0.4 to 2.1. NASA TM X-996, 1964.

2. McGhee, Robert J.; and Pierpont, P. Kenneth: Supersonic Characteristics of Both Launch and Flyback Configurations of a VTO Reusable Launch Vehicle. NASA TM X-1095, 1965.

3. McGhee, Robert J.: Aerodynamic Characteristics of a Complete VTO Launch Vehicle and Reusable Flyback Configuration From Mach 3.0 to 6.0. NASA TM X-1155, 1965.

4. Mechtly, E. A.: The International System of Units - Physical Constants and Conversion Factors. NASA SP-7012, 1964.

5. Norris, John D.: Transonic Wind-Tunnel Investigation of the Aerodynamic Characteristics of Various Saturn V Configurations. NASA TM X-953, 1964.

TABLE I.- GEOMETRIC CHARACTERISTICS

Reusable flyback vehicle -	
Body:	
Length, overall, in. (cm)	13.14 (33.38)
Diameter, in. (cm)	3.17 (8.05)
Base area, sq in. (cm^2)	7.88 (50.84)
Length/Diameter, cylindrical body	3.65
Moment reference from base, in. (cm)	2.85 (7.24)
Shrouds:	
Length, 15° and parabolic, in. (cm)	2.52 (6.40)
Base area (per shroud), 15°, sq in. (cm^2)	0.93 (6.00)
Base area (per shroud), parabolic, sq in. (cm^2)	0.68 (4.39)
Wing:	
Total area, including trailing-edge extension, sq in. (cm^2)	122.60 (790.97)
Exposed area, including trailing-edge extension, sq in. (cm^2)	88.00 (567.74)
Exposed area, neglecting trailing-edge extension, sq in. (cm^2)	75.40 (486.45)
Root chord at fuselage juncture, in. (cm)	9.38 (23.83)
Tip chord, in. (cm)	3.28 (8.33)
Span (total), in. (cm)	15.05 (38.23)
Leading-edge sweep, deg	65
Positive dihedral, deg	5
$(t/c)_{max}$	0.10
Leading-edge radius	$t_{max}/6$
Trailing-edge thickness	$t_{max}/3$
Airfoil section	Circular arc
$\bar{c}$, based on exposed area, in. (cm)	6.83 (17.35)
Moment reference, from leading-edge wing	$0.22\bar{c}$
Moment reference, distance from body base, in. (cm)	2.85 (7.24)
Aspect ratio, design	2.08
Vertical tail:	
Area, each, sq in. (cm^2)	9.43 (60.84)
Root chord, in. (cm)	3.65 (9.27)
Tip chord, in. (cm)	2.19 (5.56)
Height, in. (cm)	3.23 (8.20)
Leading-edge sweep, deg	30
$(t/c)_{max}$	0.10
Leading-edge radius	$t_{max}/6$
Trailing-edge thickness	$t_{max}/3$
Airfoil section	Circular arc
Toe-in, deg	0 and 5
Cant, deg	15
Tail moment arm, c.g. to $(\bar{c}/4)$ tail, in. (cm)	7.51 (19.08)
Second-stage expendable rocket booster -	
Length, in. (cm)	9.25 (23.50)
Diameter, in. (cm)	3.17 (8.05)
Length/Diameter	2.92
Spacecraft -	
Length, in. (cm)	7 (17.78)
Diameter, base, in. (cm)	3.17 (8.05)
Length/Diameter	2.21

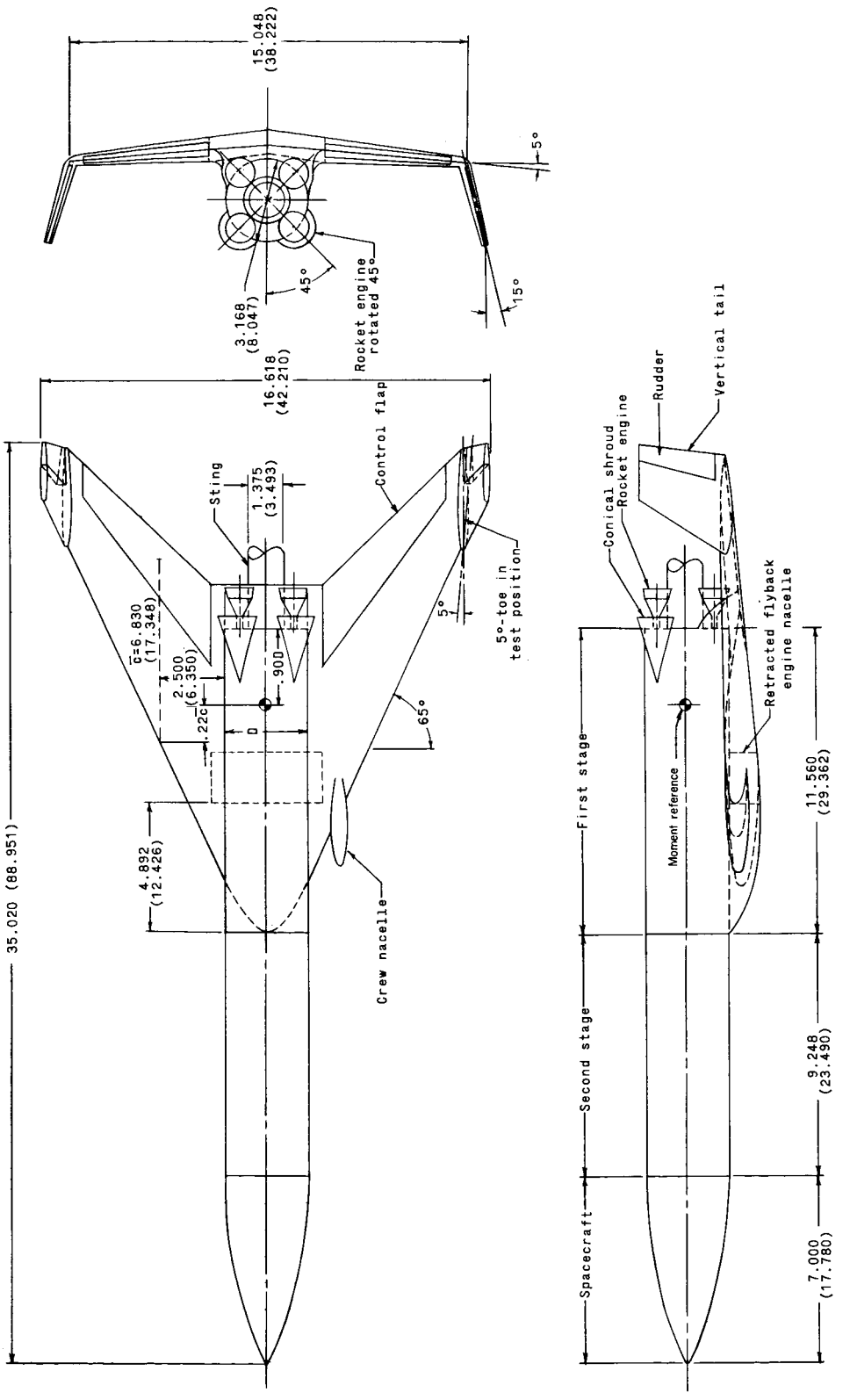

(a) General arrangement of vertical-take-off launch vehicle.

Figure 1.- Arrangement and geometric details of launch vehicle with first-stage flyback vehicle. (All dimensions are in inches (cm) unless otherwise noted.)

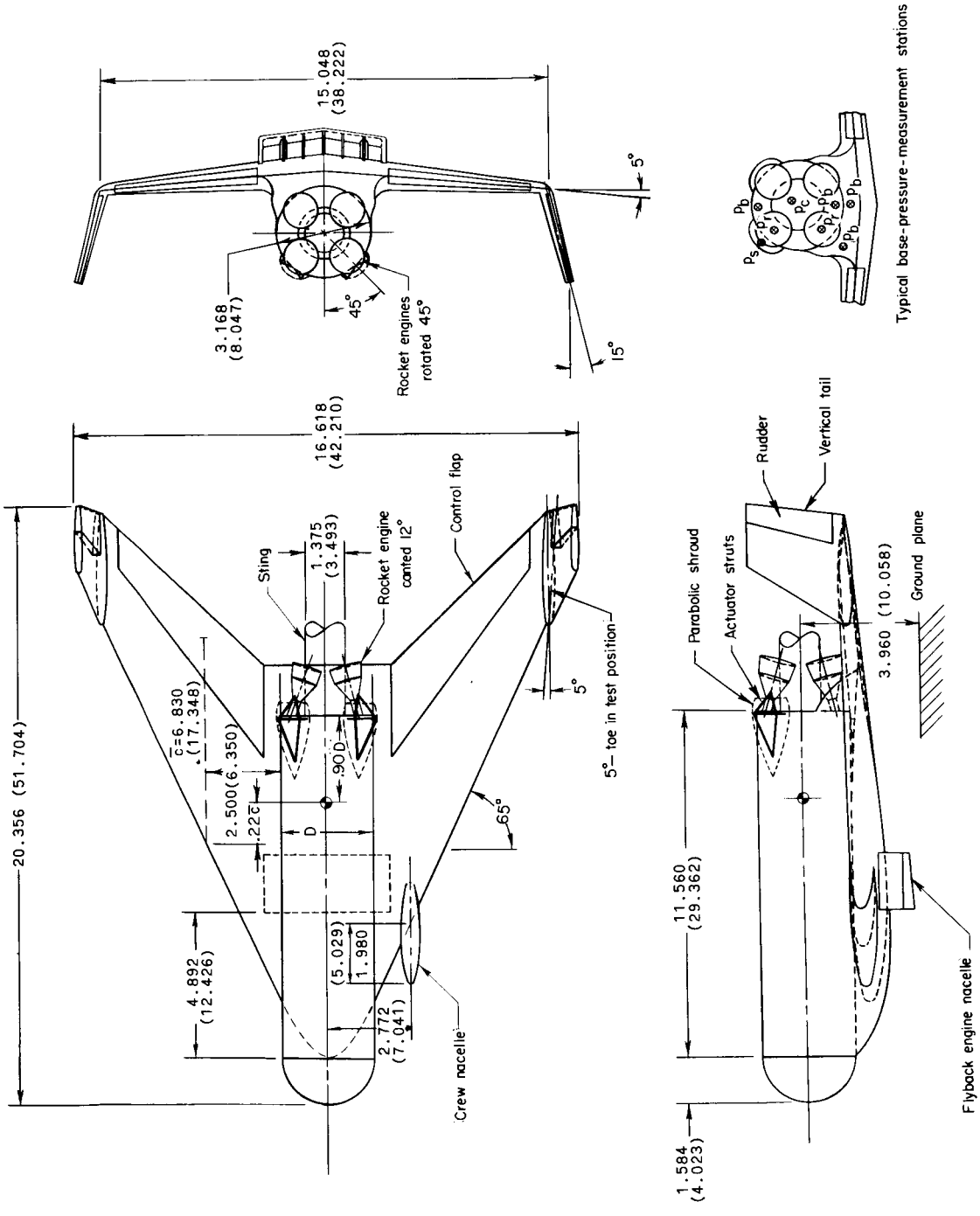

(b) Reusable first-stage flyback vehicle.

Figure 1.- Concluded.

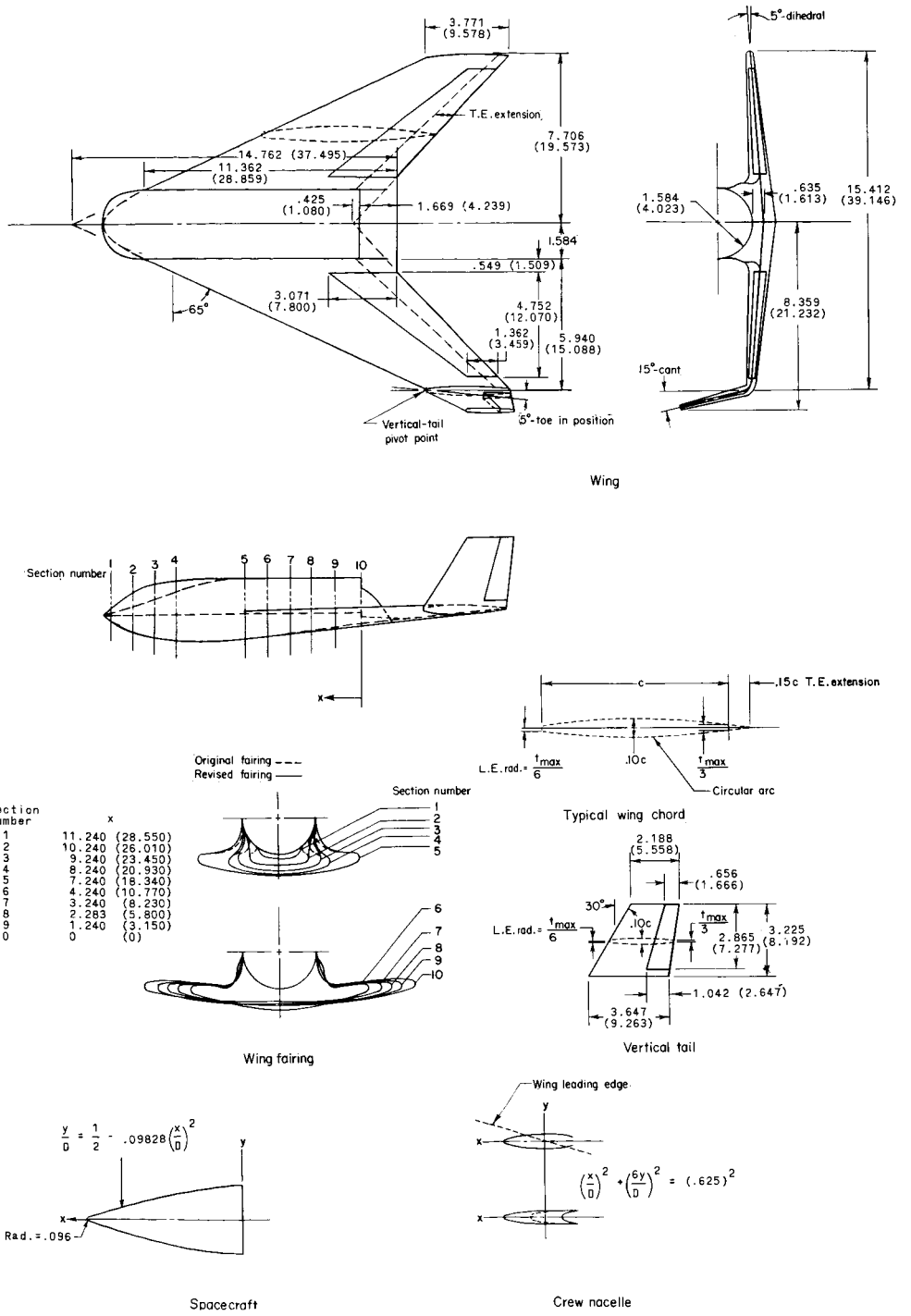

(a) Wing, vertical tail, crew nacelle, wing fairings, and spacecraft.

Figure 2.- Details of model components. (All dimensions are in inches (cm) unless otherwise noted.)

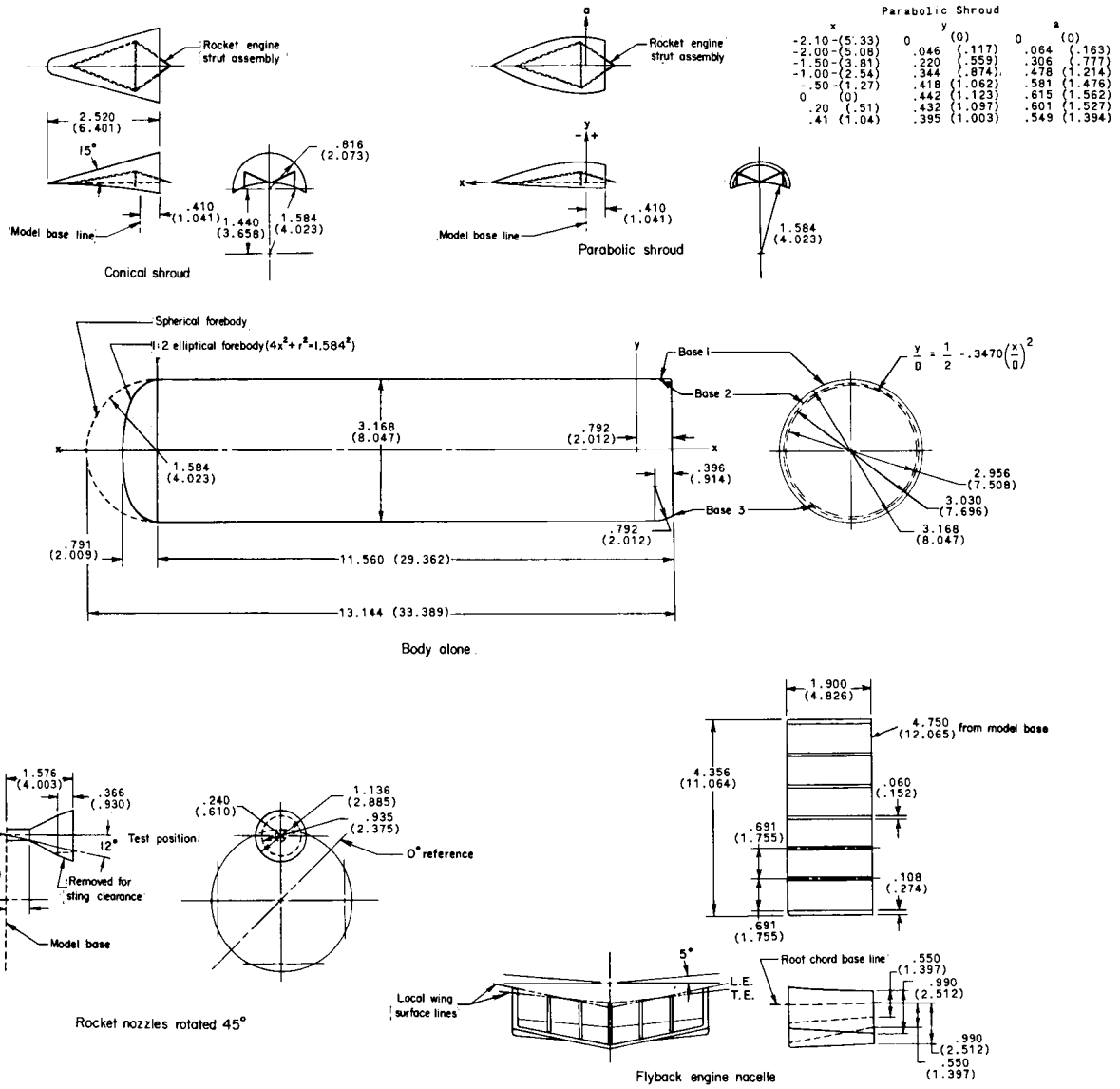

(b) Shrouds, body alone with base modifications and forebody arrangements, rocket nozzles, and flyback engine nacelle.

Figure 2.- Concluded.

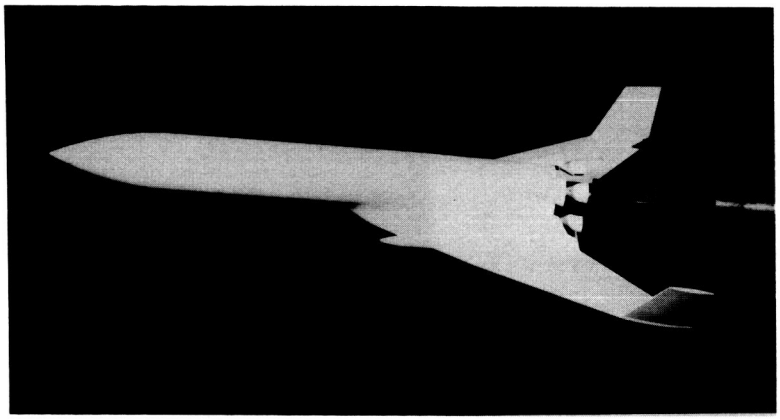

Launch configuration. L-64-7561

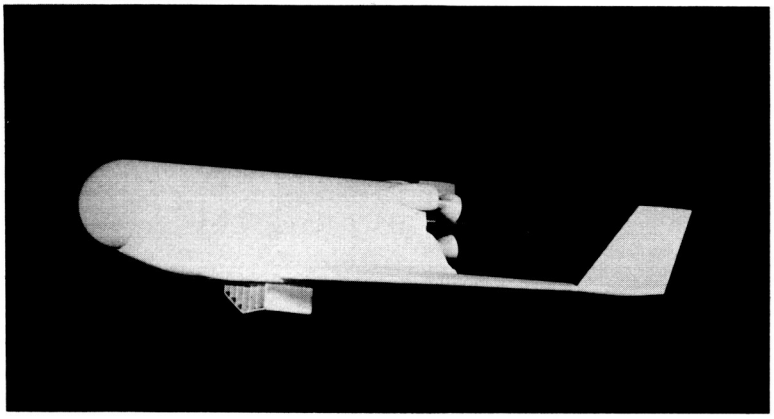

First stage with parabolic shrouds. L-64-7567

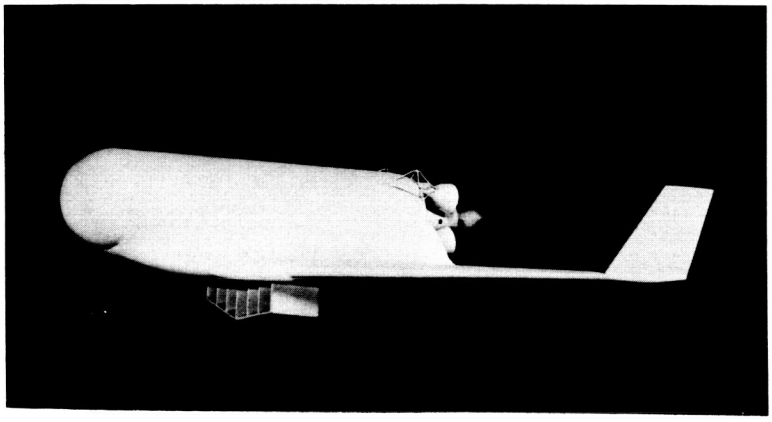

First stage with exposed actuator struts.

Figure 3.- Photographs of representative configuration. L-64-7559

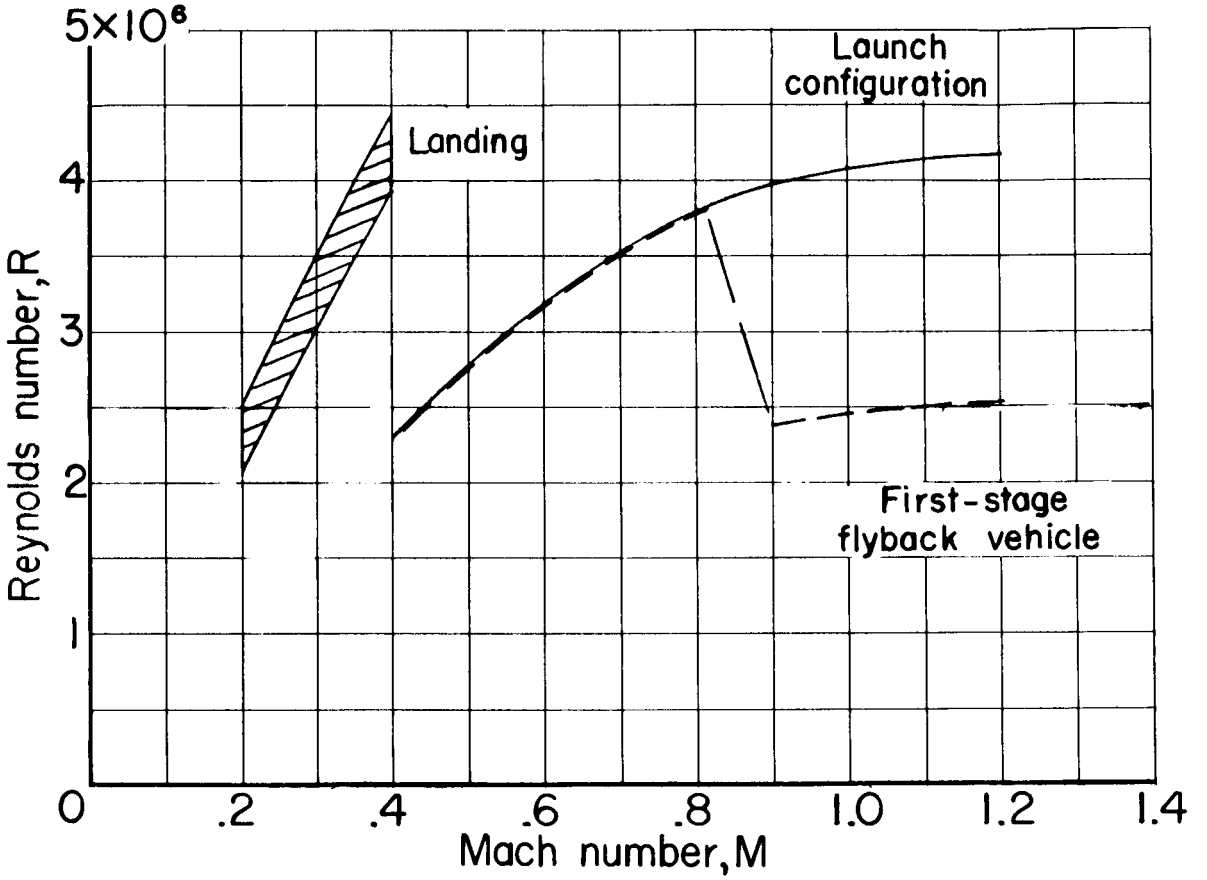

Figure 4.- Variation with Mach number of test Reynolds number per foot (per 0.305 m).

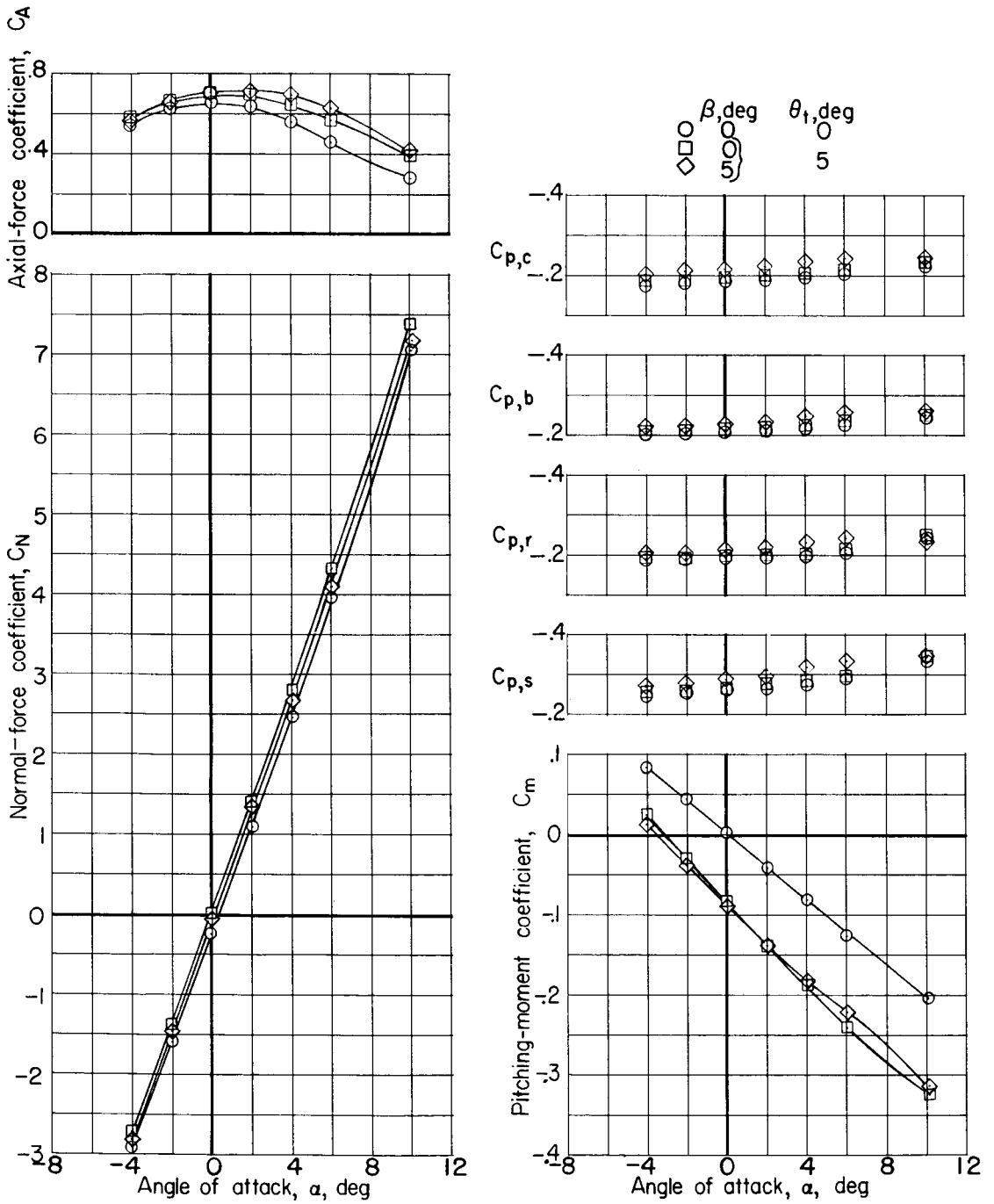

(a) M = 0.40.

Figure 5.- Longitudinal aerodynamic characteristics of complete launch vehicle. 15° conical shrouds; retracted engine nacelle; $\gamma = 0^0$; $\theta_c = 15^0$.

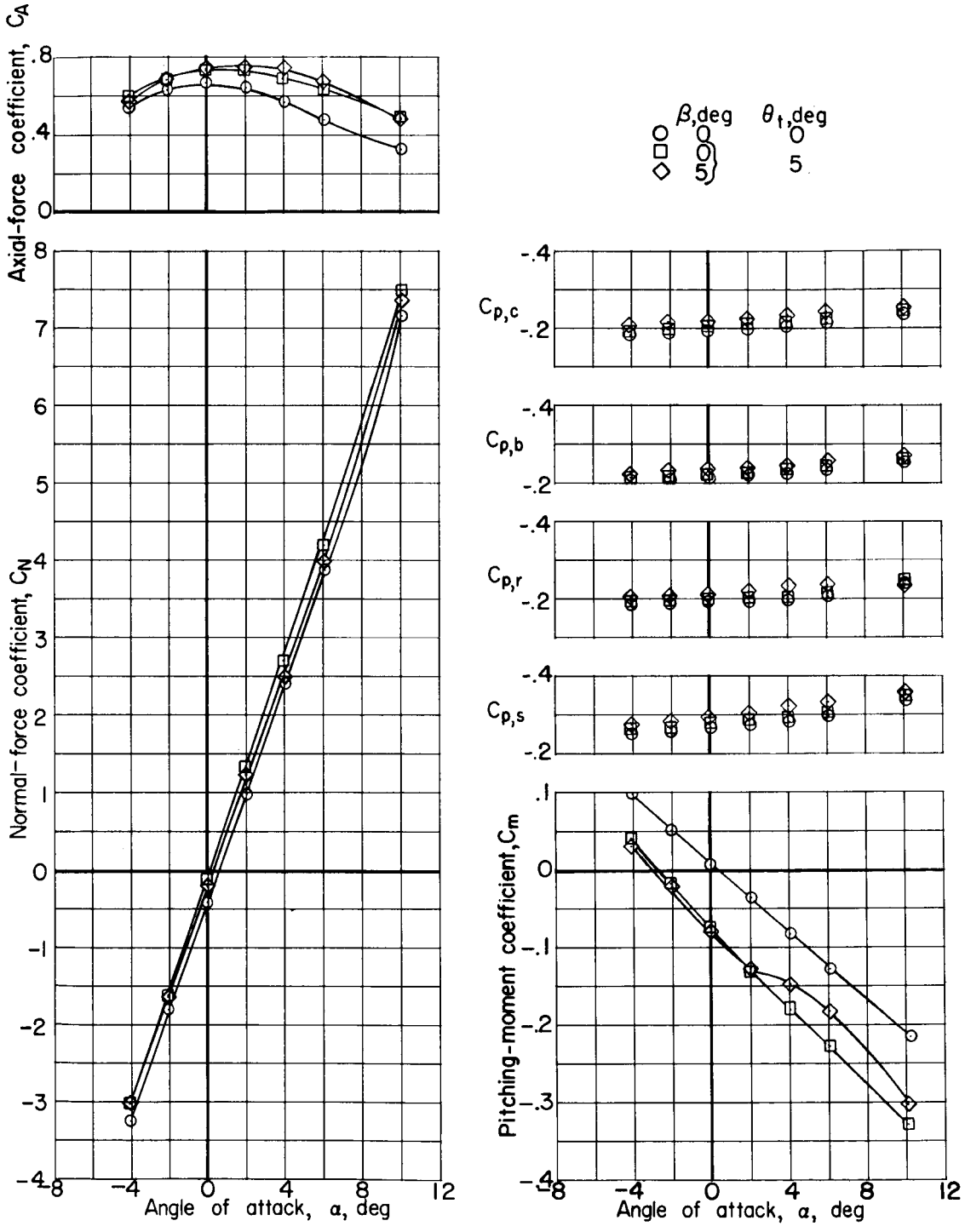

(b) M = 0.60.

Figure 5.- Continued.

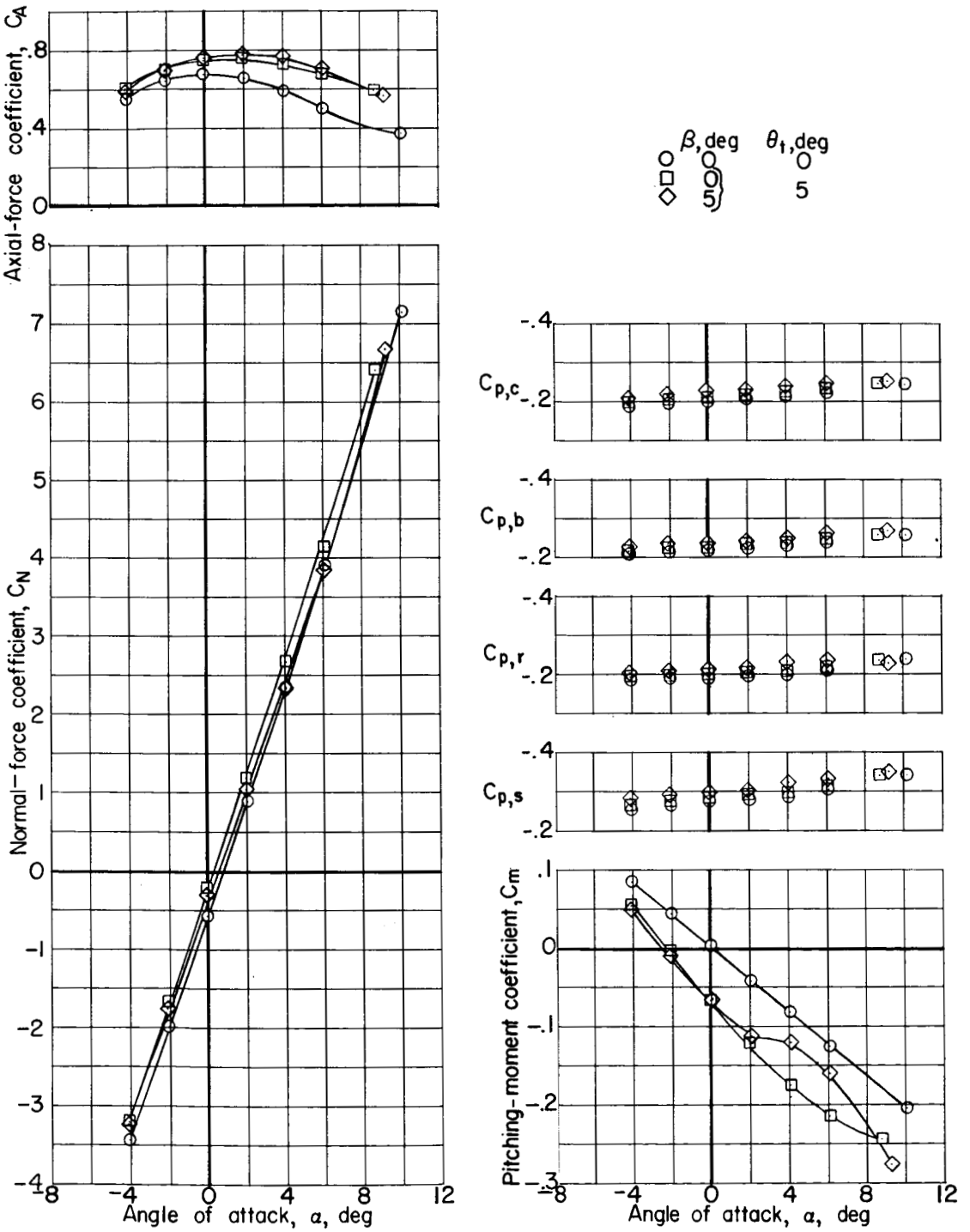

(c) M = 0.70.

Figure 5.- Continued.

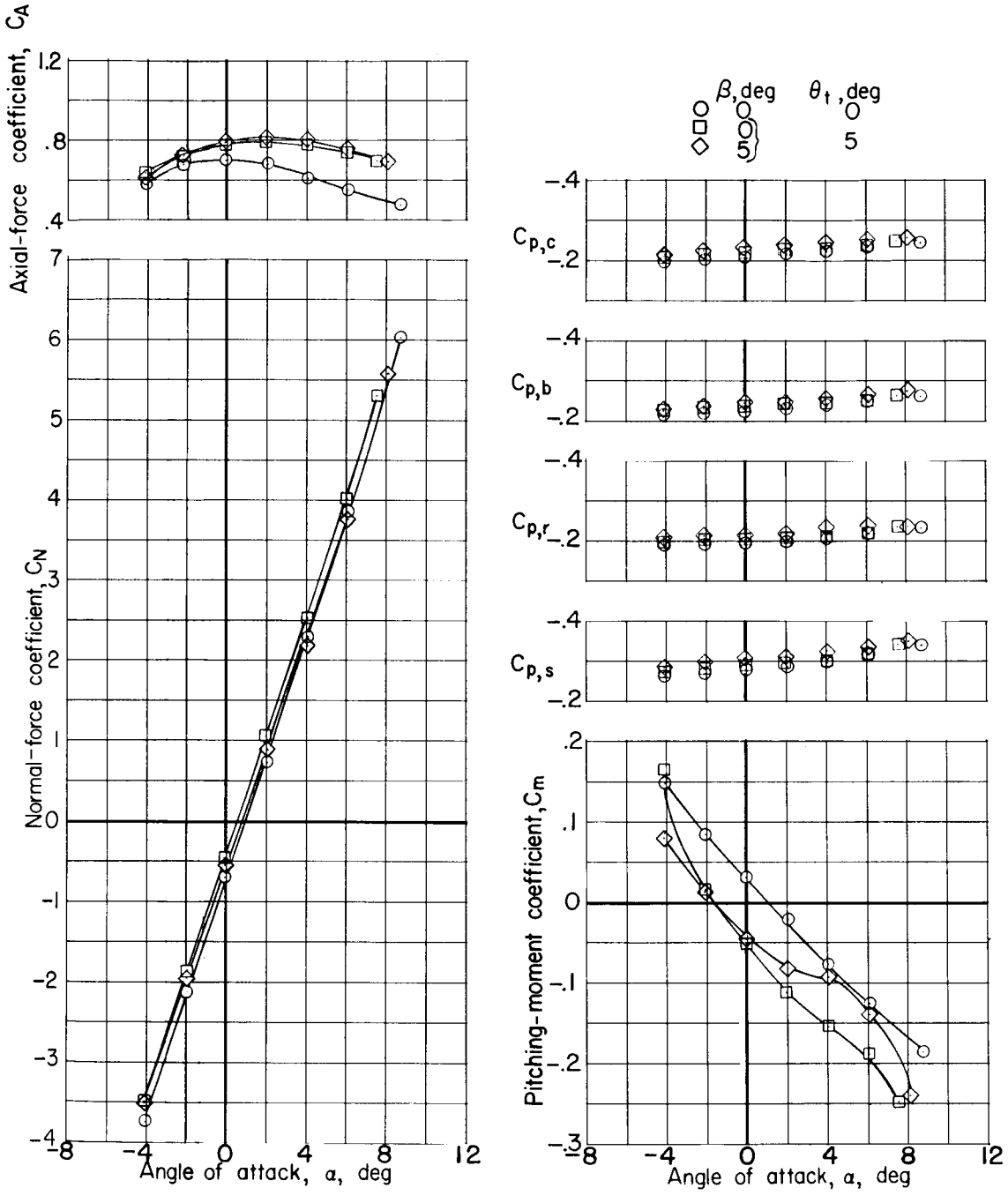

(d) M = 0.80.

Figure 5.- Continued.

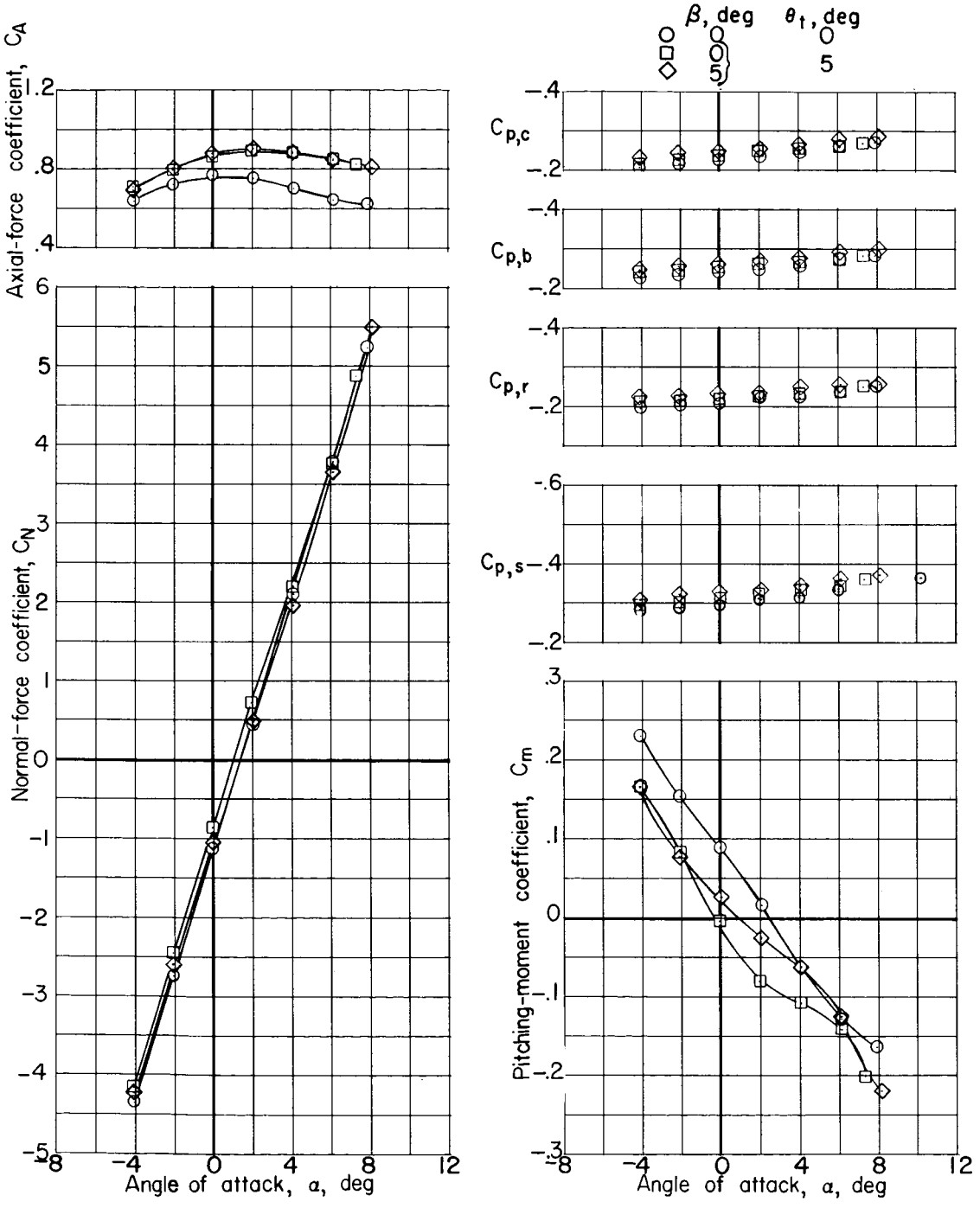

(e) M = 0.90.

Figure 5.- Continued.

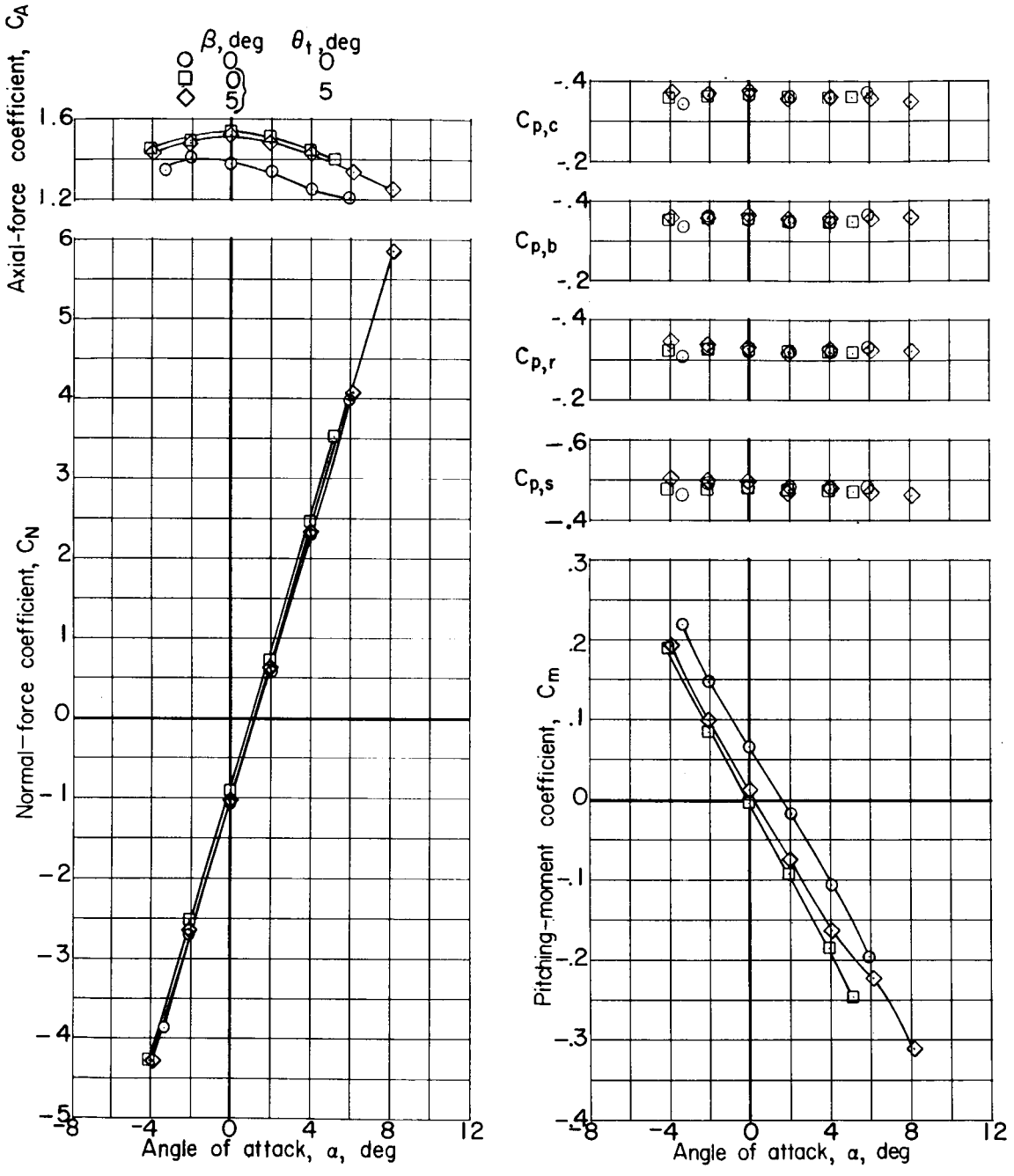

(f) M = 1.03.

Figure 5.- Continued.

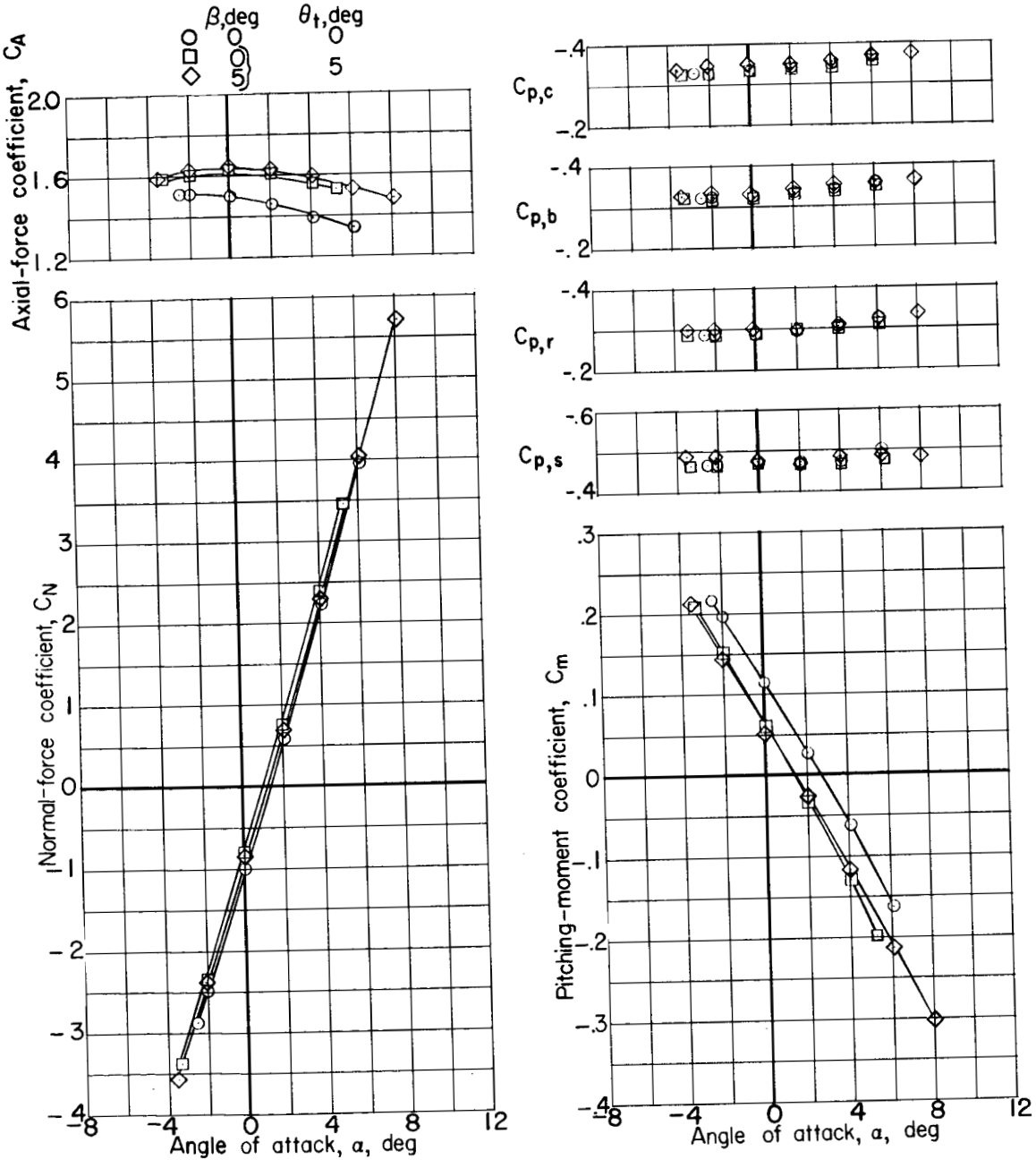

(g) M = 1.20.

Figure 5.- Concluded.

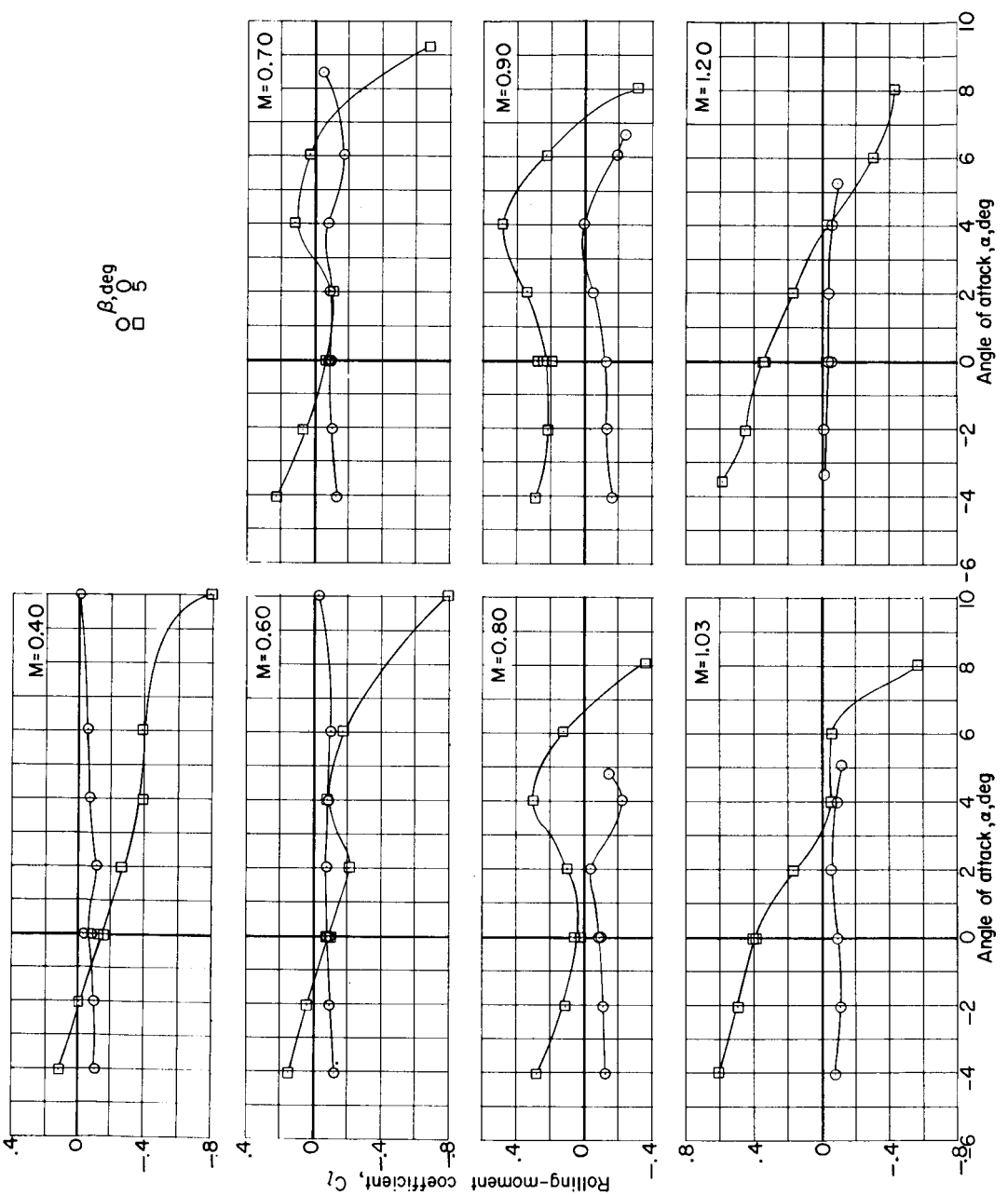

(a) C_l plotted against α.

Figure 6.- Lateral aerodynamic characteristics of the complete launch vehicle. 15° conical shrouds; retracted engine nacelle; $\gamma = 0°$; $\theta_c = 15°$; $\theta_t = 5°$.

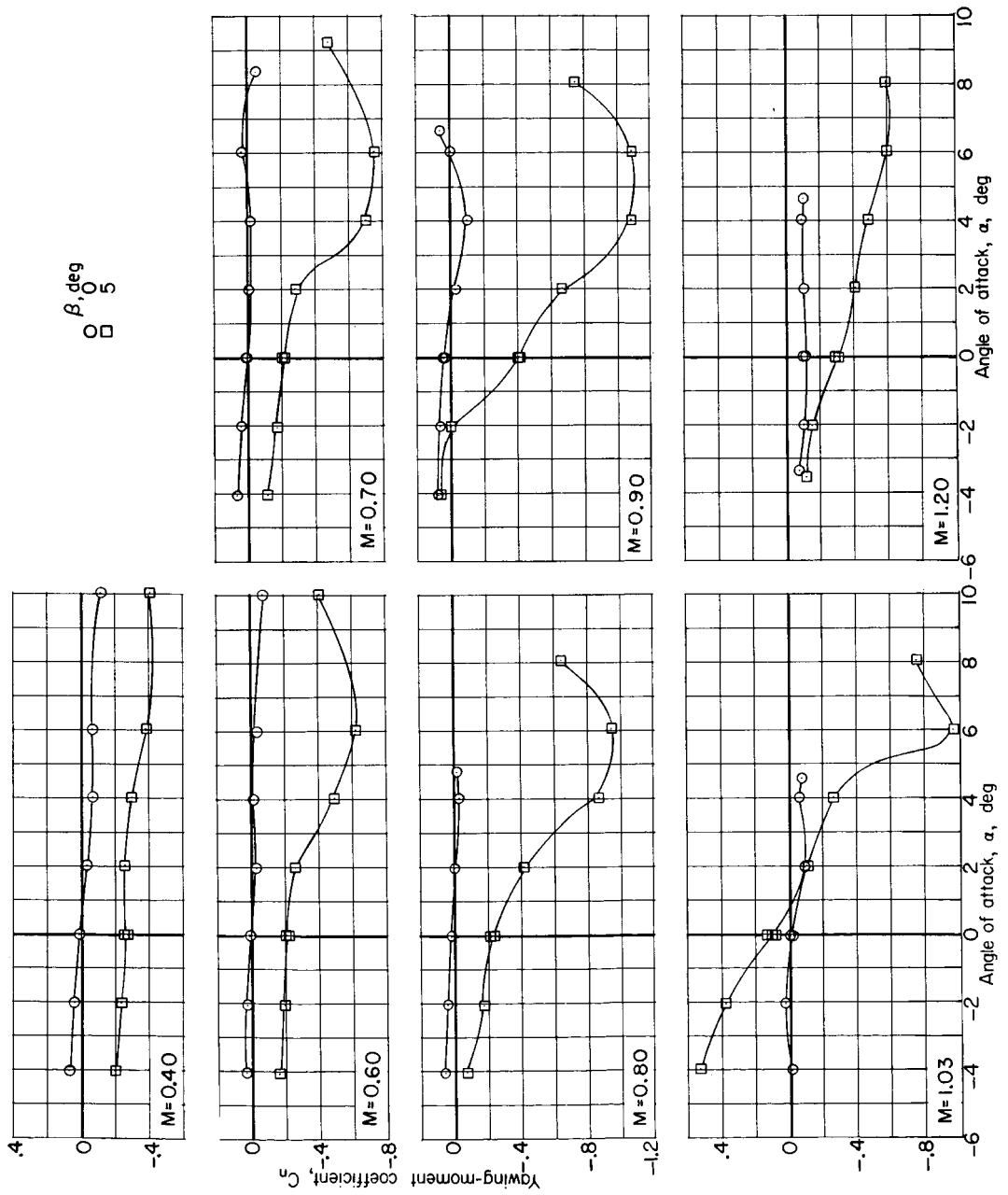

(b) C_n plotted against α.

Figure 6.- Continued.

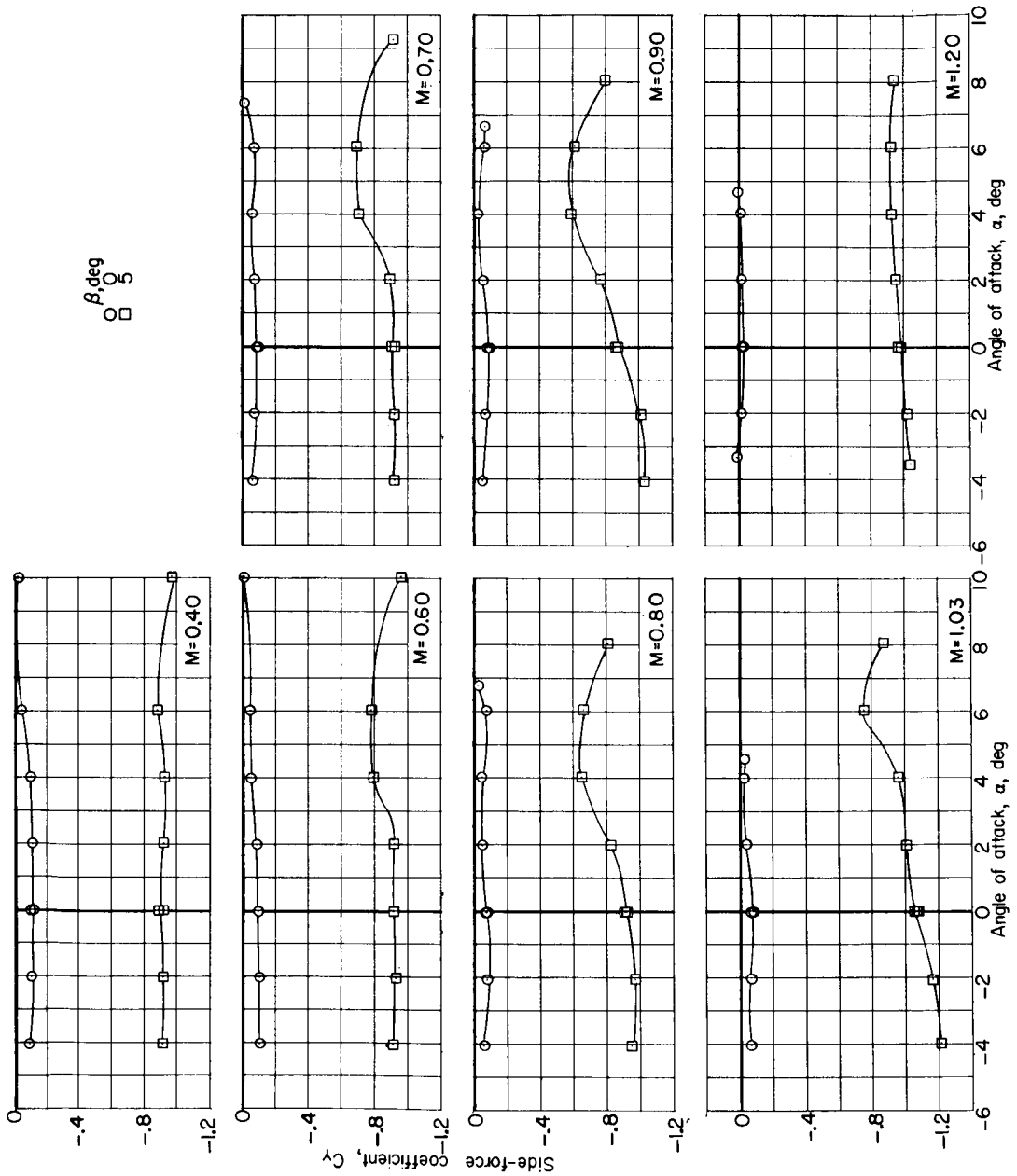

(c) Cy plotted against α.

Figure 6.- Concluded.

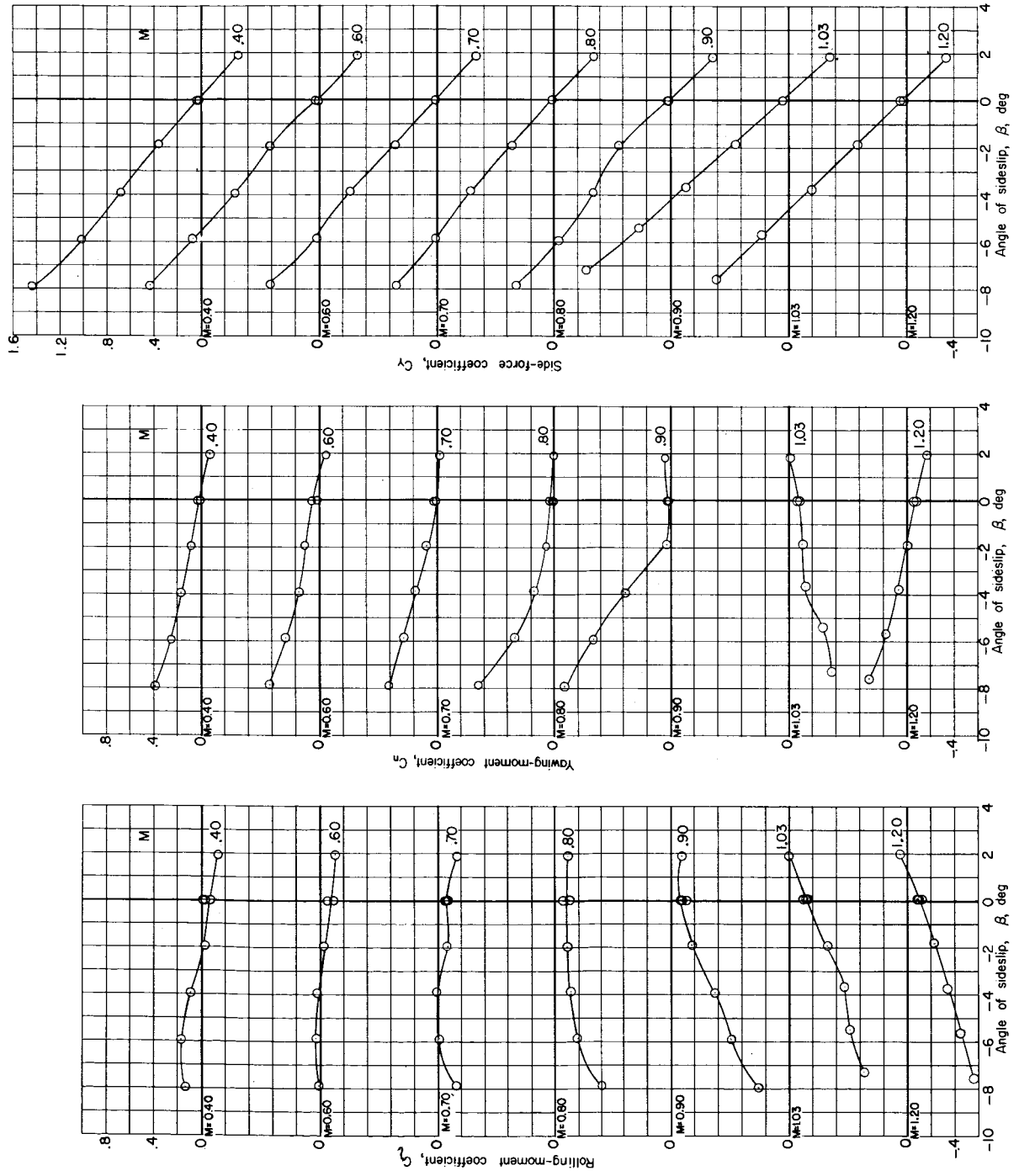

Figure 7.- Lateral aerodynamic characteristics of complete launch vehicle. 15^0 conical shrouds; retracted engine nacelle; $\gamma = 0^0$; $\theta_c = 15^0$; $\theta_t = 5^0$; $\alpha = 0^0$.

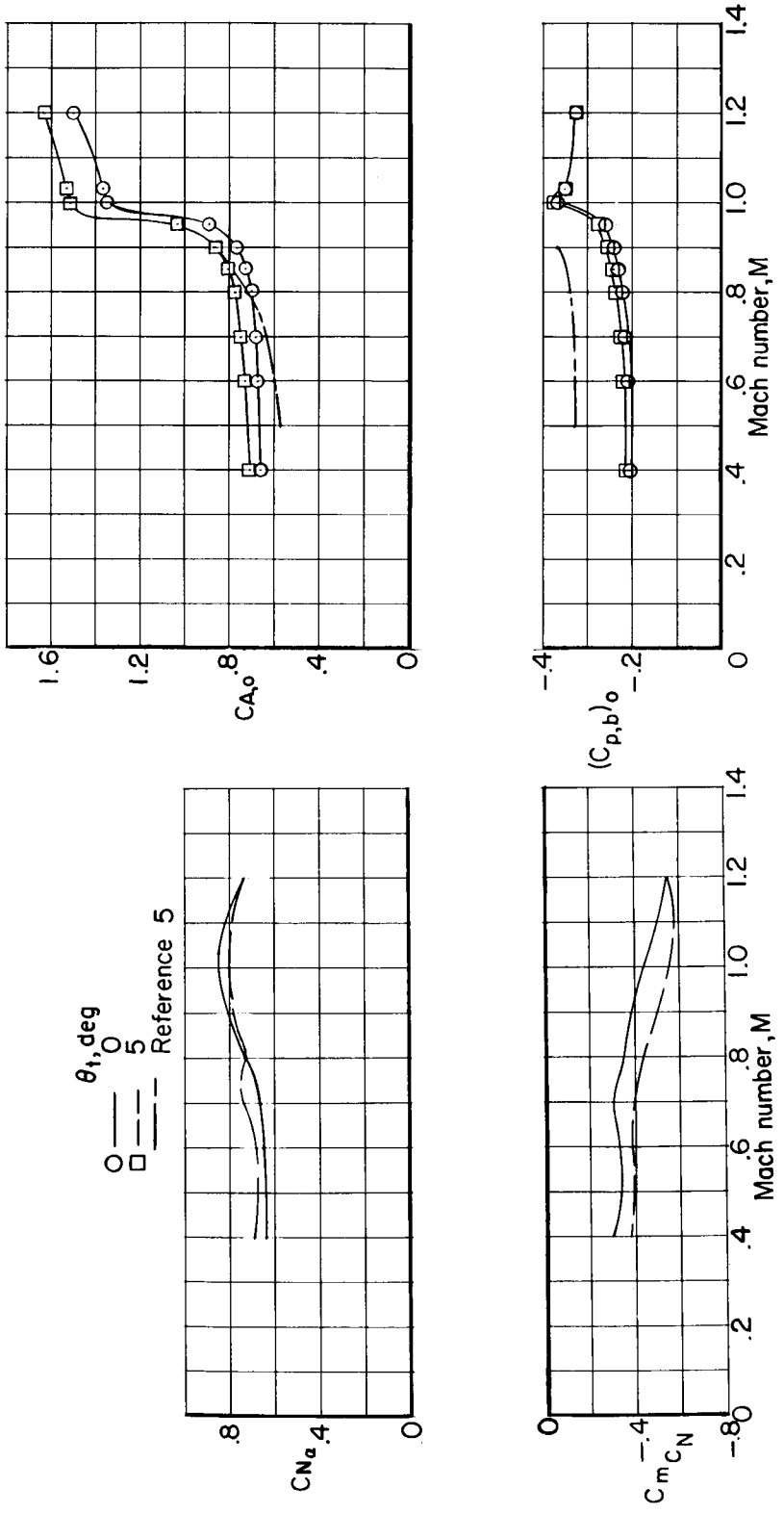

Figure 8.- Variation with Mach number of longitudinal-stability and drag parameters for complete launch vehicle. 15^0 conical shrouds; retracted engine nacelle; $\gamma = 0^0$; $\theta_c = 15^0$; $\beta = 0^0$.

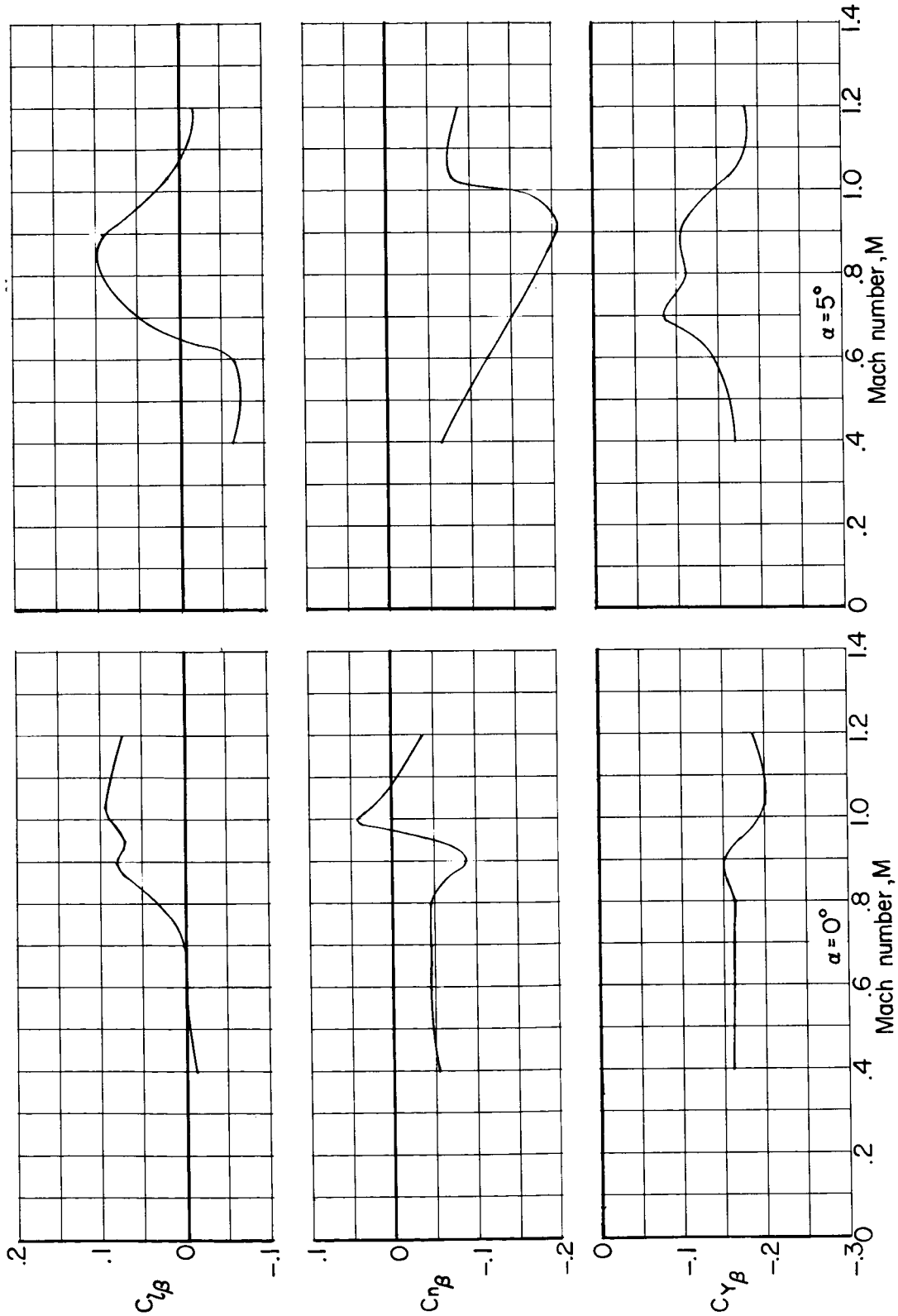

Figure 9.- Variation with Mach number of lateral-directional-stability parameters for complete launch vehicle. 15^0 conical shrouds; retracted engine nacelle; $\gamma = 0^0$; $\theta_c = 15^0$; $\theta_t = 5^0$.

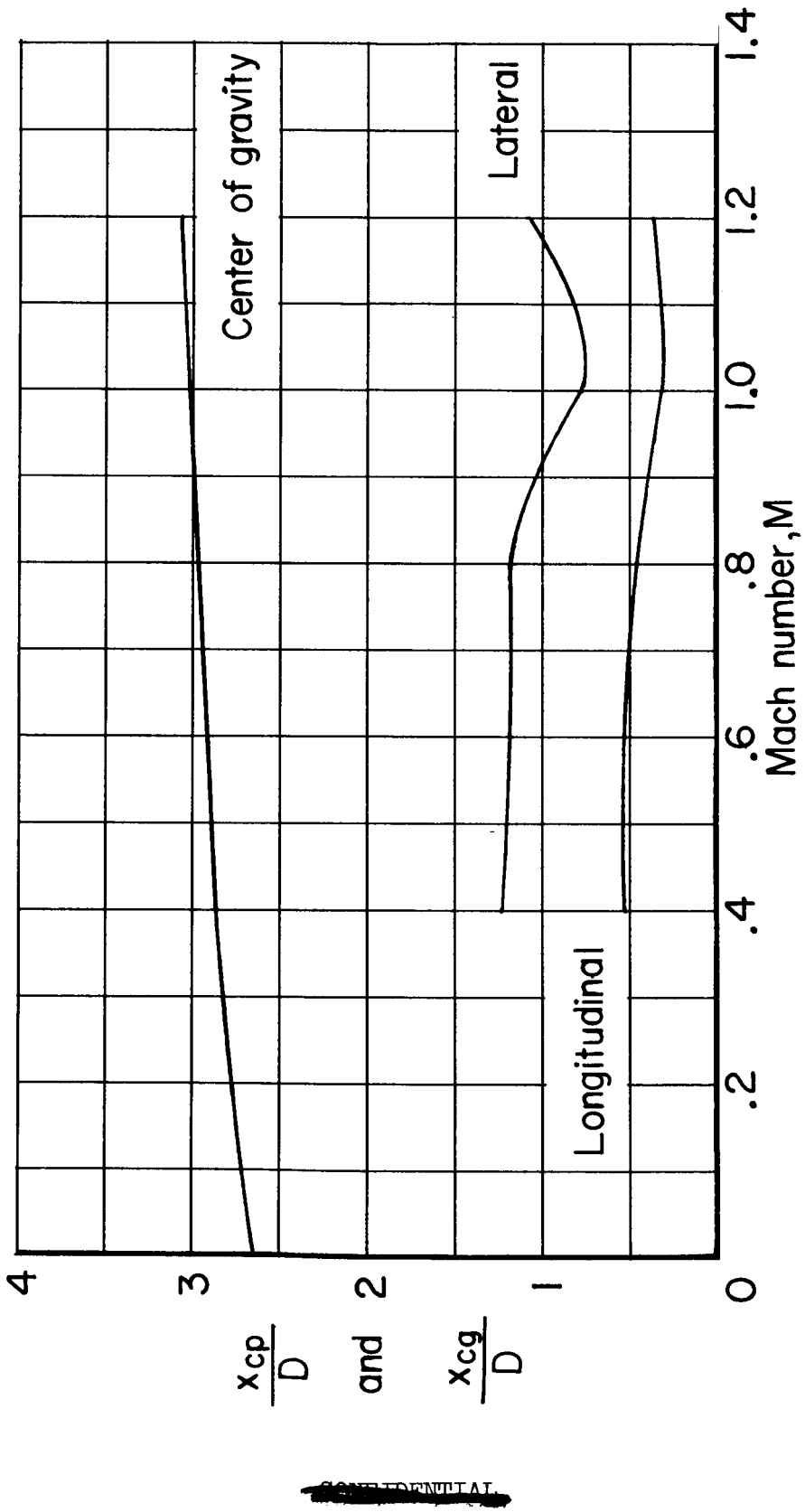

Figure 10.- Comparison of longitudinal and lateral center of pressure for complete launch vehicle with estimated flight center of gravity. $\alpha = 0^{\circ}$.

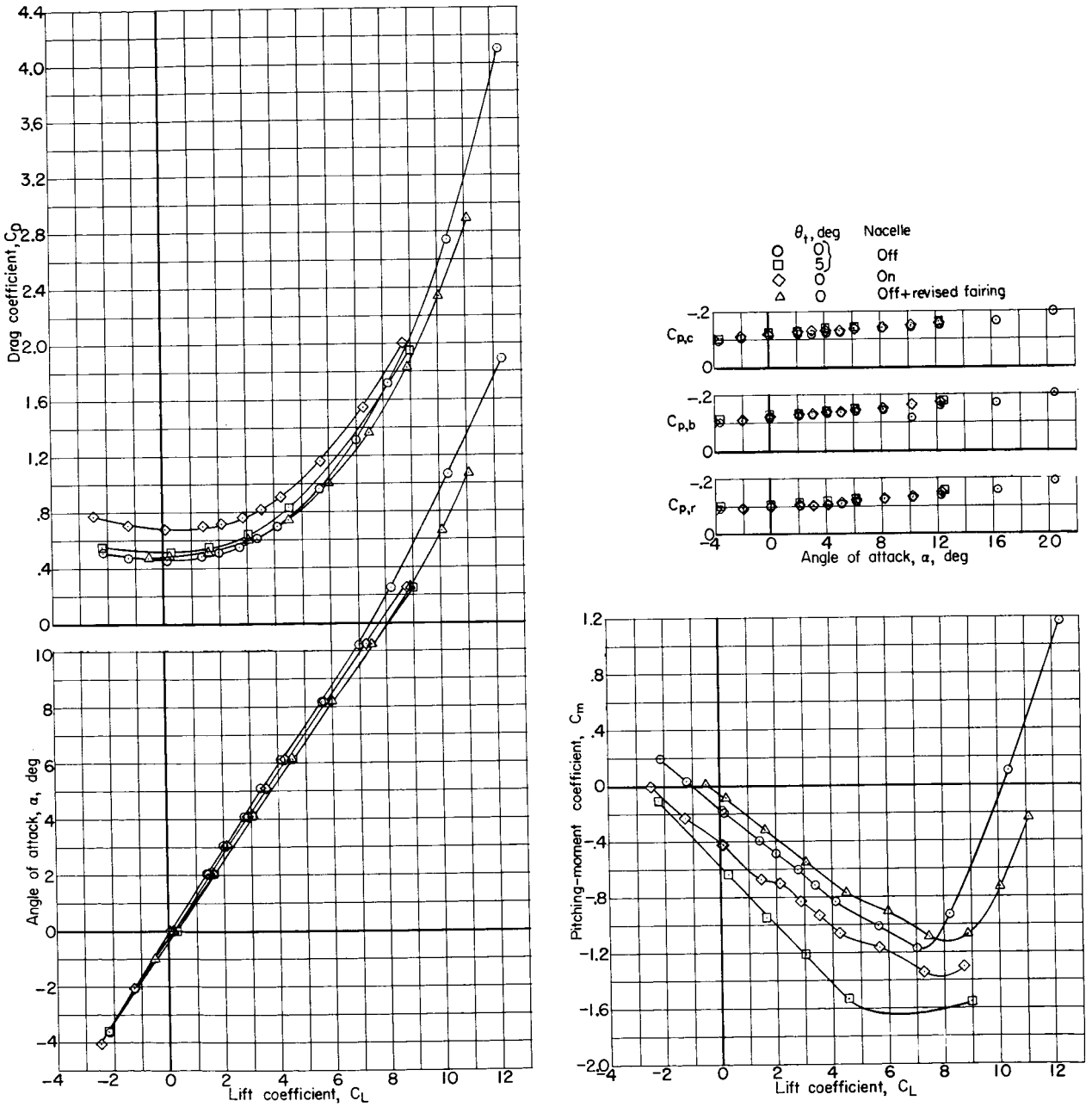

(a) M = 0.40.

Figure 11.- Longitudinal aerodynamic characteristics of first-stage flyback vehicle. Exposed rocket engine actuator struts; no shrouds; $\gamma = 12^0$; $\theta_c = 15^0$; $\beta = 0^0$.

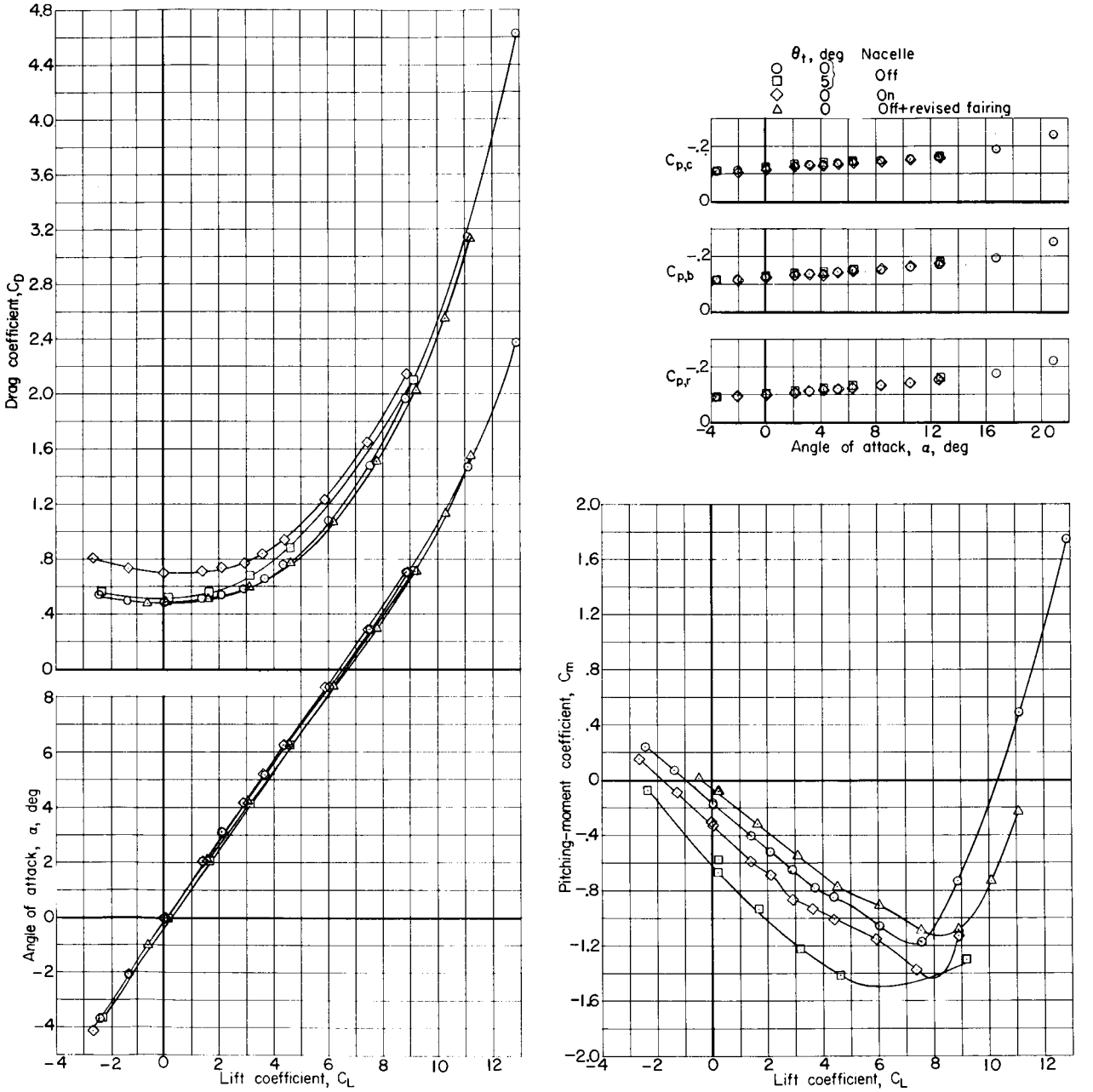

(b) M = 0.60.

Figure 11.- Continued.

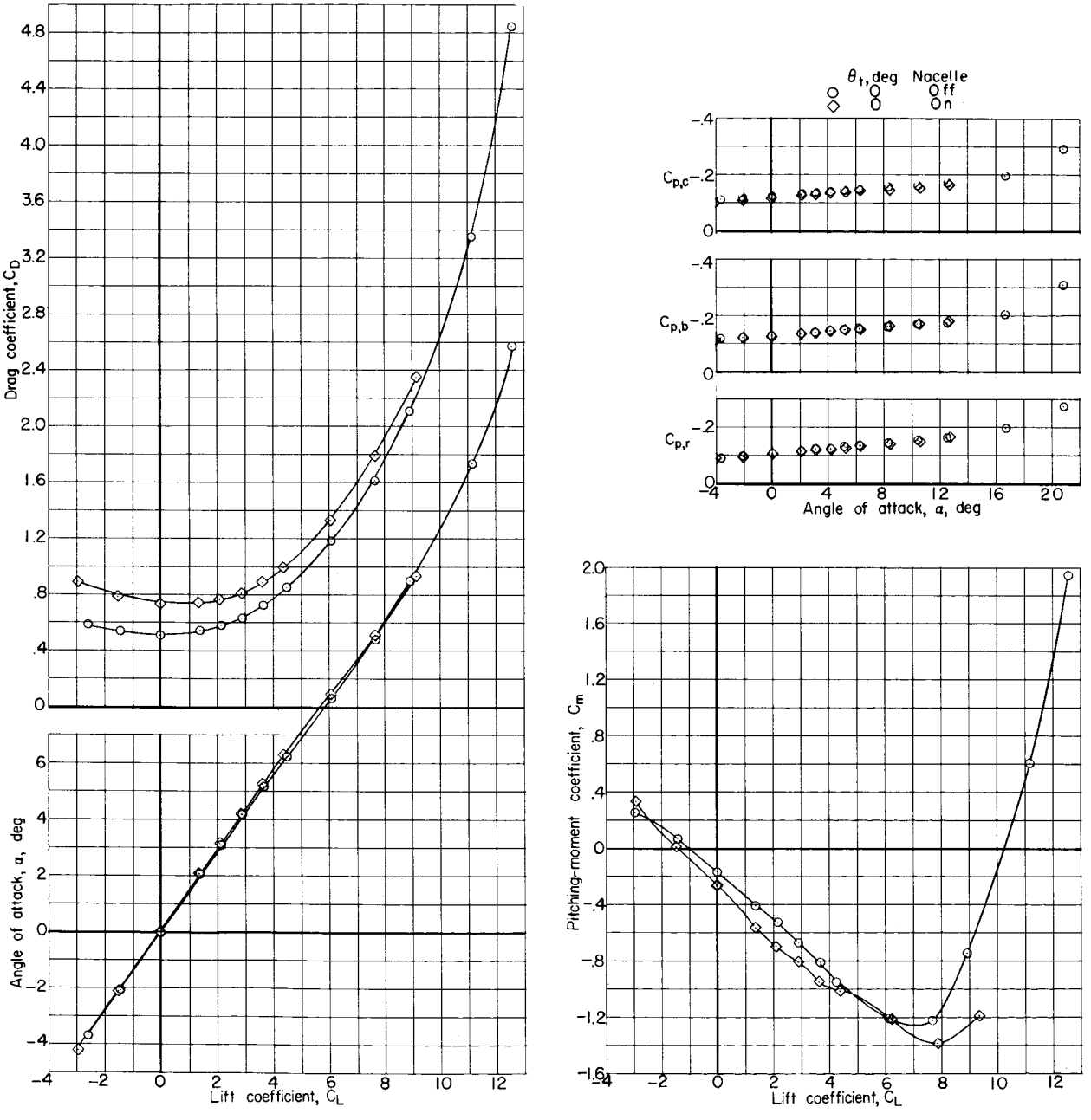

(c) M = 0.70.

Figure 11.- Continued.

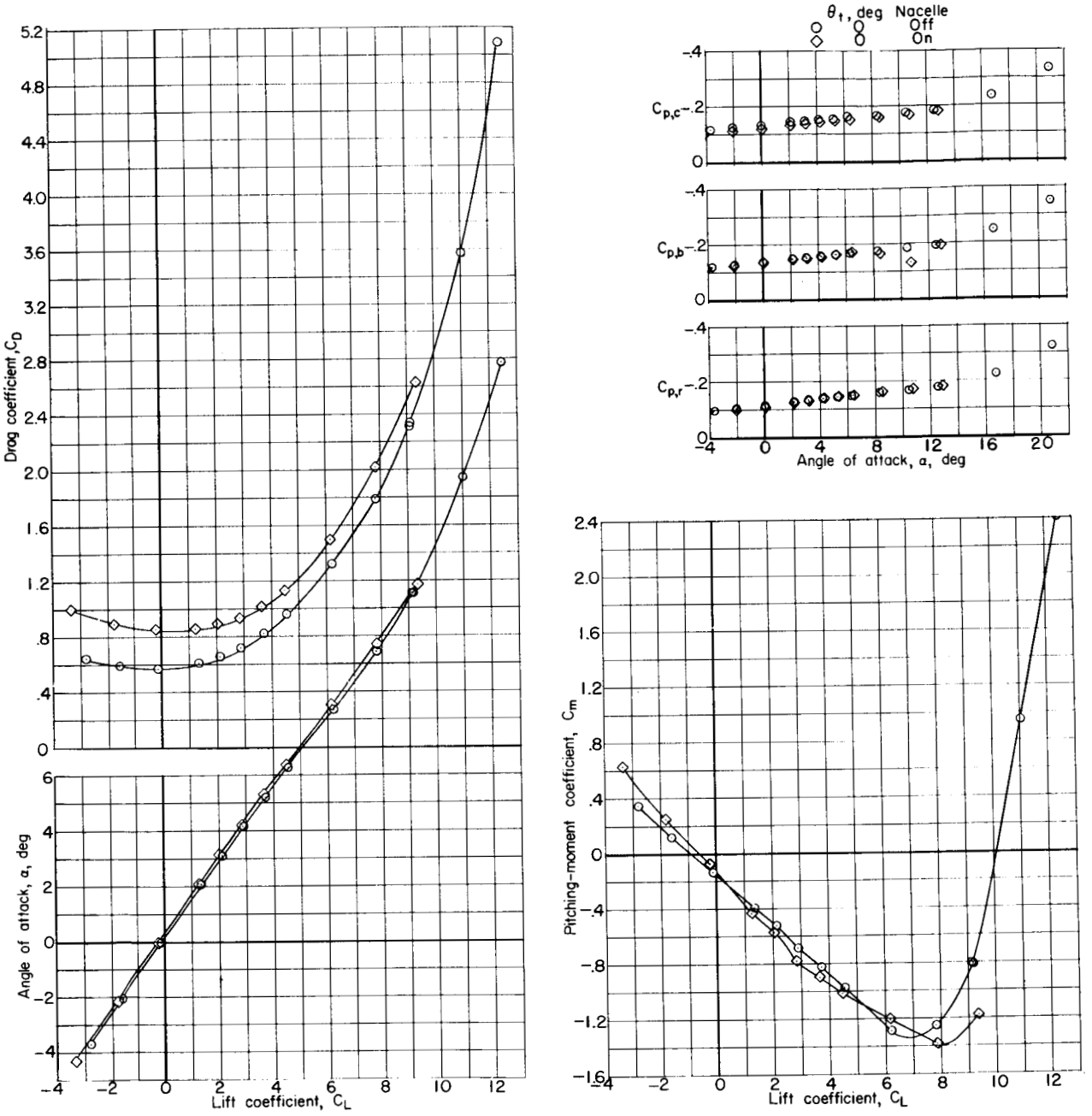

(d) M = 0.80.

Figure 11.- Continued.

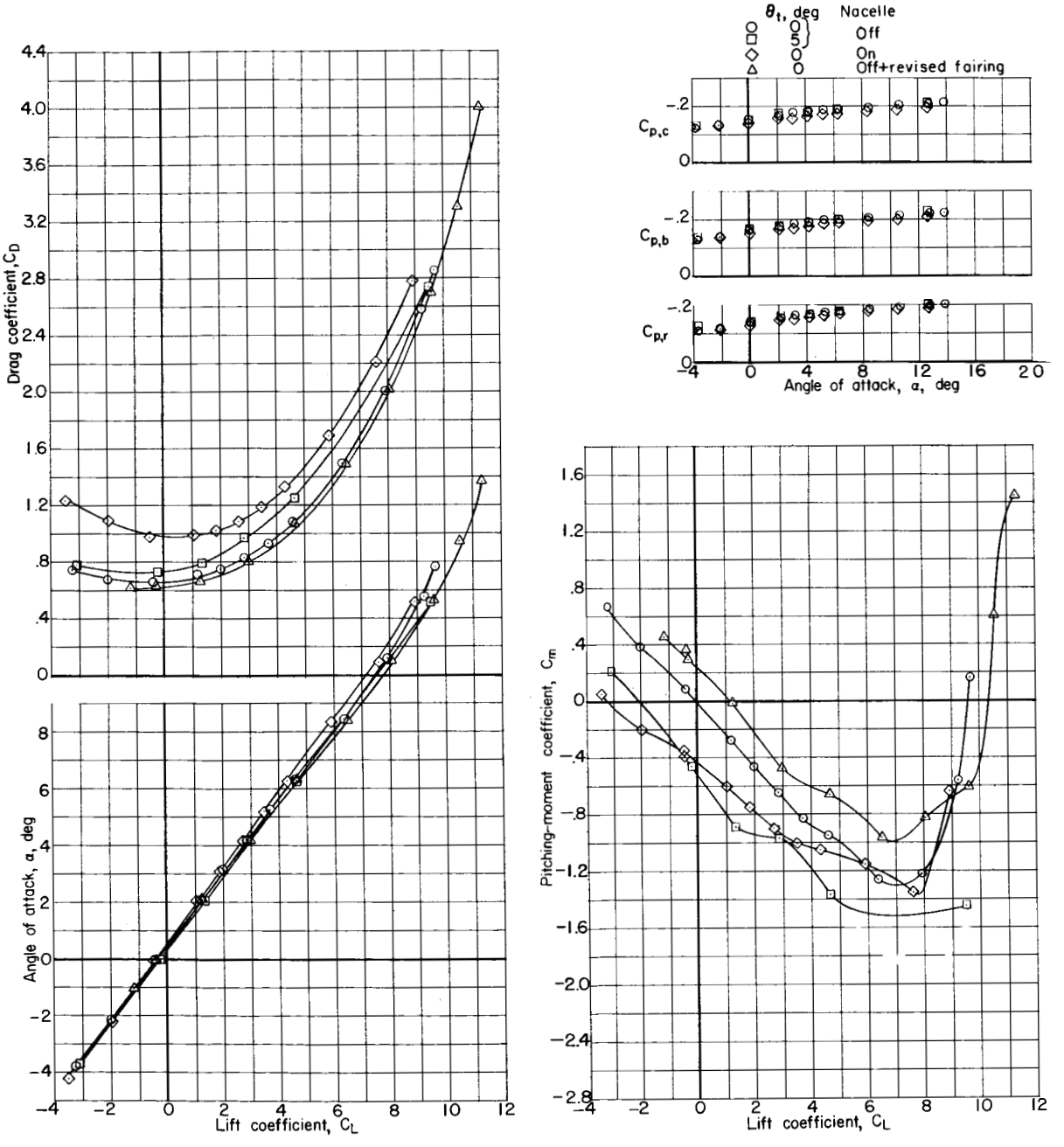

(e) M = 0.90.

Figure 11.- Continued.

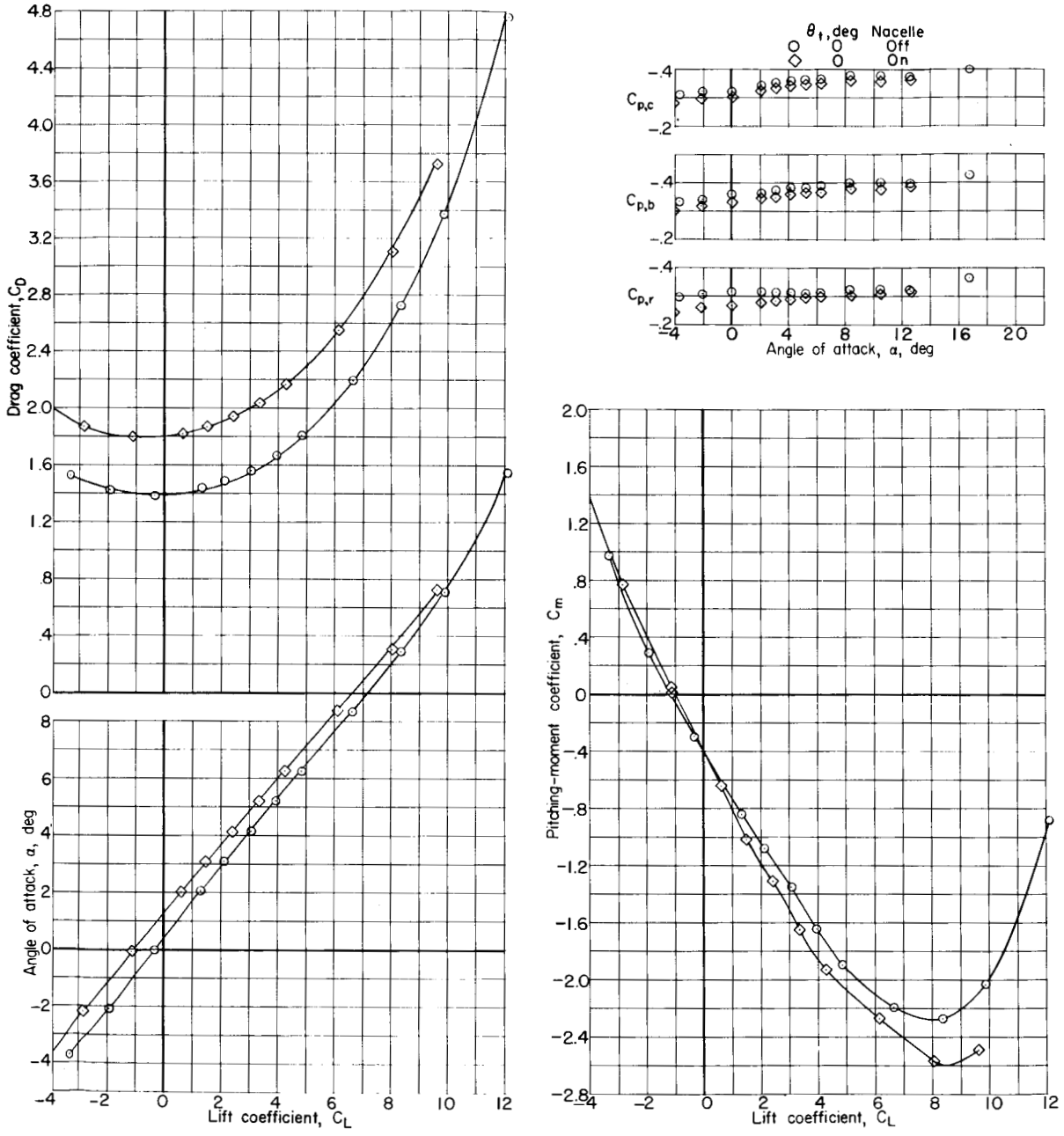

(f) M = 1.03.

Figure 11.- Continued.

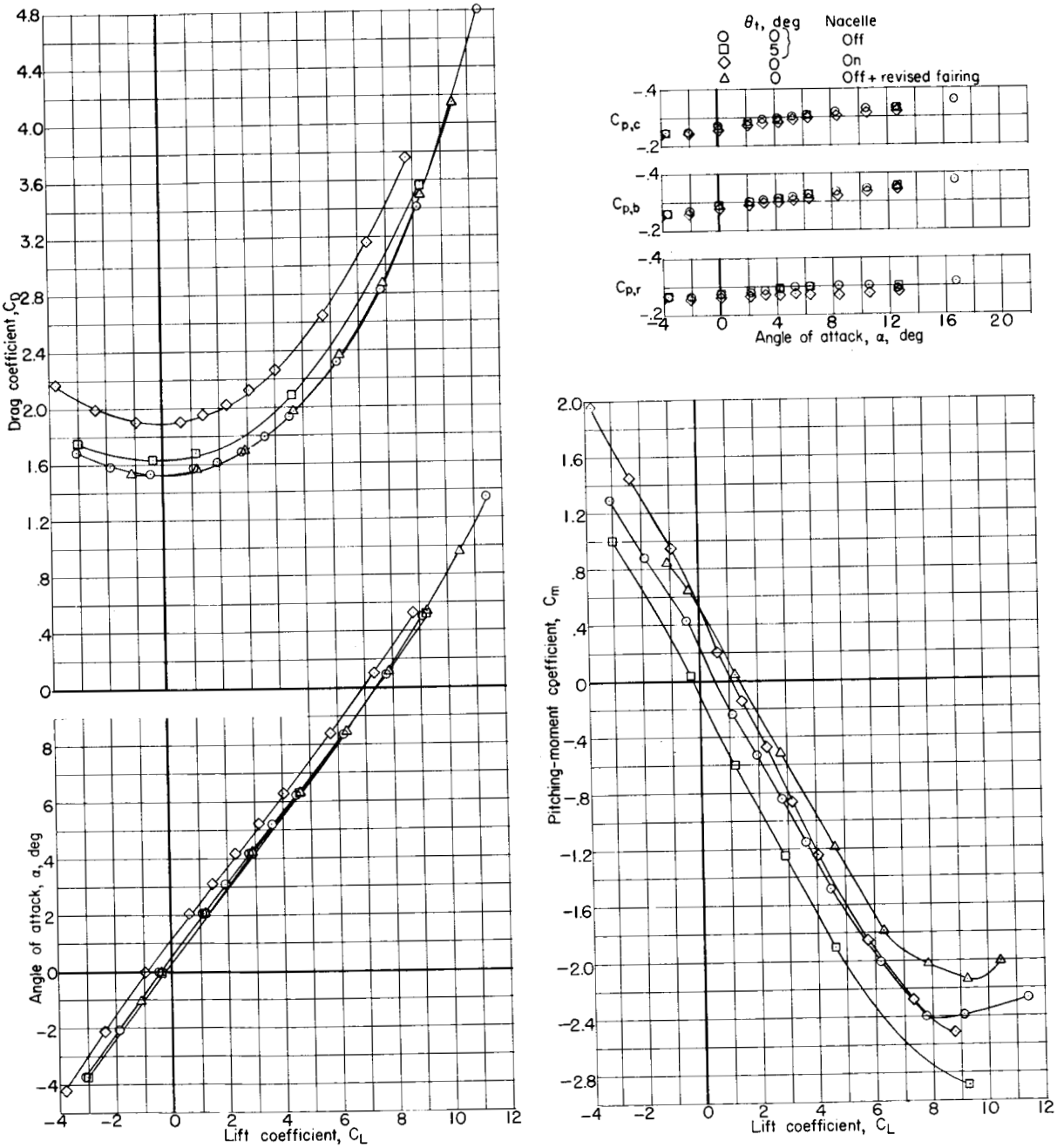

(g) M = 1.20.

Figure 11.- Concluded.

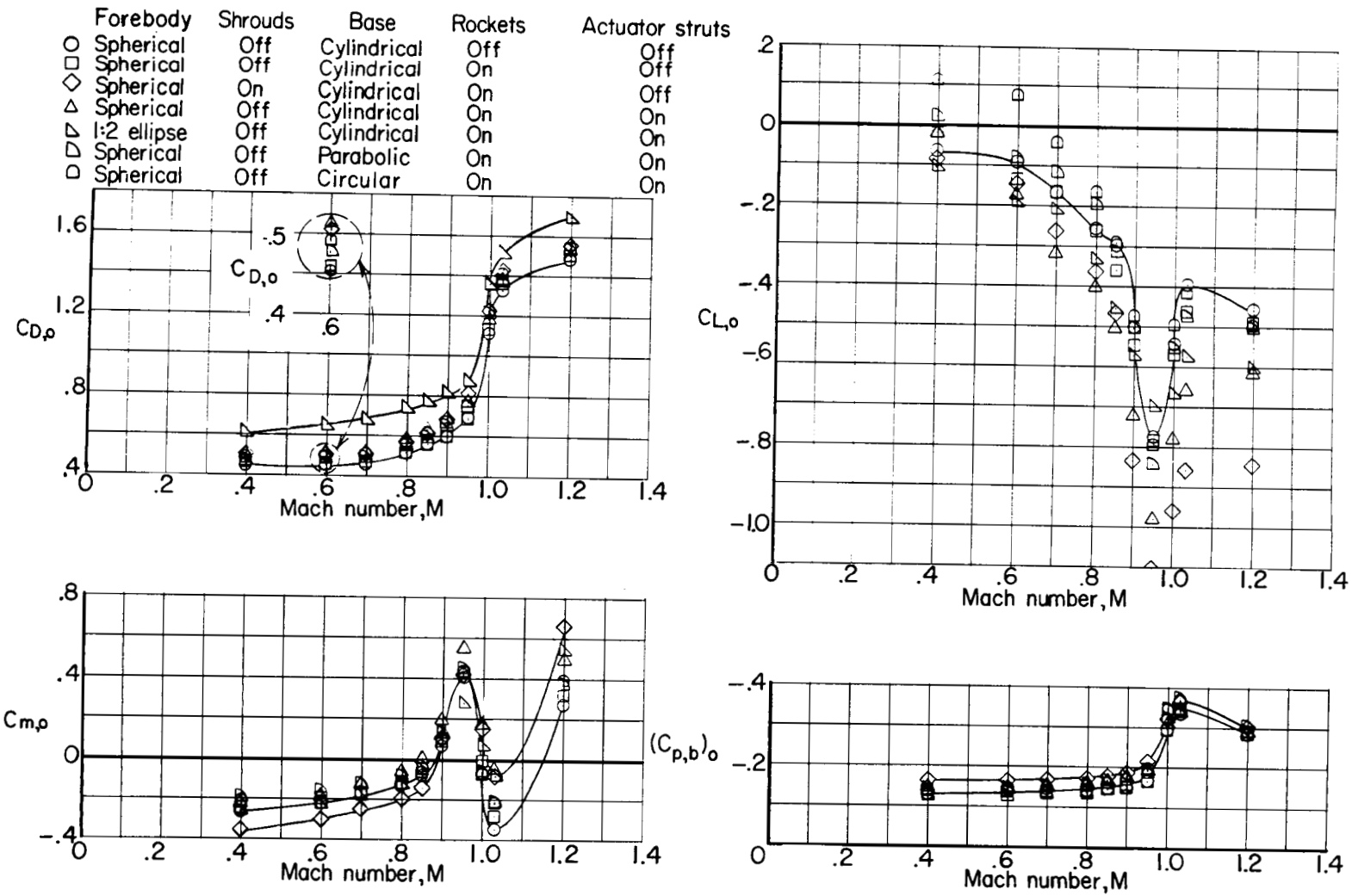

Figure 12.- Effect of various forebody and afterbody configurations on aerodynamic characteristics of first-stage flyback vehicle. Engine nacelle off; $\gamma = 12^0$; $\theta_c = 15^0$; $\theta_t = 0^0$; $\beta = 0^0$; $\alpha = 0^0$.

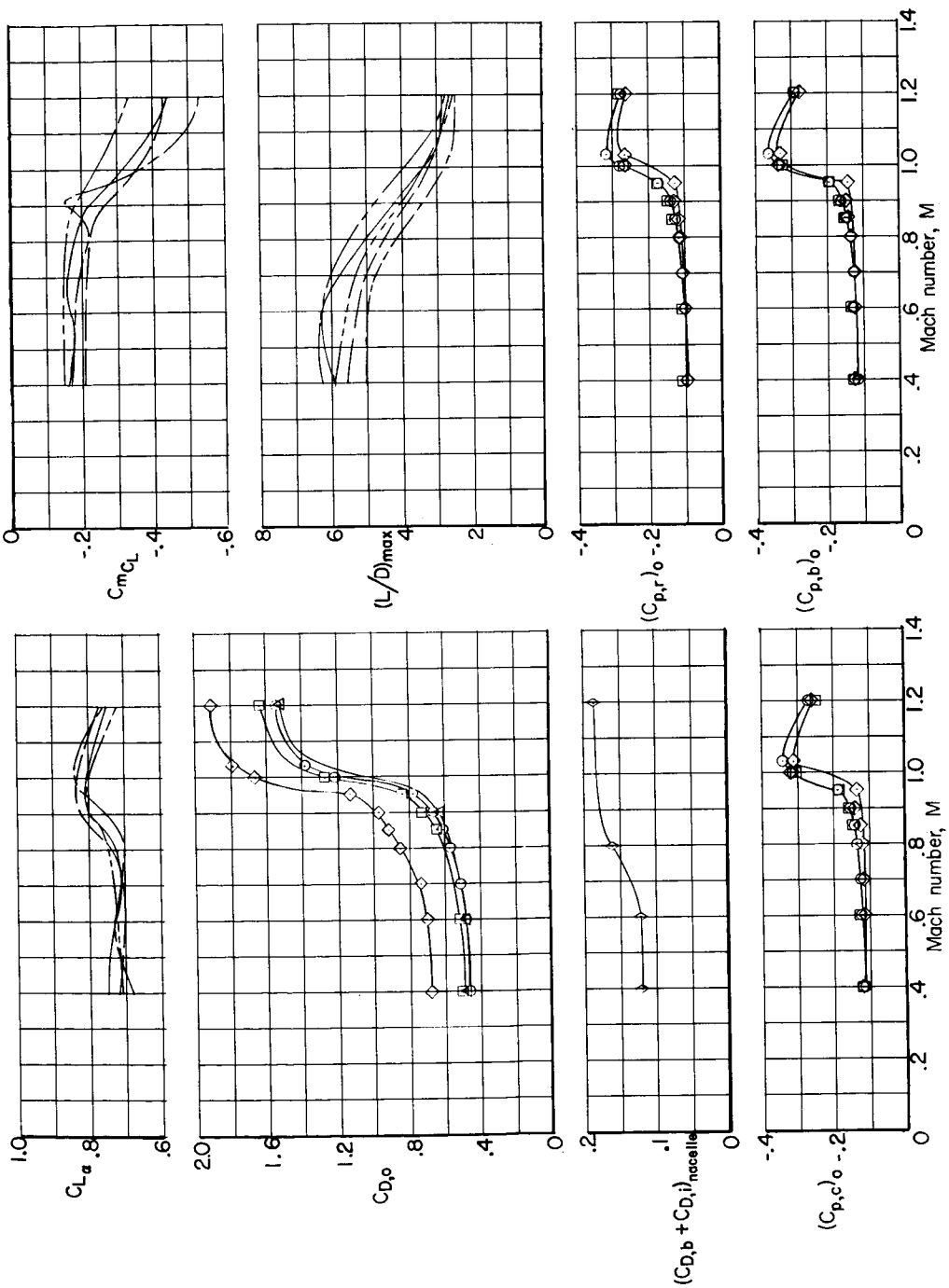

Figure 13.- Variation with Mach number of longitudinal-stability and drag parameters for first-stage flyback vehicle. Exposed rocket engine actuator struts; no shrouds; $\gamma = 12^0$; $\theta_c = 15^0$; $\beta = 0^0$.

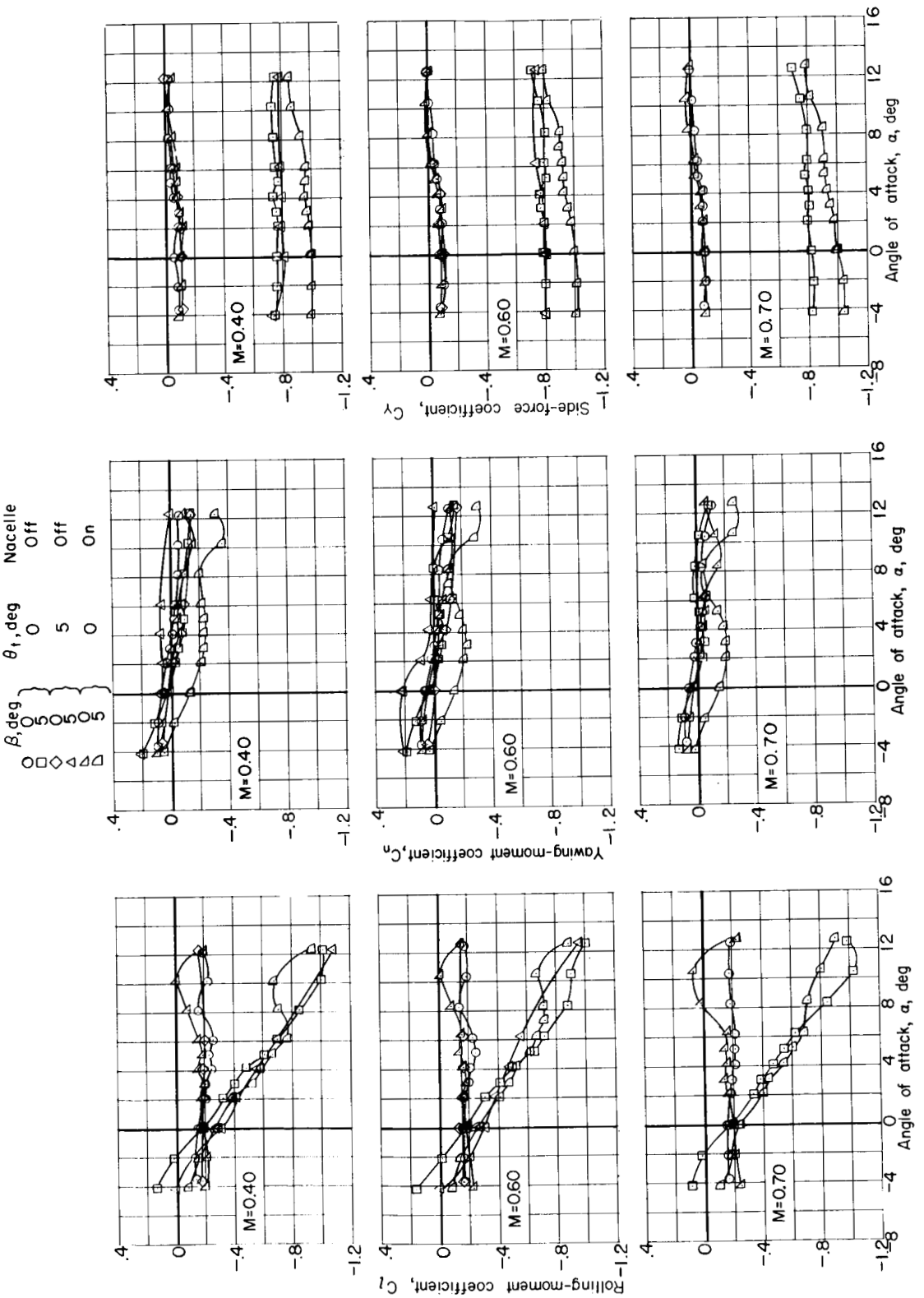

Figure 14.- Lateral aerodynamic characteristics of first-stage flyback vehicle. Exposed rocket engine actuator struts; no shrouds; $\gamma = 12^{0}$; $\theta_c = 15^{0}$.

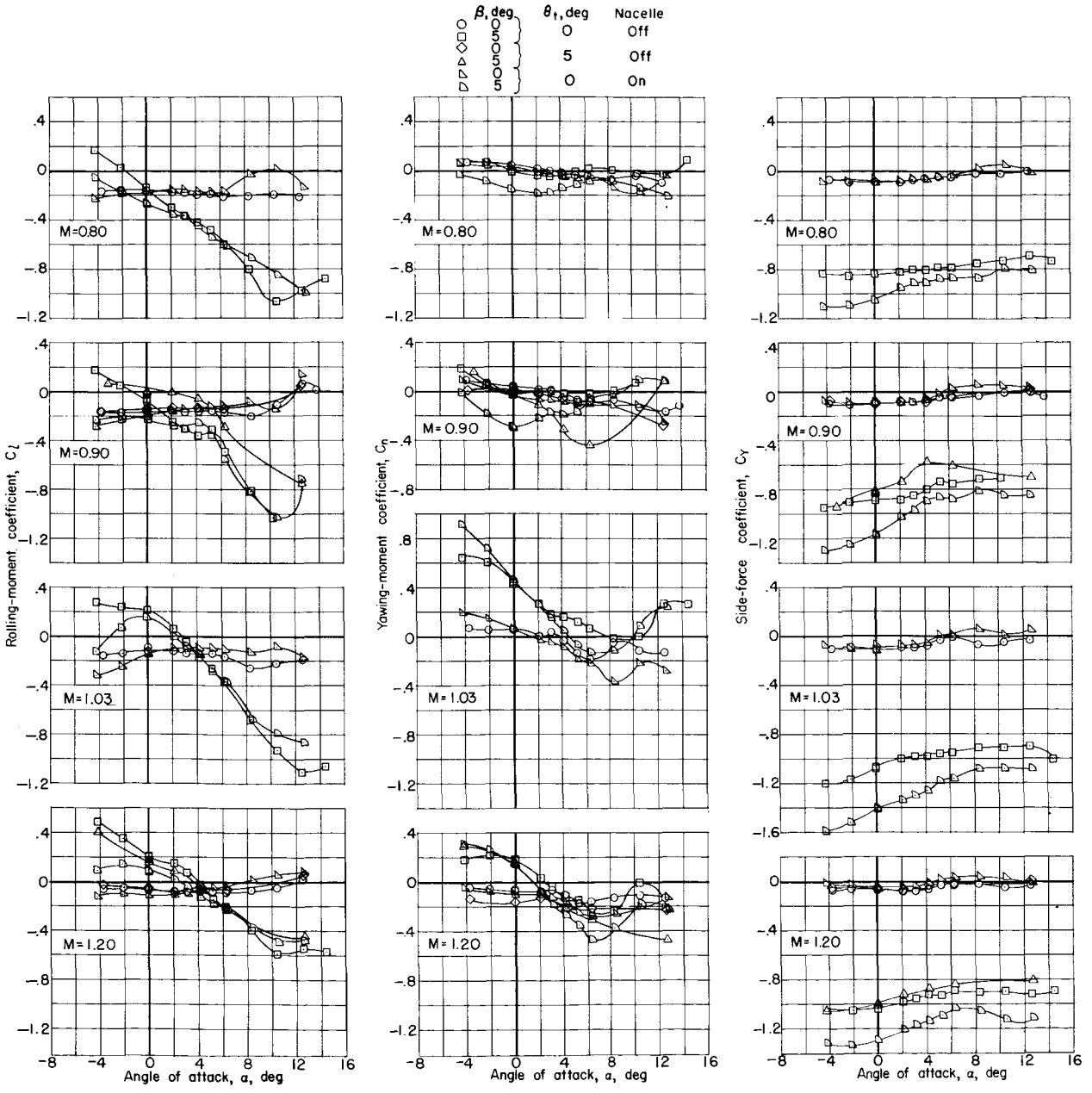

Figure 14.- Concluded.

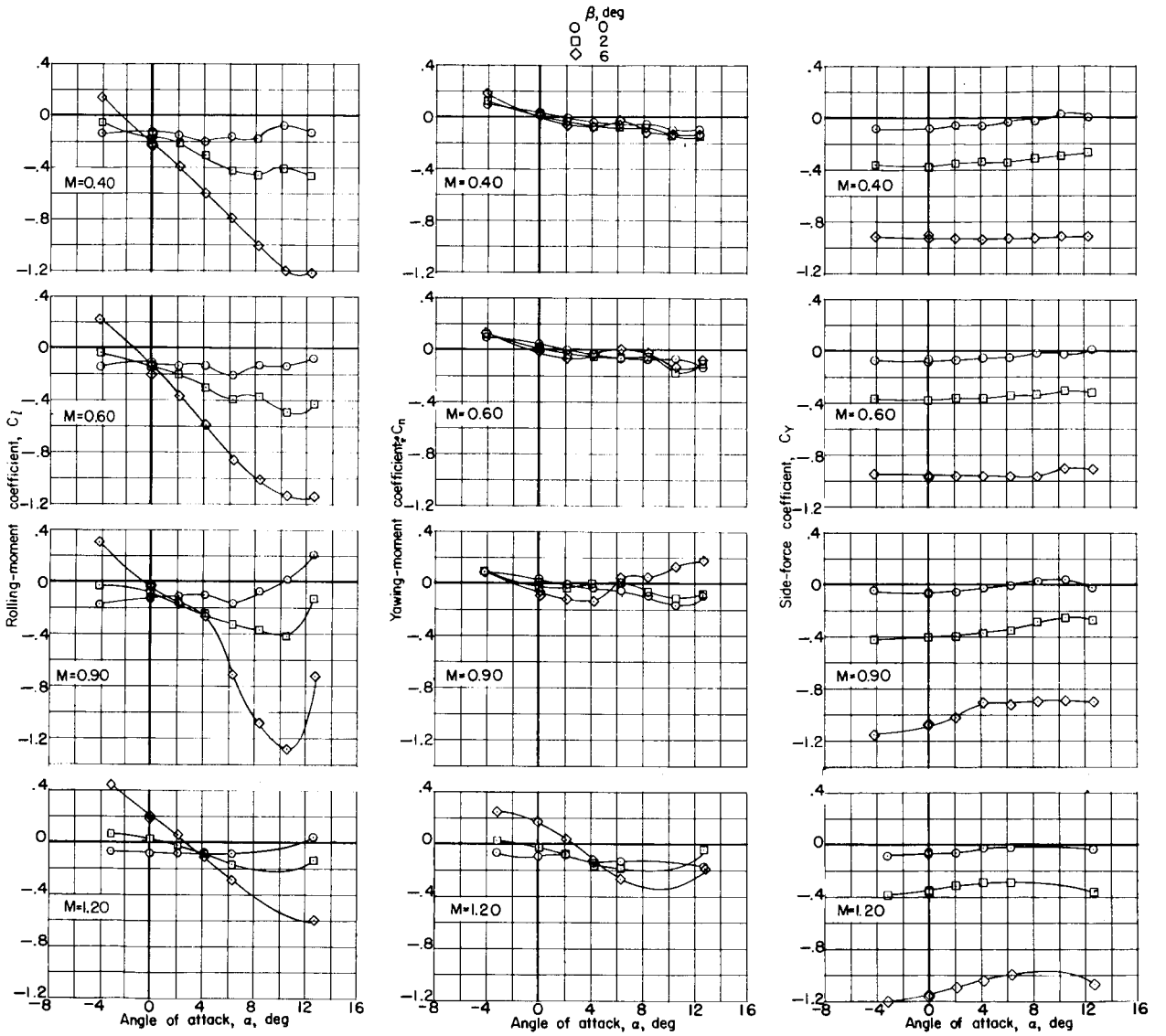

Figure 15.- Lateral aerodynamic characteristics of first-stage reusable flyback vehicle at several angles of sideslip. Exposed rocket engine actuator struts; no shrouds; engine nacelle off; $\gamma = 12^0$; $\theta_c = 15^0$; $\theta_t = 0^0$.

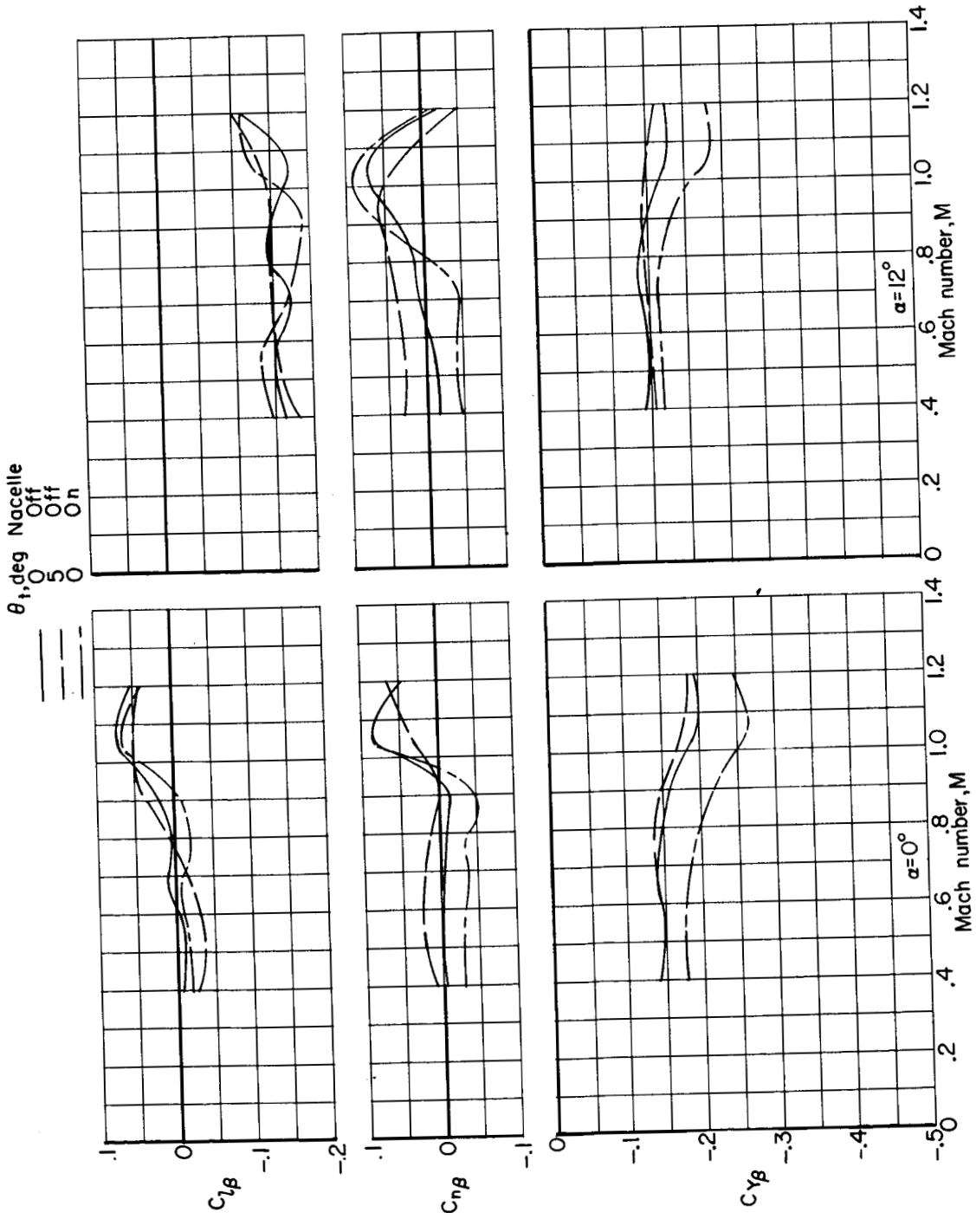

Figure 16.- Variation with Mach number of lateral-directional-stability parameters for first-stage reusable flyback vehicle. Exposed rocket engine actuator struts; no shrouds; $\gamma = 12^0$; $\theta_c = 15^0$.

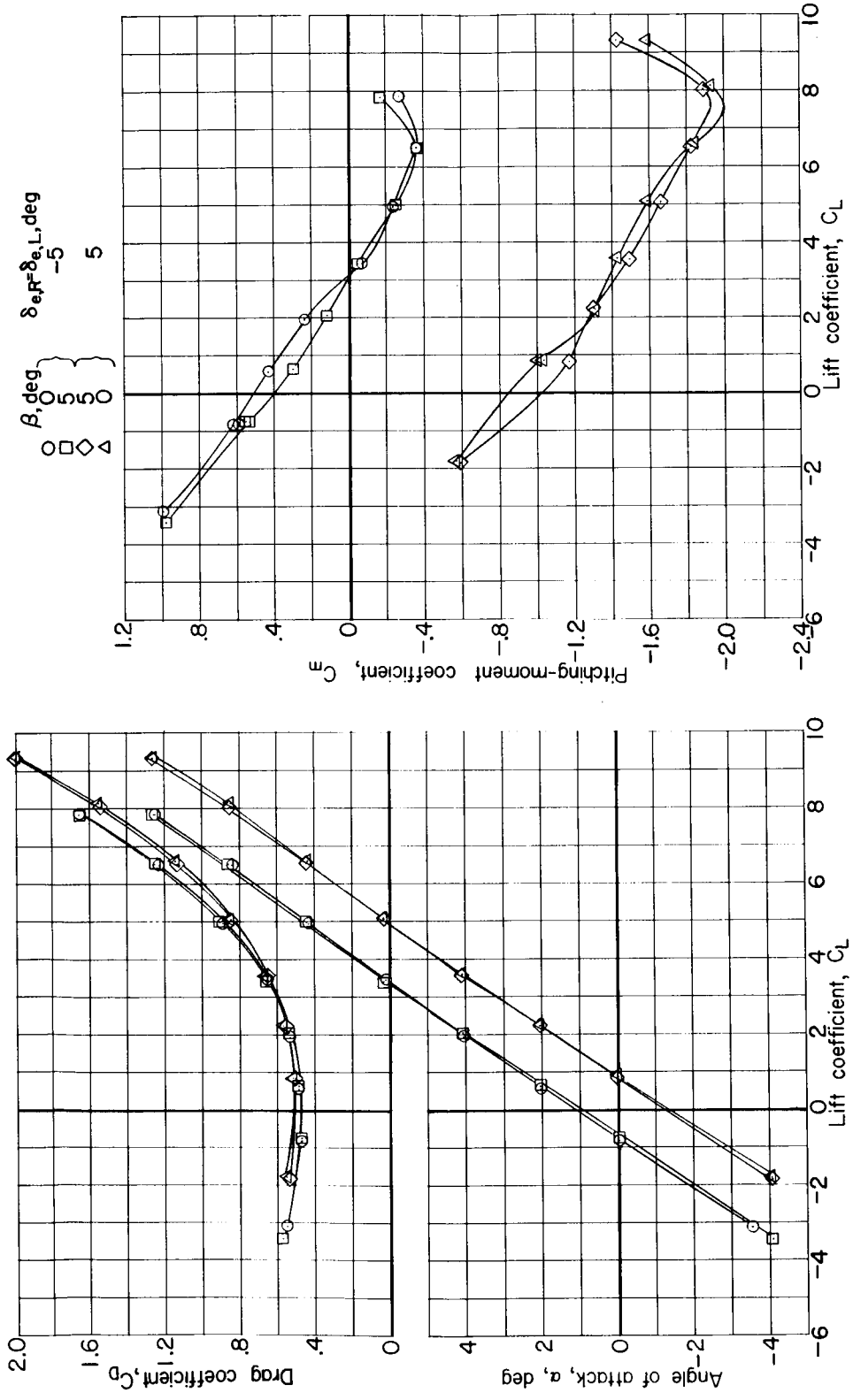

(a) Longitudinal characteristics. M = 0.40.

Figure 17.- Aerodynamic characteristics with deflected longitudinal control surfaces of first-stage reusable flyback vehicle. Exposed rocket engine actuator struts; no shrouds; engine nacelle off; $\gamma = 12^0$; $\theta_c = 15^0$; $\theta_t = 0^0$.

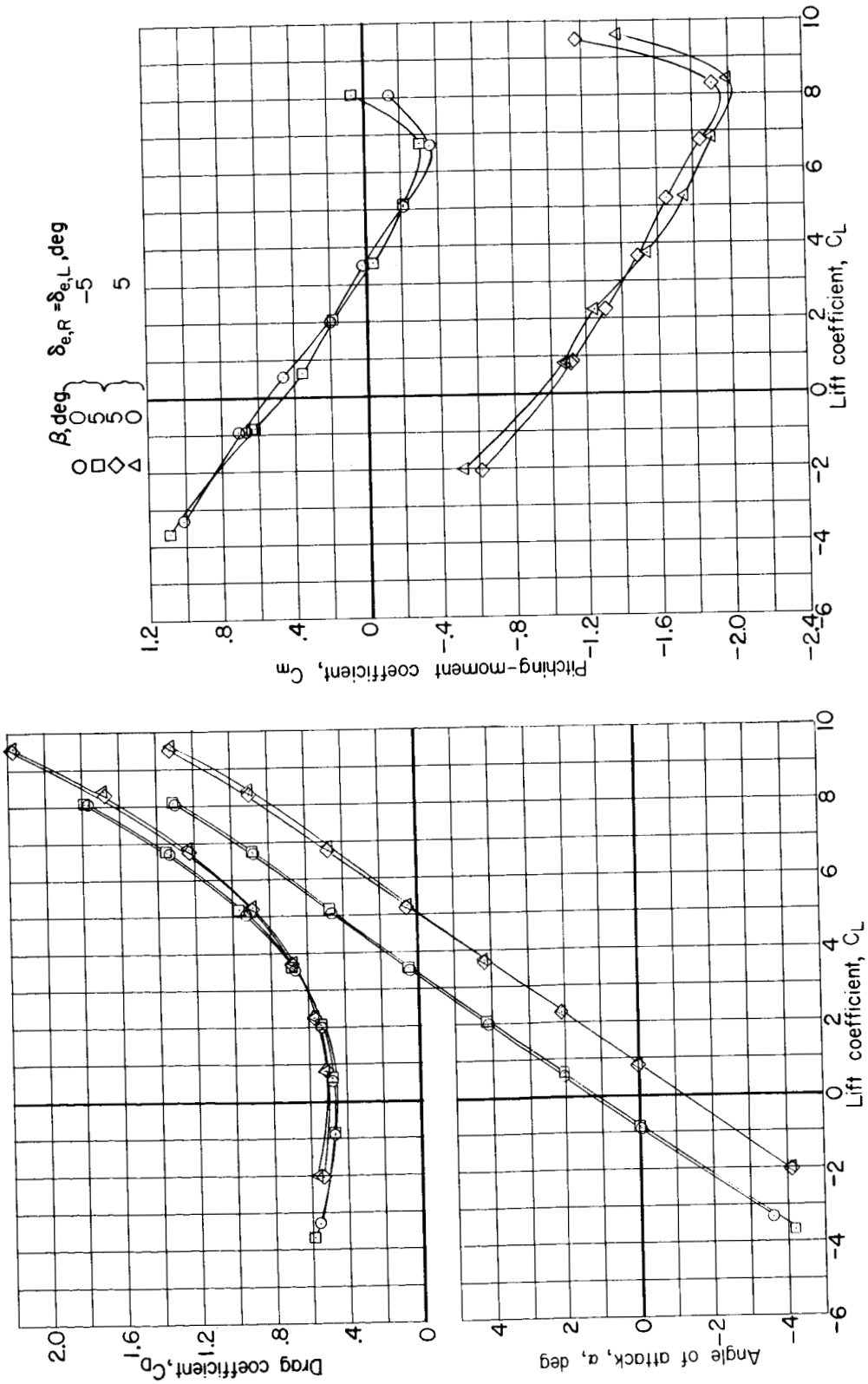

(a) Continued. M = 0.60.

Figure 17.- Continued.

(a) Continued. M = 0.90.

Figure 17.- Continued.

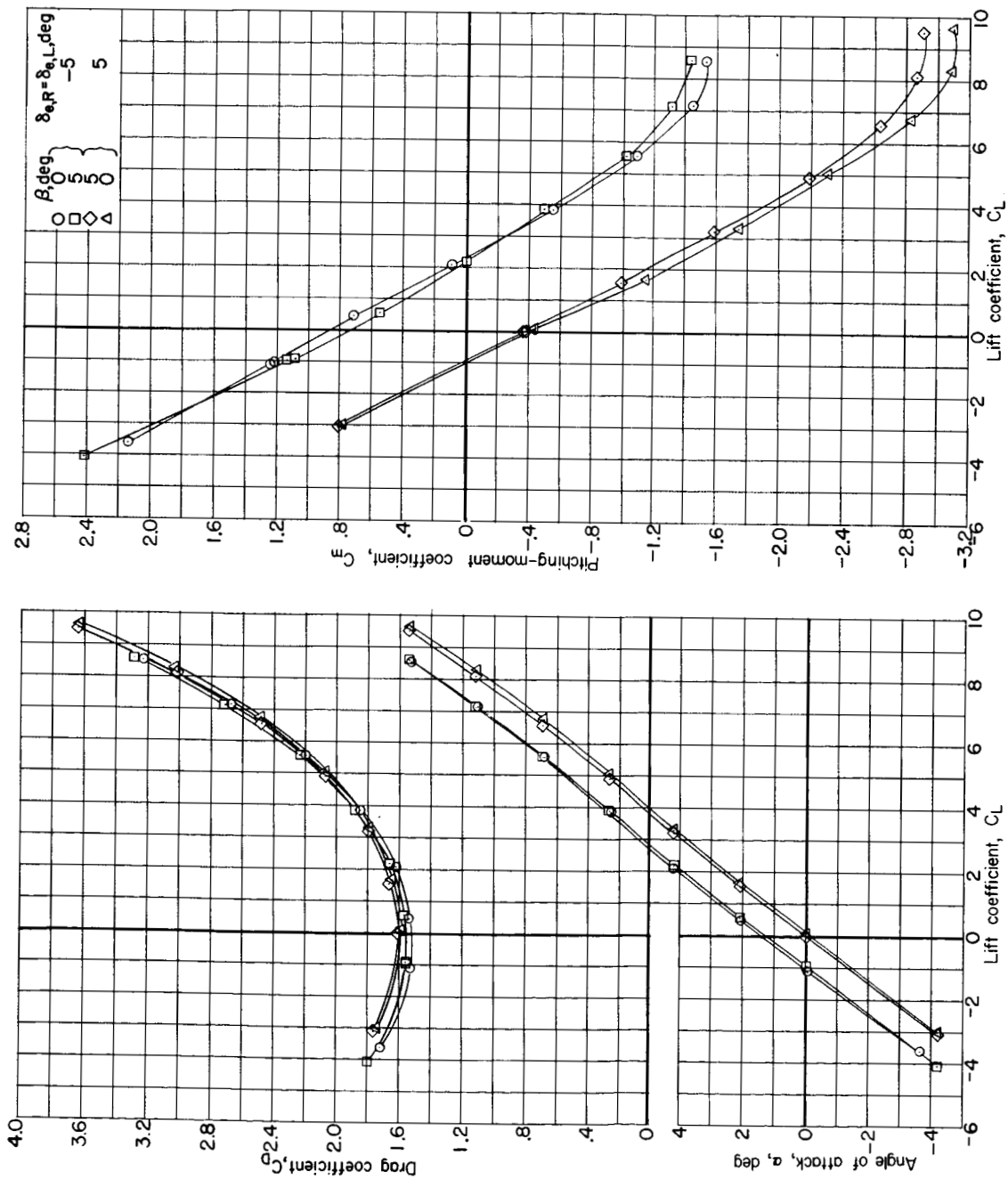

(a) Concluded. M = 1.20.

Figure 17.- Continued.

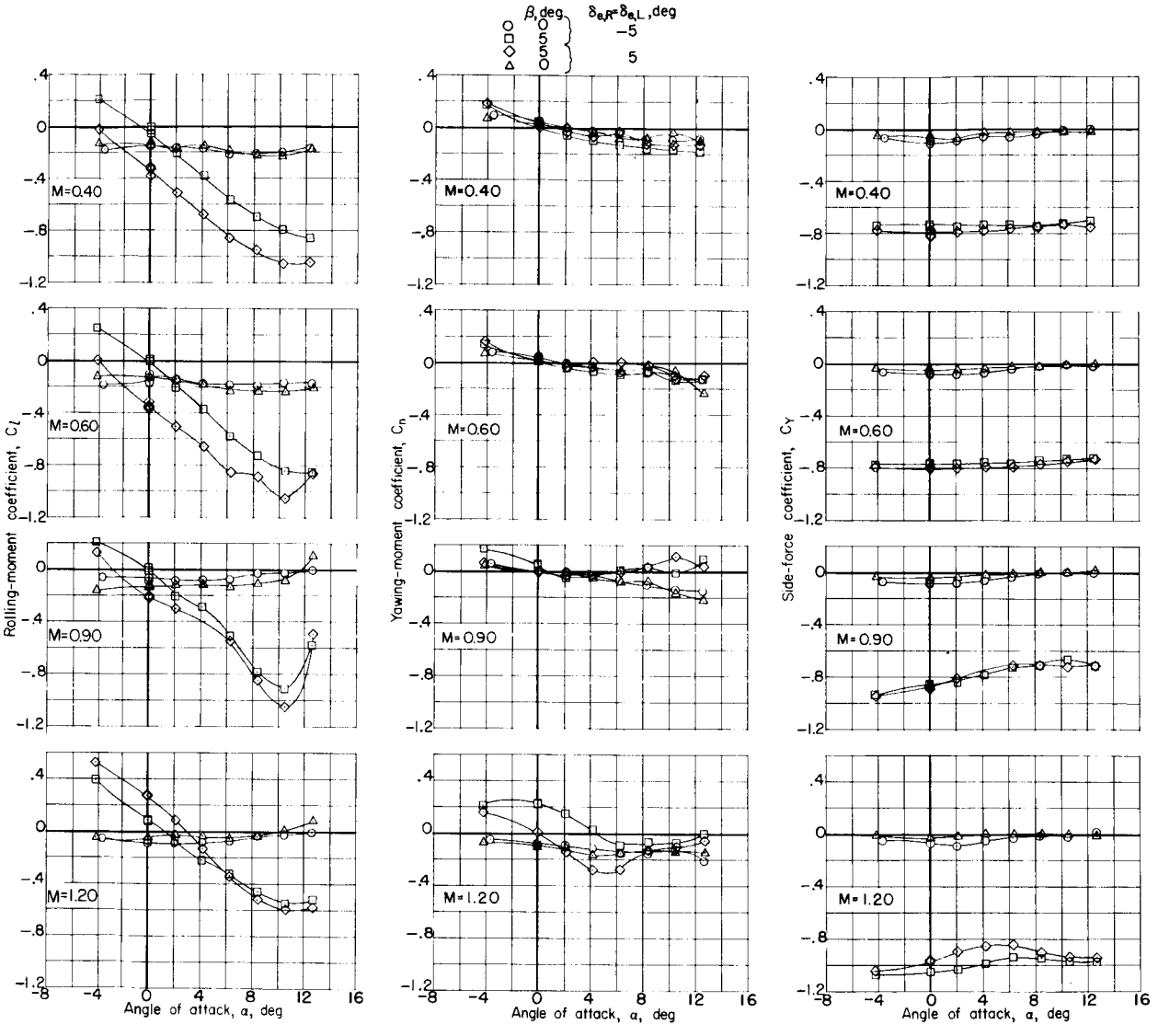

(b) Lateral directional characteristics.

Figure 17.- Concluded.

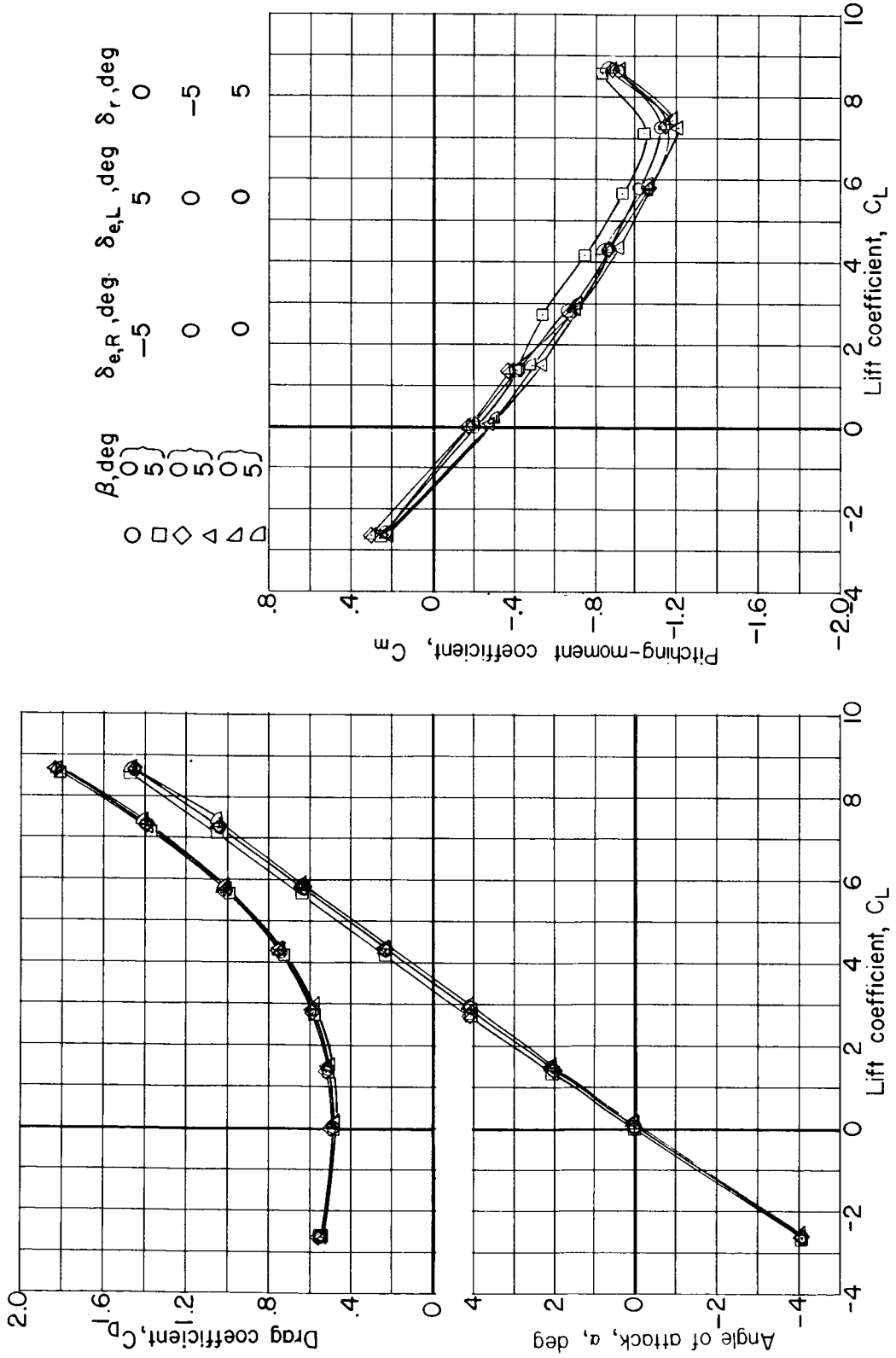

(a) Longitudinal characteristics. M = 0.40.

Figure 18.- Aerodynamic characteristics with deflected lateral or directional control surfaces of first-stage reusable flyback vehicle. Exposed rocket engine actuator struts; no shrouds; engine nacelle off; $\gamma = 12^{0}$; $\theta_c = 15^{0}$; $\theta_t = 0^{0}$.

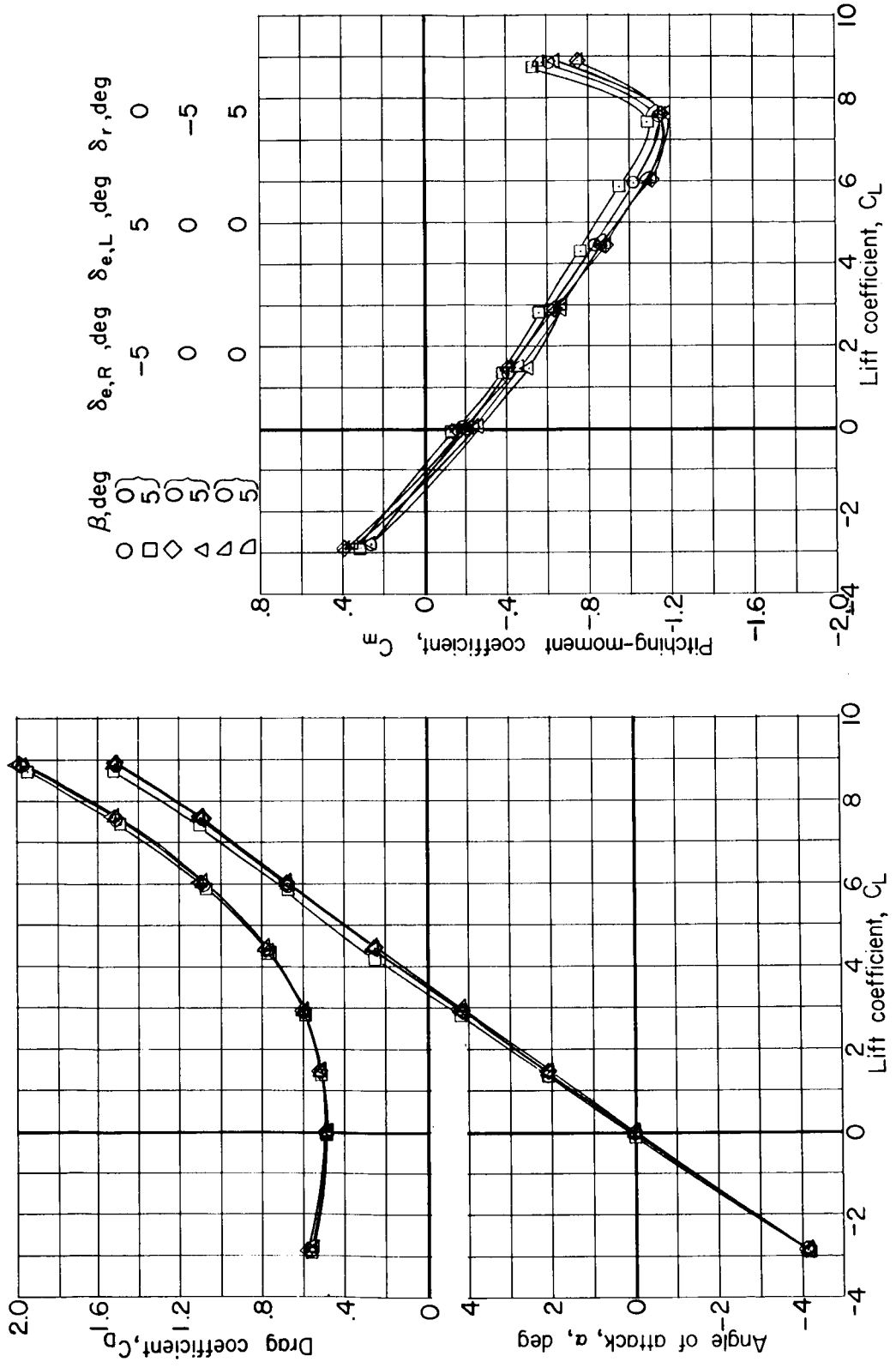

(a) Continued. M = 0.60.

Figure 18.- Continued.

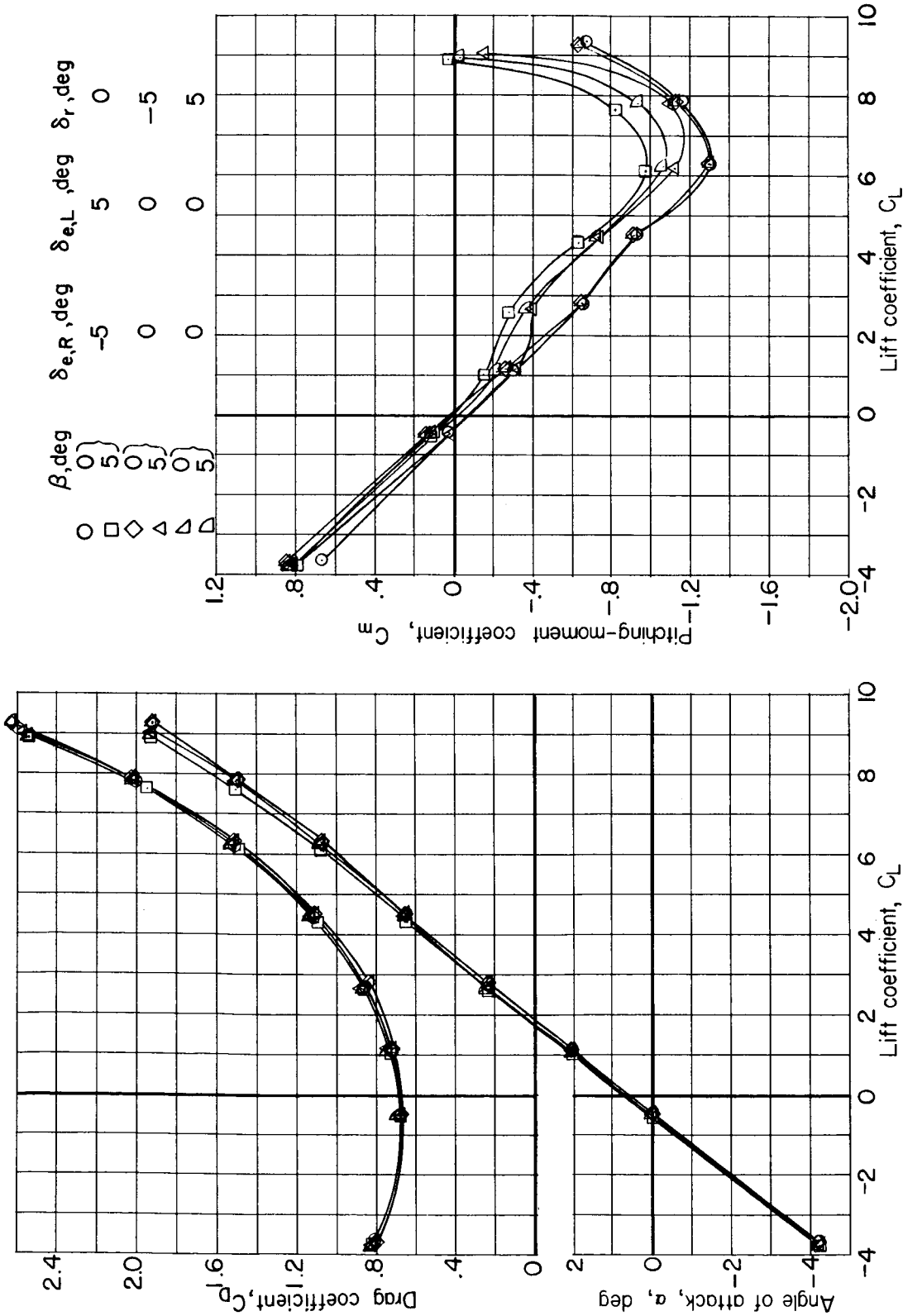

(a) Continued. M = 0.90.

Figure 18.- Continued.

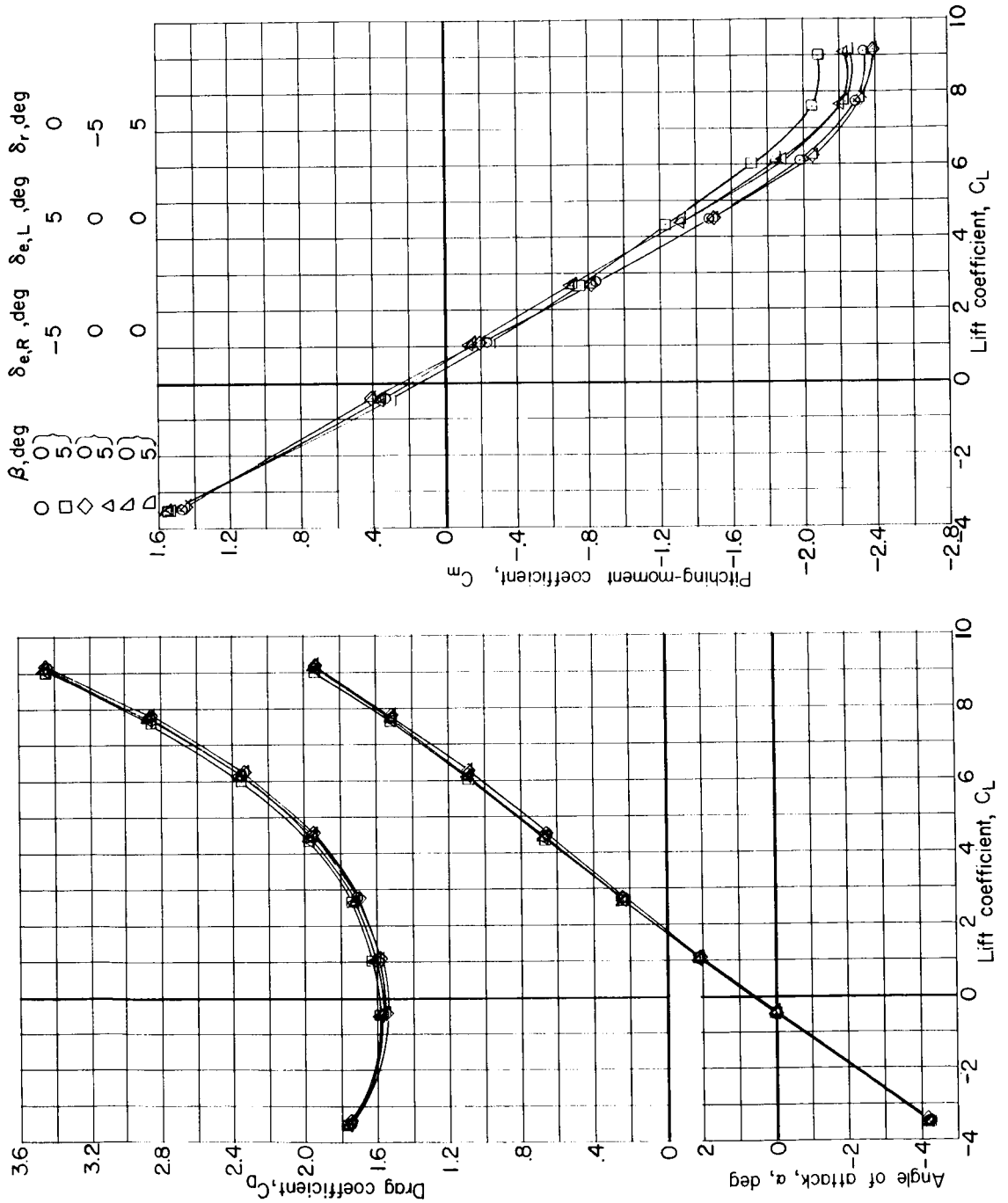

(a) Concluded. M = 1.20.

Figure 18.- Continued.

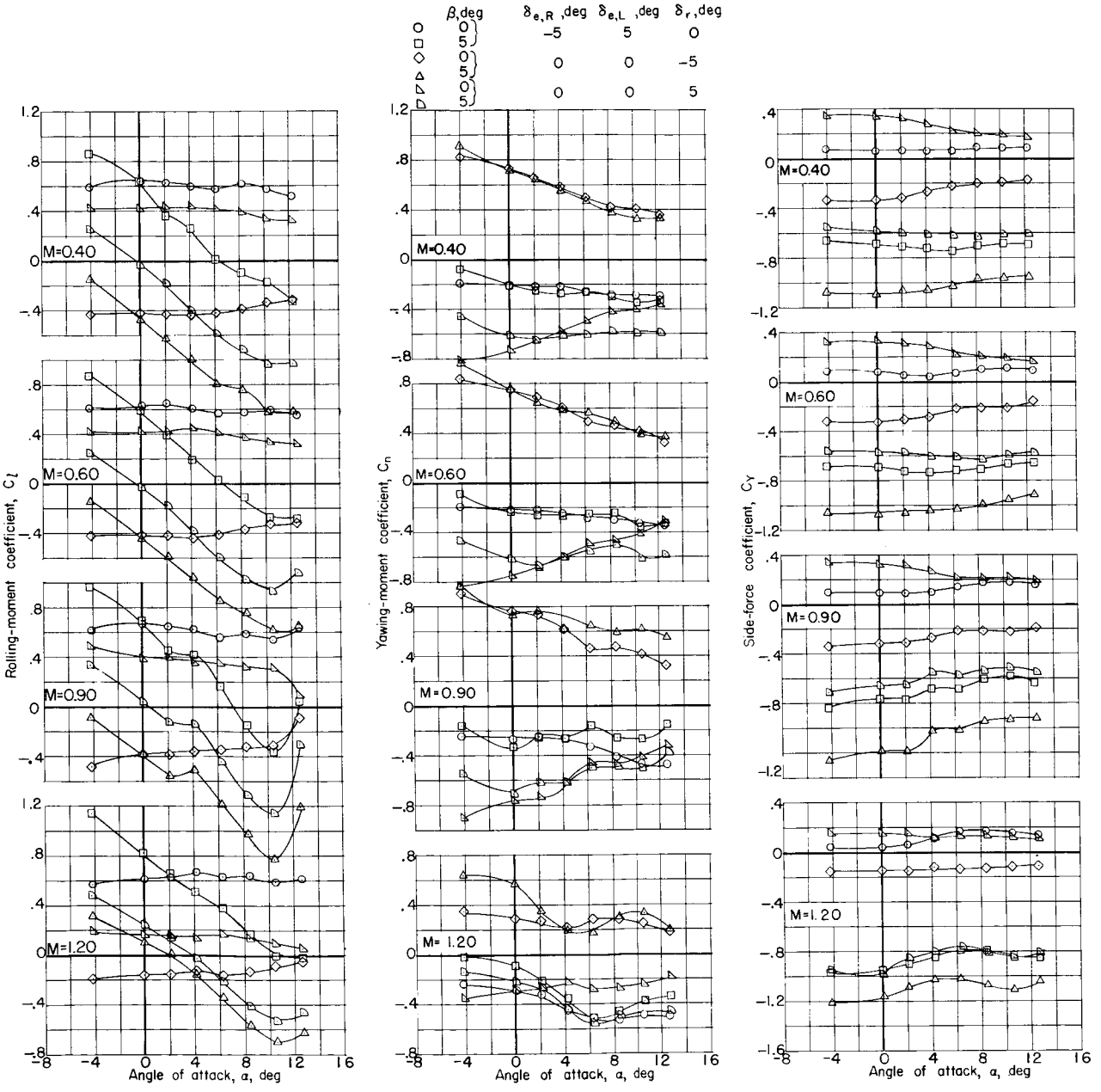

(b) Lateral-directional characteristics.

Figure 18.- Concluded.

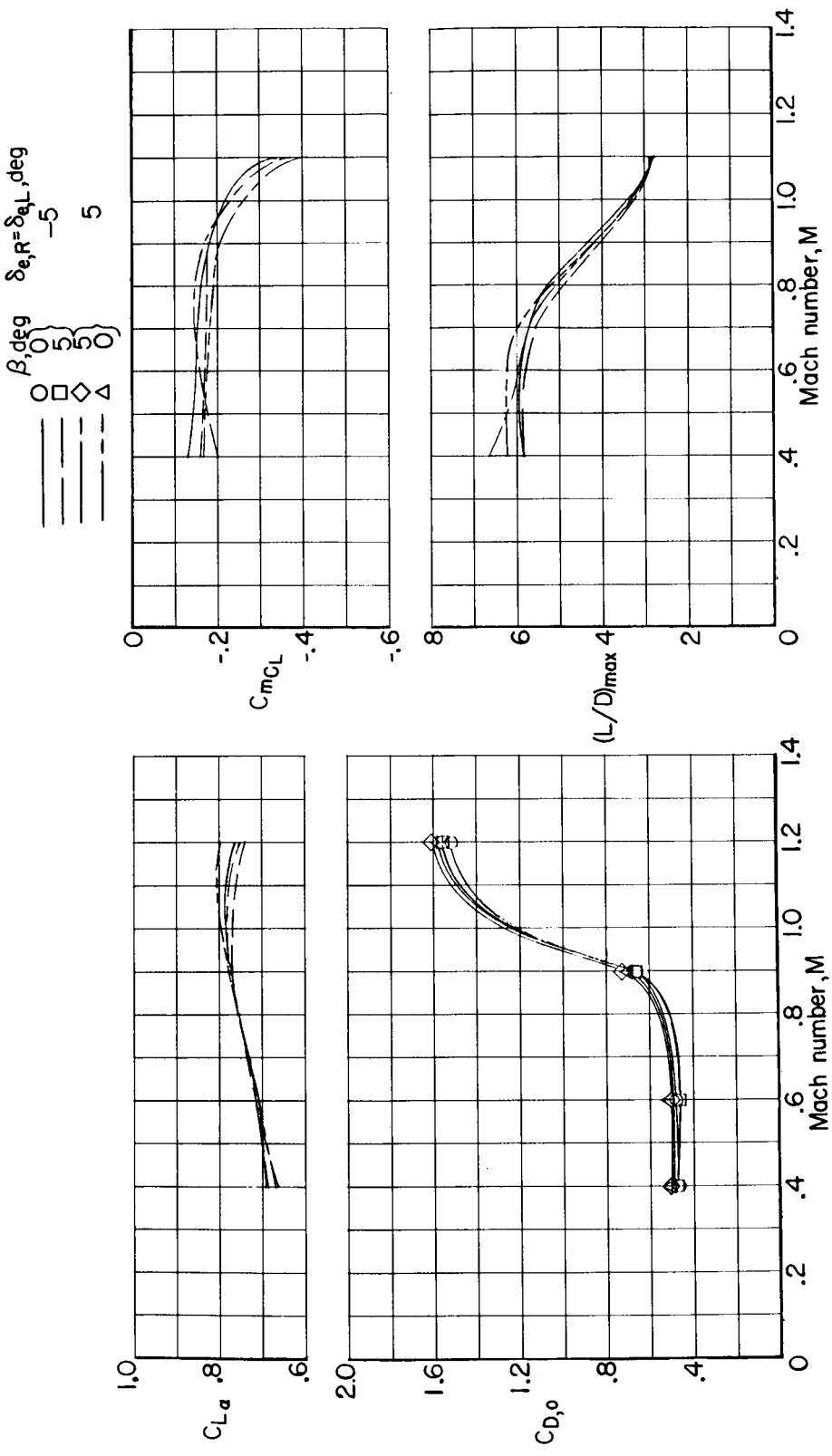

Figure 19.- Variation with Mach number of longitudinal-stability and drag parameters for first-stage reusable flyback vehicle showing effects of longitudinal control deflection. Exposed rocket engine actuator struts; no shrouds; engine nacelle off; $\gamma = 12^0$; $\theta_c = 15^0$; $\theta_t = 0^0$.

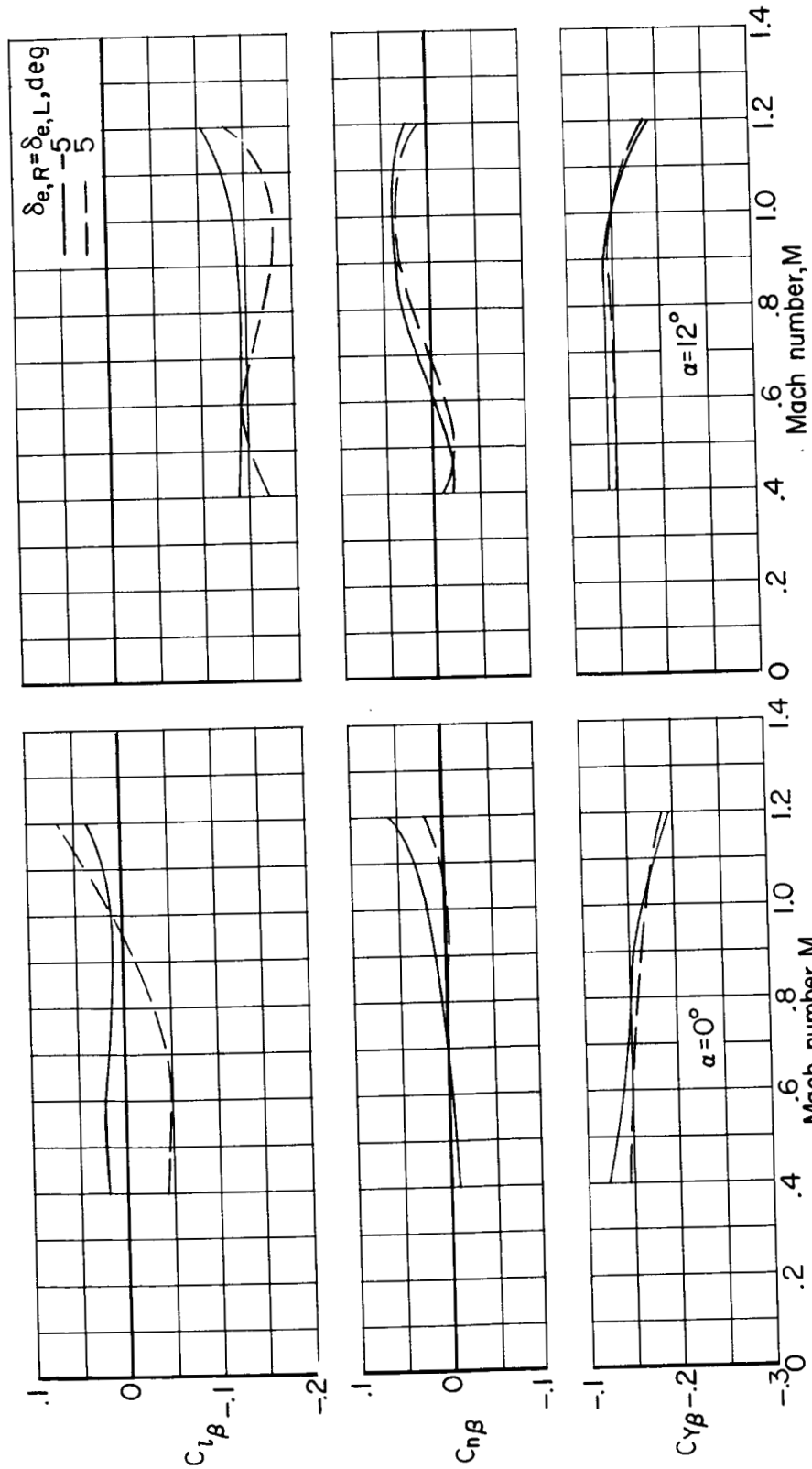

Figure 20.- Variation with Mach number of lateral-directional-stability parameters for first-stage reusable flyback vehicle showing effects of longitudinal control deflections. Exposed rocket engine actuator struts; no shrouds; engine nacelle off; $\gamma = 12^0$; $\theta_c = 15^0$; $\theta_t = 0^0$.

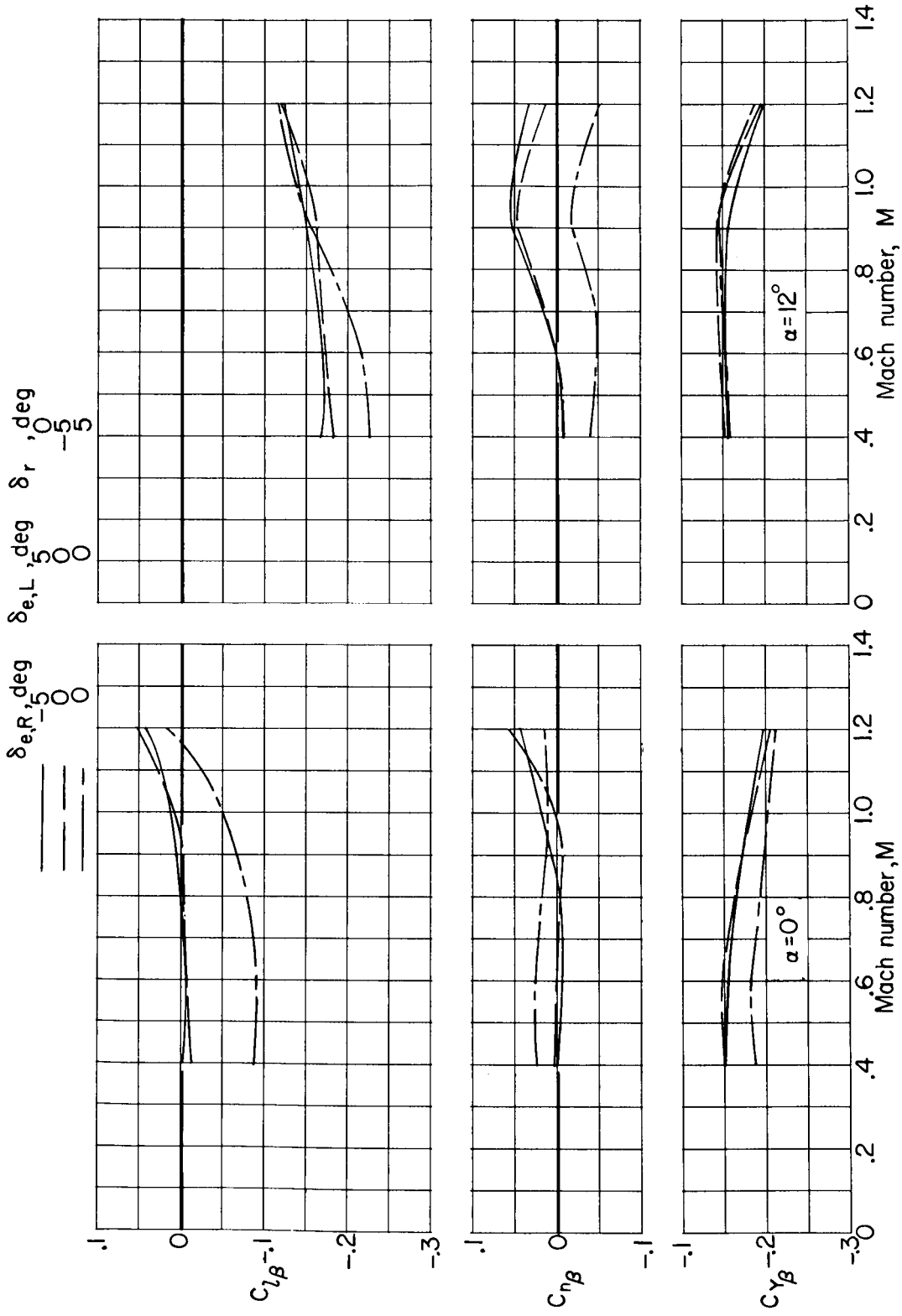

Figure 21.- Variation with Mach number of lateral-directional-stability parameters for first-stage reusable flyback vehicle showing effects of lateral-directional control deflections. Exposed rocket engine actuator struts; no shrouds; engine nacelle off; $\gamma = 12^0$; $\theta_c = 15^0$; $\theta_t = 0^0$.

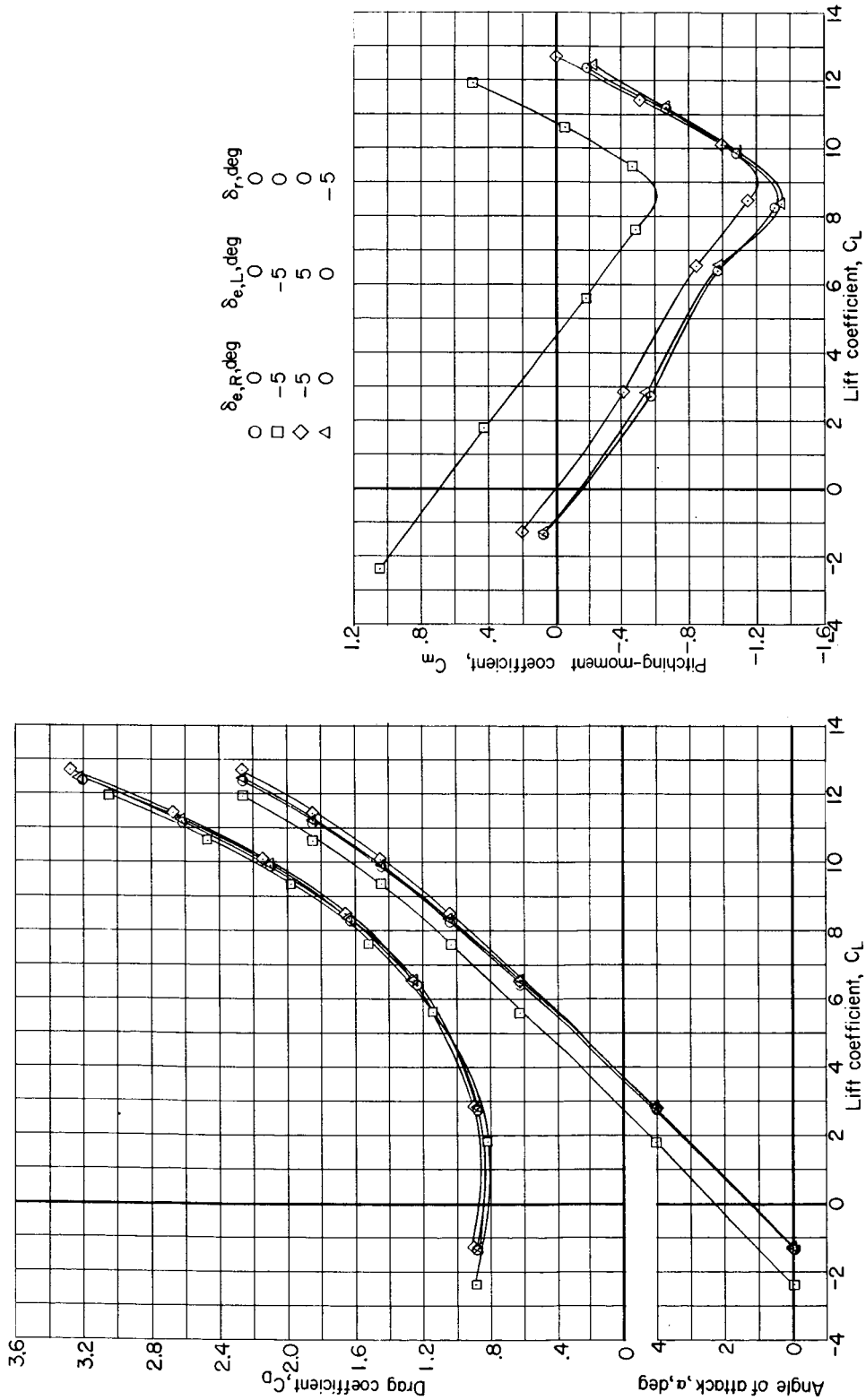

(a) Longitudinal characteristics. M = 0.20.

Figure 22.- Landing characteristics of first-stage reusable flyback vehicle at 0° sideslip with and without control deflections. Exposed rocket engine actuator struts; no shrouds; engine nacelle on; $\gamma = 12^0$; $\theta_c = 15^0$; $\theta_t = 0^0$; $\beta = 0^0$.

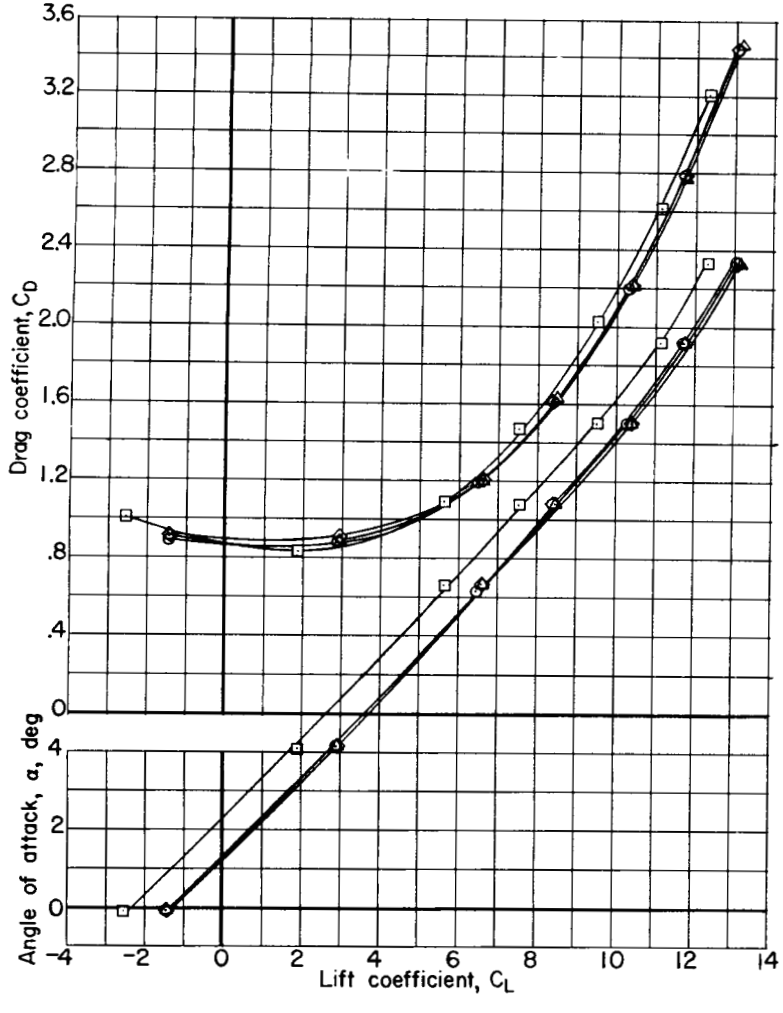

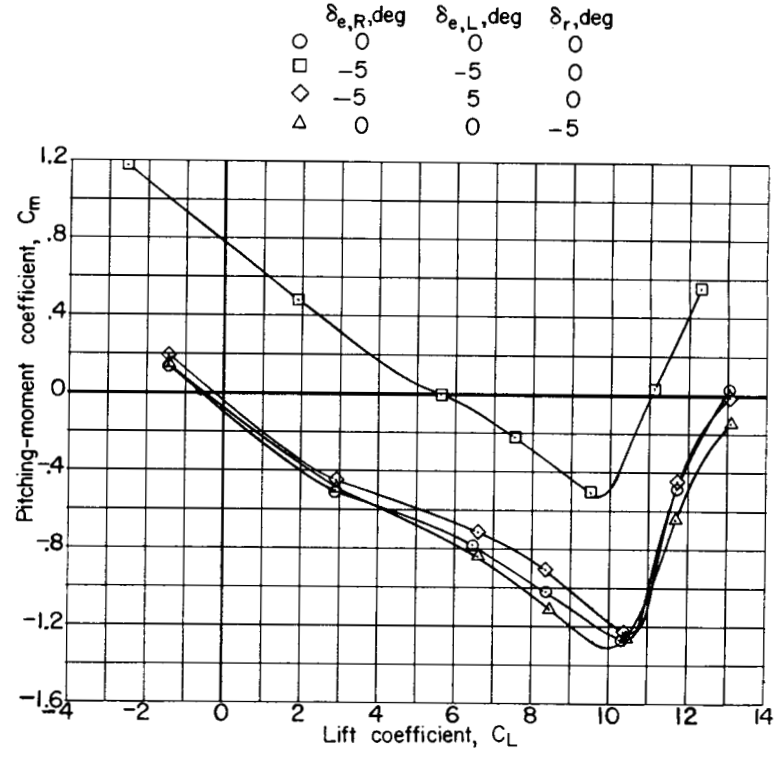

(a) Continued. M = 0.30.

Figure 22.- Continued.

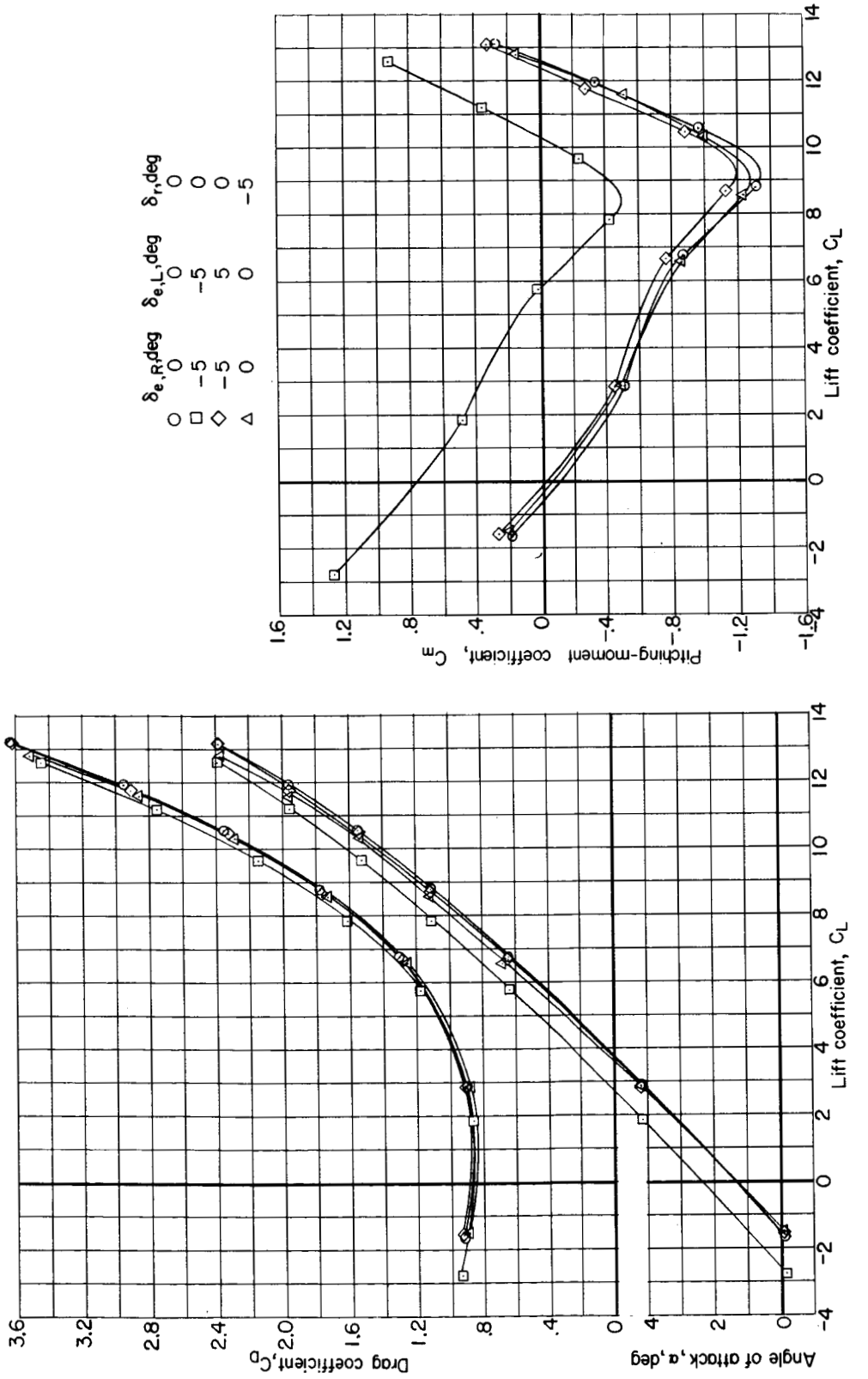

(a) Concluded. M = 0.40.

Figure 22.- Continued.

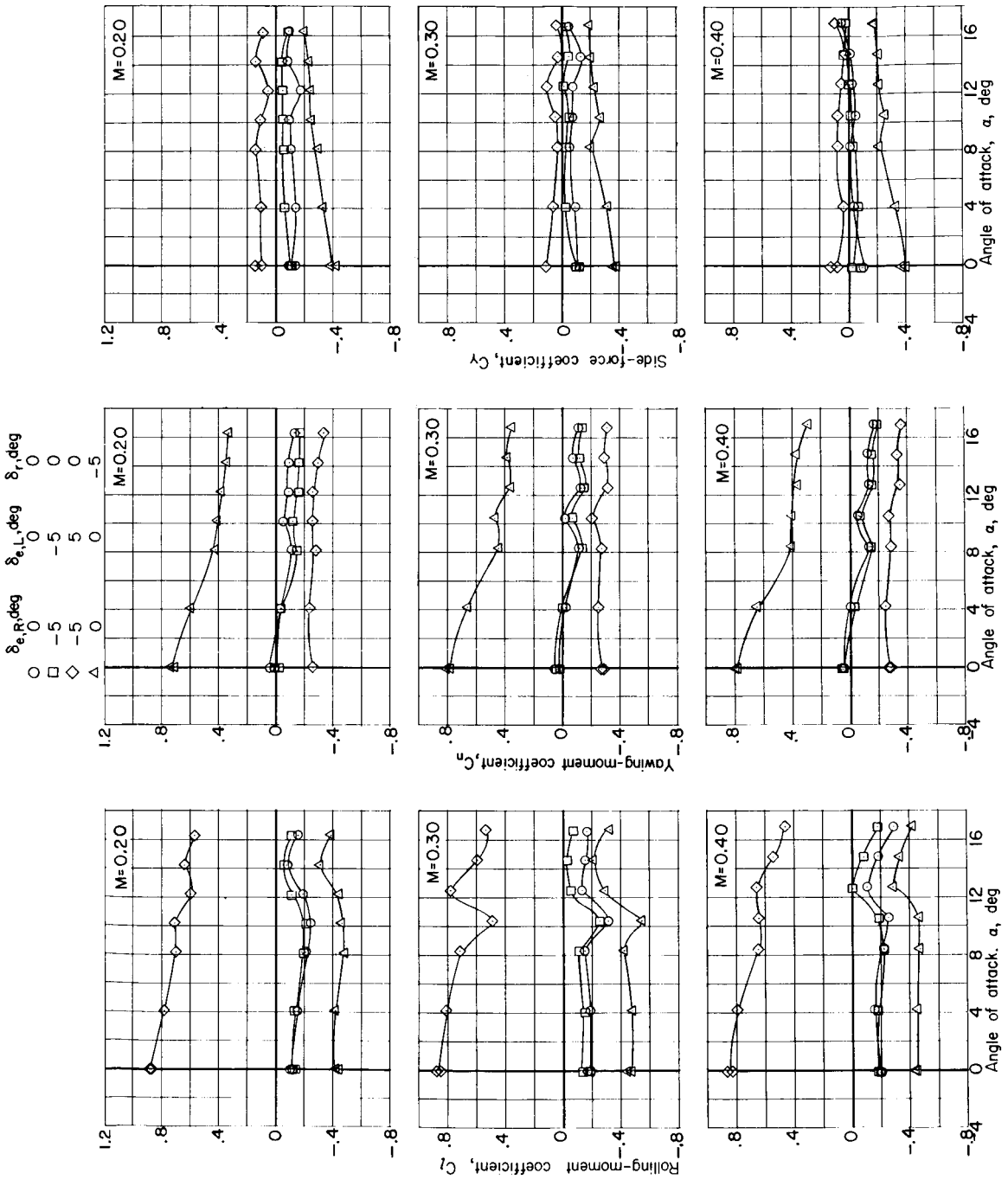

(b) Lateral directional characteristics.

Figure 22.- Concluded.

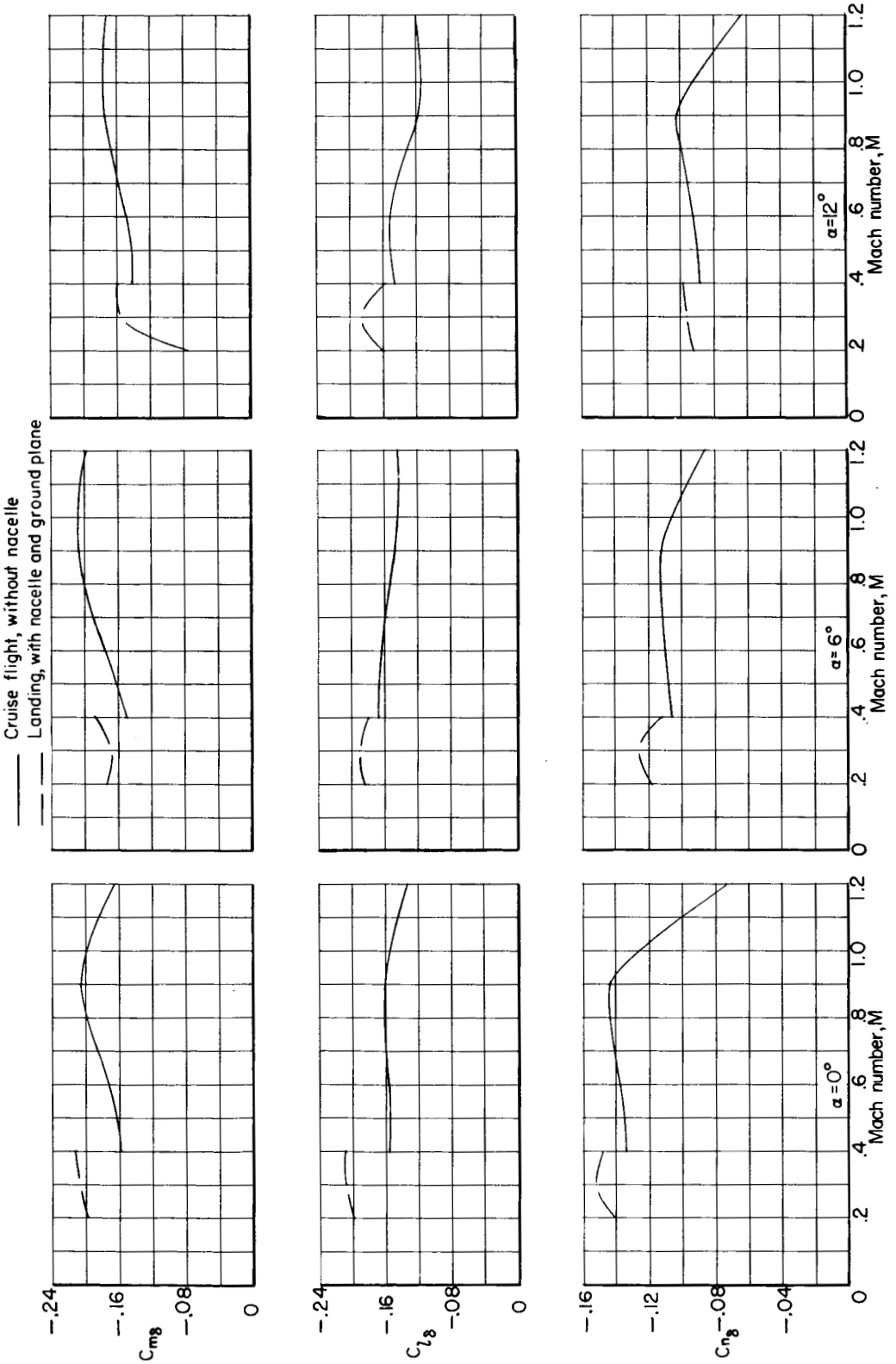

Figure 23.- Control effectiveness at cruise flight and landing conditions of first-stage reusable flyback vehicle. Exposed rocket engine actuator struts; no shrouds; $\gamma = 12^0$; $\theta_c = 15^0$; $\theta_t = 0^0$; $\beta = 0^0$.

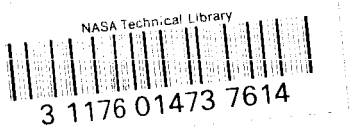

"The aeronautical and space activities of the United States shall be conducted so as to contribute . . . to the expansion of human knowledge of phenomena in the atmosphere and space. The Administration shall provide for the widest practicable and appropriate dissemination of information concerning its activities and the results thereof."

—NATIONAL AERONAUTICS AND SPACE ACT OF 1958

NASA SCIENTIFIC AND TECHNICAL PUBLICATIONS

TECHNICAL REPORTS: Scientific and technical information considered important, complete, and a lasting contribution to existing knowledge.

TECHNICAL NOTES: Information less broad in scope but nevertheless of importance as a contribution to existing knowledge.

TECHNICAL MEMORANDUMS: Information receiving limited distribution because of preliminary data, security classification, or other reasons.

CONTRACTOR REPORTS: Technical information generated in connection with a NASA contract or grant and released under NASA auspices.

TECHNICAL TRANSLATIONS: Information published in a foreign language considered to merit NASA distribution in English.

TECHNICAL REPRINTS: Information derived from NASA activities and initially published in the form of journal articles.

SPECIAL PUBLICATIONS: Information derived from or of value to NASA activities but not necessarily reporting the results of individual NASA-programmed scientific efforts. Publications include conference proceedings, monographs, data compilations, handbooks, sourcebooks, and special bibliographies.

Details on the availability of these publications may be obtained from:

SCIENTIFIC AND TECHNICAL INFORMATION DIVISION

NATIONAL AERONAUTICS AND SPACE ADMINISTRATION

Washington, D.C. 20546